University of Trento

Department of Psychology and Cognitive Science

Ph.D. in Cognitive Science

~ · ~

Academic Year 2025–2026

Not the Pearls but the Thread: Using fNIRS Hyperscanning to Investigate Real-Life Social Interactions

Supervisors
Prof. Gianluca Esposito
Prof. Andrea Bizzego
Prof. Dagmara Dimitriou

Ph.D. Candidate
Alessandro Carollo

Acknowledgments

I wish to express my deepest gratitude to my whole family, my girlfriend, my Ph.D. supervisors, working colleagues, and friends. You are the pearls that have made this work possible: your encouragement, guidance, and companionship have been the thread sustaining me throughout this journey.

Abstract

Hyperscanning refers to the simultaneous recording of brain activity from two or more individuals. Since its introduction in 2002, this approach has represented a major methodological advance in social neuroscience, enabling researchers to directly investigate the neural mechanisms underlying active social exchange. Around the early 2010s, the use of functional near-infrared spectroscopy (fNIRS) became increasingly popular in hyperscanning research. This trend was driven by the technique's high tolerance for head and body movements, its noninvasive nature, and its portability, which together made it particularly suitable for examining neural dynamics during naturalistic social interactions. Over time, the hyperscanning literature has evolved along two main and interrelated trajectories. The first is methodological, focusing on improving the acquisition and analysis of brain signals in experimental settings that allow greater freedom of movement and more ecologically valid social interactions. The second is conceptual, aiming to elucidate how the brain supports active social engagement at both the intra- and interpersonal levels. In line with these directions, the present thesis is based on five experimental studies encompassing both methodological and conceptual investigations. On one side, Chapter 2 presents two experimental studies aimed at improving the identification and correction of motion artifacts in fNIRS data. The first study introduces and demonstrates the feasibility of a computer vision approach for extracting head movement information from video recordings. Using these ground-truth movement features, the second study examines the relationship between specific movement characteristics and the corresponding noise patterns in fNIRS signals. On the other side, the thesis includes three additional experimental studies

designed to examine how relational factors influence patterns of interpersonal neural synchrony and functional connectivity. Specifically, Chapter 3 presents studies investigating how the linguistic features and emotional content of dialogues are associated with, and supported by, patterns of prefrontal interpersonal synchrony and within-brain functional connectivity. Chapter 4 reports a large-scale hyperscanning study involving 284 participants, which examines how interpersonal closeness and task interactivity modulate interpersonal neural synchrony. Methodologically, this thesis demonstrates the feasibility of using computer vision techniques to extract reliable movement features during fNIRS acquisition and to link these features to motion-induced artifacts. These results provide an empirical foundation for developing more robust, movement-informed pre-processing pipelines. Conceptually, the findings show that emotional content and linguistic complexity modulate both interpersonal and intrapersonal neural coupling, suggesting that cognitive and affective dimensions of communication jointly shape the coordination of neural activity between and within interacting individuals. Moreover, interpersonal closeness and task interactivity were found to differentially influence synchrony patterns across prefrontal and temporo-parietal regions. Overall, this work highlights the interdependence between methodological innovation and conceptual understanding in social neuroscience. By presenting works on both computer vision–based movement annotations and naturalistic hyperscanning paradigms, the thesis contributes to a more ecologically grounded framework for studying interpersonal neural synchrony. These insights hold both theoretical significance for models of social cognition and practical potential for applications in educational, clinical, and everyday interactive contexts.

Contents

Chapter 1

Introduction to Hyperscanning

The content of this chapter is based on the publication: **Carollo, A.**, & Esposito, G. (2024). Hyperscanning literature after two decades of neuroscientific research: A scientometric review. *Neuroscience, 551*, 345-354. https://doi.org/10.1016/j.neuroscience.2024.05.045.

In some parts, the text has been modified for consistency with the dissertation style.

1.1 Pearls and Threads

> "Les perles composent le collier, mais c'est le fil qui fait le collier. Or, enfiler les perles sans en perdre une seule et toujours tenir son fil de l'autre main, voilà la malice...
>
> [The pearls compose the necklace, but it is the string that makes it a necklace. Now, to thread the pearls without losing a single one and always to hold one's string with the other

> hand, there's the trick...]" (*Gustave Flaubert, letter to Louise Colet, 26 August 1853*)

When Gustave Flaubert wrote the first draft of Madame Bovary, the novel that would make him famous worldwide, he remarked to some of his friends that "It is not the pearls that make the necklace but the thread that joins them together". In this way, Flaubert emphasized that the value of individual elements, in his case, scenes, characters, or episodes, does not lie in their isolated quality, but in the structure that binds them into a coherent whole. Likewise, in a novel, characters acquire their true significance only when the narrative thread weaves them into an integrated and meaningful unity.

Similarly, this thesis argues that social interactions emerge and are sustained not merely by the qualities of their pearls — that is, the individuals — but, above all, by the properties and strength of the thread that connects them: interpersonal synchrony. For this reason, in recent years the field of social neuroscience has undergone a profound conceptual shift. Its focus has moved from studying individuals in isolation to investigating multiple individuals engaged in dynamic, real-life social exchanges. This paradigm shift, made possible by the development of the hyperscanning approach, has transformed our understanding of social behavior — from a view centered on social cognition and processes within the individual to one that recognizes the crucial role of interpersonal phenomena, such as synchrony, in shaping everyday social interaction. Throughout this thesis, I will show how contemporary research in social neuroscience explores both the pearls and the threads that compose social exchanges.

1.2 A Revolution in Social Neuroscience

The concept of hyperscanning describes a neuroimaging approach based on the simultaneous recording of brain activity from two or more individuals. This approach was originally introduced by Montague et al. (2002) to explore the neural mechanisms supporting real-time social interaction. According to Hasson et al. (2012), the advent of hyperscanning and the broader second-person neuroscience framework marked a "Copernican revolution" in cognitive and social neuroscience. Whereas conventional neuroimaging paradigms have provided valuable insights into the functioning of the "social brain", they typically rely on data collected from one person at a time, often through tasks involving the passive exposure to social stimuli in different contexts (e.g., face perception as in Kanwisher et al., 1997). As a result, these approaches have illuminated how individuals perceive and interpret social information, yet they have fallen short of capturing the inherently interactive and enactive nature of real-life social behavior (Czeszumski et al., 2020). By contrast, hyperscanning has enabled the investigation of interpersonal and collective neural dynamics that emerge during active, real-life social interactions, offering a more ecologically grounded understanding of the neural basis of human exchanges.

1.3 Methods in Hyperscanning

Recent methodological and technological developments have significantly driven progress in hyperscanning research. Originally, hyperscanning was conceived for use with functional magnetic resonance imaging (fMRI). In their pioneering study, Montague et al. (2002) demonstrated the feasibil-

ity of acquiring simultaneous fMRI data from two participants, showing this through an experiment in which nine dyads engaged in a deception game. Since then, the hyperscanning framework has been successfully extended to other neuroimaging modalities, including magnetoencephalography (MEG; Baess et al., 2012), electroencephalography (EEG; F. Babiloni et al., 2007), and, more recently, functional near-infrared spectroscopy (fNIRS; Cui et al., 2012; Funane et al., 2011).

Each of these neuroimaging methods offers specific advantages and limitations when applied to hyperscanning designs (Carollo et al., 2022; Martin & Huettel, 2022). For example, fMRI provides superior spatial resolution compared to fNIRS and EEG but requires participants to remain supine within the scanner, thereby restricting the range of possible interactive tasks. EEG, on the other hand, affords high temporal precision, yet is highly susceptible to motion artifacts that may compromise data quality.

By contrast, fNIRS represents a valuable middle ground between these two modalities. It offers sufficient spatial resolution for recording activity from superficial cortical regions and is relatively robust to participant movement. Furthermore, fNIRS devices are portable and considerably more cost-effective than fMRI, enabling data collection in more naturalistic settings such as classrooms, dyadic interactions, or parent–child play sessions.

For these reasons, fNIRS has become particularly well-suited to studying social interaction as it naturally occurs, where individuals communicate, gesture, and move freely. Its motion tolerance and portability have been instrumental in extending hyperscanning research beyond the laboratory, paving the way for more ecologically valid investigations of real-

life social behavior, especially in developmental populations (see Figure 1.1 for an example of study setup used with mother–child dyads during free play Bizzego, Gabrieli, et al., 2022).

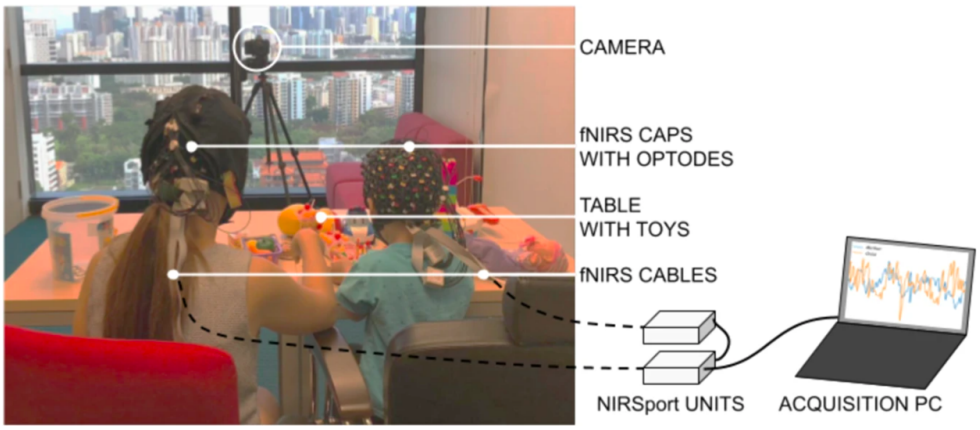

Figure 1.1: Representation of a functional near-infrared spectroscopy (fNIRS) hyperscanning setup to monitor the brain activity of mother and child during a free play session. Image from Bizzego, Gabrieli, et al. (2022).

1.4 Interpersonal Neural Synchrony

A central finding emerging from hyperscanning studies is that social exchanges are typically accompanied by the alignment (or synchronization) of neural activity between interacting partners (e.g., Dumas et al., 2010). This phenomenon, commonly referred to as interpersonal neural synchrony, can be understood as a neural-level extension of the bio-behavioral synchrony framework (Feldman, 2012a), which posits that behavioral, physiological, and hormonal processes between social partners tend to align during interaction (Carollo, Lim, et al., 2021).

The idea that two brains can align under certain circumstances was initially demonstrated using sequential fMRI scans, without employing a hyperscanning approach. In their single-participant fMRI study, Hasson

et al. (2004) showed that people's brains exhibit similar neural responses when exposed to the same video. Comparable results have been observed during story listening and memory recall tasks, suggesting a potential association between interpersonal closeness and brain activity similarity (J. Chen et al., 2017; De Felice, Chand, et al., 2024; Yeshurun et al., 2017). Interestingly, the similarity in brain activity is stronger among friends than among individuals who are not friends (Parkinson et al., 2018). However, these studies only showed that brains respond similarly when they are exposed to the same stimulus; they did not reveal how alignment between interacting individuals depends on the shared timing, rhythms, and communicative exchanges that occur during real-life social interactions. Thus, fully understanding whether and how individual neural signals align as a function of social contact requires the adoption of a hyperscanning approach.

Using the hyperscanning approach, studies have demonstrated that brain activity becomes synchronized between interacting individuals across various social tasks (e.g., Cui et al., 2012; De Felice, Hakim, et al., 2024). Notably, this synchronization exceeds what can be accounted for by shared perceptual input alone, an effect that De Felice, Chand, et al. (2024) referred to as the *hyperscanning effect*. In other words, the exposure to the same environmental stimuli cannot fully account for the *hyperscanning effect*. Rather, this effect appears to be induced by the co-presence among interacting individuals.

Not only is interpersonal neural synchrony elicited by the mere co-presence of individuals, but it is also modulated by the specific properties that characterize the social exchange itself. For instance, several studies have shown that interpersonal neural synchrony varies as a function

of the quality of the social interaction (Endevelt-Shapira & Feldman, 2023; Nguyen, Schleihauf, Kayhan, et al., 2020; Nguyen et al., 2024), suggesting that it may serve as a neural marker of social connectedness (Nguyen, Schleihauf, Kayhan, et al., 2020). For this reason, the study of interpersonal neural synchrony is particularly valuable when combined with ecologically valid paradigms as it enables researchers to link neural dynamics to behavioral, social, and developmental outcomes in naturalistic settings.

1.5 From Correlation to Causation

In recent years, the scope of hyperscanning has expanded beyond traditional brain imaging, incorporating innovative approaches based on brain stimulation techniques, such as transcranial, sensory, and optogenetic methods, to move from correlational to causal frameworks (Novembre & Iannetti, 2021) (see Figure 1.2 as an example of sensory entrainment). Conventional hyperscanning paradigms typically conceptualize interpersonal neural synchrony as a dependent variable emerging from social interaction between individuals. Although this perspective has generated important insights, it does not allow researchers to determine whether neural synchrony is simply a byproduct of shared environmental exposure and co-presence or whether it actively contributes to social coordination and connectedness. By contrast, stimulation-based hyperscanning adopts a causal logic, directly manipulating neural activity to observe its influence on interpersonal dynamics and relational outcomes (e.g., H. Lu et al., 2023. This shift enables researchers to test whether induced neural synchrony can enhance or alter social interaction processes.

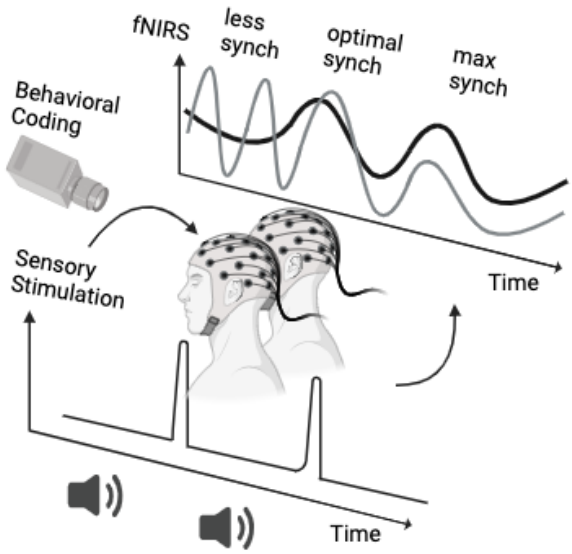

Figure 1.2: A graphical example of multi-brain modulation through rhythmic sensory stimulation. Image from Carollo and Esposito (2024).

1.6 Mapping the Hyperscanning Literature

Over the past two decades, the techniques described above have been applied in an increasing number of hyperscanning studies, each offering distinct advantages and limitations. Despite these technical progresses, the field remains characterized by methodological and conceptual heterogeneity, and no unified theoretical framework yet exists to integrate findings across domains and understand the role of interpersonal neural synchrony across social tasks and relationships (Carollo, Bizzego, Schäfer, et al., 2025; Hamilton, 2021).

To better understand how hyperscanning research has evolved, we conducted a data-driven scientometric study that mapped the field's development from 2002 to 2023 (n = 500 documents) (Carollo & Esposito, 2024). Using data retrieved from Scopus and analyzed through *bibliometrix* (Aria & Cuccurullo, 2017) and CiteSpace (C. Chen, 2006), we identified the main research domains and emerging conceptual trends.

The document co-citation network (Figure 1.3) comprised 648 publications grouped into ten major thematic clusters, spanning several domains such as affective neuroscience, verbal communication, education, parent–child interaction, and technologically mediated social exchanges.

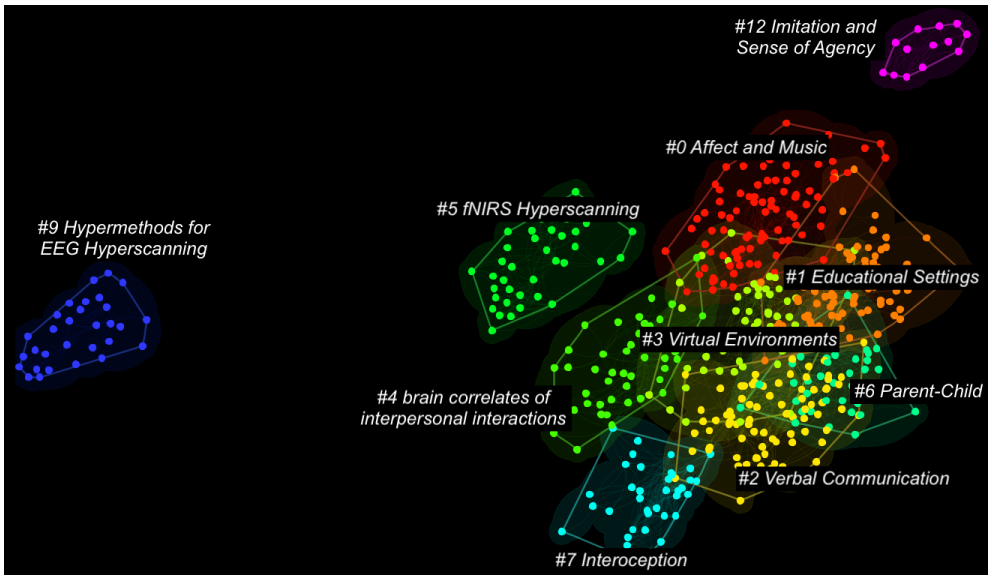

Figure 1.3: Document co-citation analysis network of the hyperscanning literature. Image from Carollo and Esposito (2024).

Building on the scientometric mapping, the next sections provide a qualitative overview of the main thematic domains that have emerged in hyperscanning research over the past two decades. Each subsection corresponds to one or more clusters identified in the document co-citation analysis (see Figure 1.3) and highlights the main characteristic research questions, methods, and/or findings associated with that domain. Together, these thematic areas illustrate the evolution of hyperscanning from its methodological foundations to its current applications in increasingly naturalistic and socially complex contexts.

1.6.1 Foundational EEG Work and "Hypermethods"

The earliest stage of hyperscanning research was characterized by pioneering efforts to demonstrate the feasibility of EEG recording and analyzing brain activity from multiple individuals simultaneously. Foundational studies (e.g., Astolfi et al., 2010; F. Babiloni et al., 2006) introduced what were later referred to as *hypermethods*: analytical techniques originally designed to measure functional connectivity and used to assess synchronization between brains. These approaches, often adapted from single-participant neuroimaging analyses (Astolfi et al., 2005; F. Babiloni et al., 2005), allowed researchers to move beyond the study of single brain activity and to explore the dynamics supporting interacting individuals, providing the first empirical evidence of interpersonal neural synchrony.

Building on this methodological foundation, subsequent research began to explore how such inter-brain synchronization relates to social-cognitive processes such as imitation and the sense of agency in controlled tasks. A seminal contribution in this direction came from Dumas et al. (2012), who investigated how the brain distinguishes between self-generated and other-generated actions by experimentally controlling the interpersonal imitation patterns within dyadic interactions.

In designing their experiments and interpreting the observed results, early hyperscanning studies often drew on the literature on the mirror neuron system (Rizzolatti & Craighero, 2004) and behavioral mimicry (Ashton–James et al., 2007), extending these concepts from single-brain frameworks to interactive contexts. Collectively, this initial body of work established both the methodological and conceptual foundations for un-

derstanding how neural synchronization emerges and potentially supports joint action in controlled social exchanges.

1.6.2 fNIRS and Ecological Validity

During the early 2010s, hyperscanning research entered a new phase in which researchers sought to address two main challenges: first, to employ neuroimaging techniques with higher spatial resolution, and second, to design experimental paradigms with greater ecological validity (Astolfi, Toppi, Fallani, et al., 2011; Dumas et al., 2011; Funane et al., 2011). While fMRI offered excellent spatial resolution and allowed researchers to map the neural substrates of social interaction (e.g., Abe et al., 2019), its characteristics constrained the use of naturalistic tasks. Because fMRI is highly sensitive to movement and requires participants to lie supine inside the scanner, it constrains the ecological validity of interactive paradigms. For this reason, the introduction of fNIRS provided an elegant solution, combining moderate spatial precision for monitoring cortical layer of the brain with portability, movement tolerance, and comfort suitable for studying real-life social exchanges.

A landmark study by Funane et al. (2011) marked the beginning of fNIRS hyperscanning. The authors showed that greater spatiotemporal covariance in prefrontal cortical activity between participants was associated with enhanced behavioral coordination during synchronous button-pressing tasks. As noted by F. Babiloni and Astolfi (2014), this study represented a crucial step in adapting the technical solutions developed for EEG hyperscanning to optical imaging. Shortly after, Cui et al. (2012) introduced an alternative approach, using a single NIRS system to record brain activity from two participants simultaneously by

splitting the recording optodes. Although this method reduced the number of available optodes per participant, it enabled researchers to map regions of interest while minimizing the costs associated with dual-device hyperscanning.

The adoption of fNIRS marked a methodological turning point for hyperscanning, enabling researchers to study the interpersonal and intrapersonal brain dynamics under more naturalistic social conditions. The adoption of techniques with good spatial resolution also encouraged to localize the specific brain regions where interpersonal neural synchrony systematically emerges (e.g., Astolfi et al., 2015; Balconi et al., 2018; Hirsch et al., 2017; Nozawa et al., 2016). In line with this effort, the meta-analysis by Zhao et al. (2024) observed consistent patterns of interpersonal neural synchrony in the frontal, temporal, and parietal regions across close relationships.

1.6.3 Emotion and Music

The shift toward more ecologically valid experimental paradigms in social neuroscience led to a growing interest in a fundamental yet often overlooked aspect of daily social interactions: the affective component (Balconi & Vanutelli, 2017; Cornejo et al., 2017). Emotions play a central role in shaping social cohesion, motivating joint actions, and supporting prosocial behavior (Czeszumski et al., 2020; Konvalinka et al., 2011; Lopes et al., 2005; Twenge et al., 2007). Despite their importance, emotional processes had been relatively neglected in hyperscanning research, primarily due to the complexity of including and controlling them in experimental setup (Czeszumski et al., 2020).

One innovative approach to address this challenge was proposed by

Acquadro et al. (2016), who suggested using musical interactions as naturalistic context to study the role of affect in social exchanges and coordination. Musical settings not only preserve high ecological validity but also engage participants' emotions and enable an enactive understanding of interpersonal coordination (Czeszumski et al., 2020). Building on this approach, several hyperscanning studies have used musical tasks to demonstrate that interpersonal neural synchrony underlies coordinated behavior in emotionally rich social interactions (e.g., C. Babiloni et al., 2011, 2012; Lindenberger et al., 2009; Sänger et al., 2012, 2013).

1.6.4 Communication, Education, and Virtuality

As hyperscanning research matured, scholars began applying it to increasingly complex and socially relevant contexts, such as verbal communication, learning, and technologically mediated interaction. These studies extended hyperscanning from controlled laboratory tasks to settings that more closely mirror real-life social exchanges, highlighting its potential for understanding how interpersonal neural synchrony supports communication and collaboration across diverse environments and social contexts.

A growing body of research has focused on the neural mechanisms underlying verbal communication (e.g., Jiang et al., 2021; X. Wang et al., 2022). For instance, studies have shown that the timing and turn-taking in conversations predict interpersonal neural synchrony (Nguyen, Schleihauf, Kayhan, et al., 2021; Nguyen et al., 2023). These findings suggest that effective coordination during communication depends on the dynamic coupling of neural processes between interlocutors, enabling mutual prediction and real-time adaptation.

In parallel, hyperscanning has also been used to explore how patterns of interpersonal neural synchrony emerge and predict learning outcomes in educational settings (e.g., Balters et al., 2020; K. Lu et al., 2019; Pan et al., 2021). Nozawa et al. (2019) observed that behavioral synchrony between teachers and learners enhances both the perceived quality of the interaction and interpersonal neural synchrony in the lateral prefrontal cortex. This evidence indicates that successful pedagogical interactions may be underpinned by neural alignment, which facilitates engagement and potentially effective knowledge transmission.

Additionally, an emerging body of work has examined interpersonal neural synchrony in virtual environments, where social interaction is technologically mediated (e.g., Barde et al., 2020). Early studies suggested that virtual interactions can elicit neural coupling patterns comparable to those observed in face-to-face contexts (Gumilar et al., 2021; Wikström et al., 2022). However, other research, such as Schwartz et al. (2022, 2024), found reduced interpersonal neural synchrony during virtual exchanges when compared to in-person interactions.

1.6.5 Methodological Advances and Parent-Child Interactions

A further line of research in the hyperscanning literature has concentrated on two complementary aspects: methodological development and the investigation of parent–child interactions. On the methodological side, several studies have tackled the technical and analytical challenges inherent to hyperscanning, producing concrete guidelines for EEG and fNIRS applications that have strengthened reproducibility and standard-

ization within the field (e.g., Bizzego, Azhari, and Esposito, 2021, 2022; Kayhan et al., 2022; Nguyen, Hoehl, and Vrtička, 2021; Turk et al., 2022). These contributions have been instrumental in defining best practices for data acquisition, pre-processing, and the analysis of interpersonal neural synchrony, thereby facilitating more reliable and comparable findings across studies (Holroyd, 2022; Nguyen, Hoehl, & Vrtička, 2021).

On the empirical side, hyperscanning has been increasingly applied to the study of early social bonds—particularly mother–child interactions (e.g., Azhari et al., 2022; Nguyen, Banki, et al., 2020). This research has shed light on how interpersonal neural synchrony reflects variations in caregiving behaviors and emotional state (Azhari et al., 2019). For instance, Endevelt-Shapira and Feldman (2023) demonstrated that distinct synchrony profiles differentiate caregiving styles in terms of sensitivity and intrusiveness.

1.7 Two Trajectories: Methods and Tasks

Since its introduction (Montague et al., 2002), hyperscanning has evolved from a methodological innovation into a valid framework for studying the neural basis of social interaction. Early studies focused on demonstrating the feasibility of recording neural activity from two individuals simultaneously. Using EEG, these pioneering works introduced the first analytical methods to quantify interpersonal neural synchrony, typically through well-controlled, task-oriented paradigms inspired by mirror-neuron and social coordination theories.

In 2010s, the field began to move toward more naturalistic investigations of real-life social interaction. This shift coincided with the growing

adoption of fNIRS. Compared to EEG and fMRI, fNIRS is more tolerant to motion artifacts and allows participants to move and interact more freely, making it particularly suited to studying dynamic social behaviors, especially in developmental populations (Carollo et al., 2022).

Technological advances thus supported a parallel conceptual transition—from simplified laboratory paradigms to richer, ecologically valid contexts. Research increasingly addressed the affective and communicative dimensions of social behavior, extending hyperscanning to domains such as verbal communication, social affect, and parent–child interaction.

Overall, two intertwined trajectories define the evolution of hyperscanning research: a methodological shift from EEG and fMRI to predominantly fNIRS, and a conceptual shift toward naturalistic paradigms. Accordingly, this thesis presents both methodological developments, focused on managing motion artifacts in naturalistic fNIRS studies (Chapter 2), and conceptual studies exploring factors that shape interpersonal neural synchrony during real-life social interactions (Chapters 3–4).

Chapter 2

Advancing fNIRS Pre-Processing Methods

The content of this chapter is based on two publications:

Bizzego, A., **Carollo, A.**, Senay, B., Fong, S., Furlanello, C., & Esposito, G. (2024). Computer Vision-Driven Movement Annotations to Advance fNIRS Pre-Processing Algorithms. *Sensors, 24*(21), 6821. https://doi.org/10.3390/s24216821.

Bizzego, A., **Carollo, A.**, Fong, S., Furlanello, C., & Esposito, G. (2025). Characterizing motion artifacts in functional near-infrared spectroscopy signals using ground-truth movement information and computer vision. *Biomedical Signal Processing and Control, 110*, 108256. https://doi.org/10.1016/j.bspc.2025.108256

In some parts, the text has been modified for consistency with the dissertation style and to avoid repetitions in the text.

As outlined in Chapter 1, the growing shift of hyperscanning research toward naturalistic paradigms has been facilitated by the adoption of fNIRS. This technique offers greater motion tolerance and experimental

flexibility than EEG and fMRI, making it particularly suitable for studying real-life social interactions. However, this ecological advantage comes with a major methodological challenge: the management of motion artifacts, which can still severely compromise signal quality and the validity of hyperscanning findings.

In recent years, several strategies have been proposed to detect and correct motion-related noise in fNIRS data. Yet, many of these methods have been developed using synthetic data or evaluated against theoretically expected brain signals, without access to ground-truth information on the actual movements performed during the task. Addressing these limitations is essential to ensure the robustness of fNIRS pre-processing pipelines and to guarantee that observed interpersonal neural synchrony reflects genuine neural coupling rather than motion-induced correlations.

This chapter presents a series of methodological contributions aimed at improving motion artifact management in naturalistic fNIRS hyperscanning. Specifically, it introduces a computer vision (CV)–based approach for movement annotation combined with fNIRS data collected from participants performing controlled, experimentally manipulated head movements. The following sections describe the validation of this approach in extracting reliable movement information from video recordings of experimental sessions, as well as the association between specific movement parameters and motion artifact patterns detected in the corresponding brain signals. Together, these methods lay the groundwork for CV-informed motion artifact identification and correction techniques, potentially advancing the reliability of fNIRS hyperscanning in ecologically valid contexts.

2.1 Functional Near-Infrared Spectroscopy

fNIRS is an optical neuroimaging method used to investigate brain activity by monitoring variations in cerebral blood oxygenation. The technique exploits the near-infrared optical window, transmitting light between sources and detectors through biological tissues to infer hemodynamic changes in the cerebral cortex (Jöbsis, 1977; Pinti et al., 2020).

As discussed in Chapter 1, the use of fNIRS in social neuroscience has increased markedly in recent years compared to traditional neuroimaging techniques, owing to its distinctive methodological advantages and to its greater movement tolerance (Carollo & Esposito, 2024; Carollo et al., 2022). Altogether, its characteristics make fNIRS particularly suitable for monitoring the brain activity during ecologically valid and participant-friendly experimental designs (Bizzego, Gabrieli, et al., 2022; Lim et al., 2024a).

Despite these strengths, fNIRS remains a relatively young technique and continues to face methodological challenges for reproducibility and cross-study comparability (Bizzego, Carollo, Lim, & Esposito, 2024; Yücel et al., 2025). In particular, residual motion artifacts can still compromise fNIRS signal quality and affect estimates of coherence among signals. For this reason, there is ongoing work to develop more reliable strategies for their detection and correction (Bizzego, Neoh, et al., 2022; Bizzego et al., 2020).

2.2 Managing Motion Artifacts: To Correct or Not?

Two main types of motion artifacts are commonly observed in fNIRS data: movement shifts and spikes. Movement shifts refer to slow, baseline drifts in the signal. In contrast, spikes are characterized by abrupt, transient signal fluctuations. These two types of artifacts are illustrated in Figure 2.1, which shows the raw signal (in orange) and its corrected version (in red). If not properly handled, motion artifacts can distort hemodynamic responses and lead to spurious or misleading results when estimating the correlation/coherence among signals (Fishburn et al., 2019).

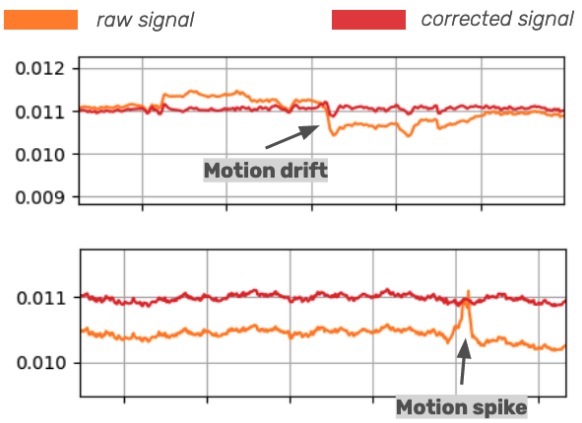

Figure 2.1: Motion artifacts (motion drifts and motion spikes) in functional near-infrared spectroscopy (fNIRS) signal pre- (in orange) and post-correction (in red). Image from Bizzego, Carollo, Senay, et al. (2024).

Hence, while fNIRS is less susceptible to motion than other neuroimaging techniques, properly handling motion artifacts is still critical to ensure the validity of the results (Perpetuini et al., 2021). This is particularly relevant in naturalistic paradigms, where participants' movements are often unavoidable.

So far, the fNIRS literature has not achieved a consensus on the optimal approach to use for managing motion artifacts. Two main strategies are commonly employed (Brigadoi et al., 2014). The first involves discarding the affected data, using only clean signals for the subsequent analyses. While this approach preserves the integrity of the original measurements, without altering the signal characteristics, it can be wasteful and sometimes unfeasible, especially in experiments that inherently involve participant movement (Virtanen et al., 2011). The second strategy consists of correcting the contaminated signals. This allows researchers to retain more data, which is particularly valuable given the challenges of collecting fNIRS signals. However, the success of this approach depends heavily on the reliability and accuracy of the methods used to identify and correct motion artifacts.

2.3 Managing Motion Artifacts: How to Correct?

Several methods have been developed to detect and correct motion artifacts in fNIRS data (e.g., Fishburn et al., 2019; Izzetoglu et al., 2005, 2010; Molavi and Dumont, 2012; Scholkmann et al., 2010; Yücel et al., 2014). Among these, a combination of spline interpolation and wavelet filtering is currently regarded as the gold standard correction approach (Brigadoi et al., 2014). This is because spline interpolation is particularly effective in correcting slow baseline drifts (motion shifts), whereas wavelet filtering is better suited for removing spikes.

Despite their widespread adoption, these algorithms rely on theoretical assumptions about expected hemodynamic responses rather than on

actual movement data. Because manually annotating motion events in fNIRS experiments is highly labor-intensive, most correction methods have been developed and evaluated without access to ground-truth information about the type, timing, or intensity of actual movements. As a result, their performance is typically assessed using simulated data rather than real motion-annotated datasets (e.g., Gao et al., 2022; M. Kim et al., 2022).

This lack of ground-truth information poses a critical limitation: it prevents researchers from determining whether correction algorithms are effectively targeting motion-related artifacts or inadvertently removing genuine neural signals. The availability of objective movement data would therefore be essential for accurately validating motion artifact identification and correction algorithms and for enabling robust comparisons across different pre-processing pipelines.

2.4 Obtaining a Ground-Truth for Movement Information

Three main approaches have been employed to obtain ground-truth information that supports robust motion artifact identification and correction in fNIRS research.

The first approach involves manual annotation of movement instances, either directly within the recorded signal or from video recordings of the experimental sessions. Although this method provides precise labeling of movement events, it is both time-consuming and labor-intensive, making it impractical for large datasets or extended experiments (Virtanen et al., 2011).

The second approach relies on the use of motion sensors, such as accelerometers, to capture head or body movements. For instance, Virtanen et al. (2011) used accelerometer data to track participants' head movements and proposed a method for motion artifact detection and correction in fNIRS signals. Several other algorithms have since been developed using accelerometer data, including adaptive filtering, active noise cancellation (C.-K. Kim et al., 2011), accelerometer-based motion artifact removal (Virtanen et al., 2011), acceleration-based reduction algorithms (Metz et al., 2015), multi-stage cascaded adaptive filtering (Islam et al., 2017), and blind source separation–based approaches (von Lühmann et al., 2019). However, not all fNIRS devices include motion sensors, and processing accelerometer data requires additional analytical steps that may complicate pre-processing pipelines unless supported by artificial intelligence (AI)–based automation.

The third approach leverages AI and CV to automatically detect and annotate movements from video recordings of experimental sessions. This method aims to identify head movements automatically, offering a more efficient, replicable, and cost-effective alternative to manual annotation. Unlike sensor-based approaches, CV-based solutions do not require additional hardware beyond standard video equipment, which is often readily available in most research settings.

2.5 Characterizing Motion Artifacts

A lack of ground-truth movement information also undermines the understanding of the specific relationship between distinct movement characteristics and the resulting artifacts in the recorded signals. To address

this gap, several studies have attempted to explore the association between movement and signal distortion. However, these investigations are often constrained by the absence of controlled movement conditions and by the limited availability of reliable annotations.

In this context, CV approaches based on AI offer a promising solution for providing objective ground-truth movement data usable to better understand how motion affects neuroimaging signals (e.g., Hu et al. 2020; Mazzonetto et al. 2022). For instance, Qian et al. (2022) demonstrated the feasibility of real-time EEG artifact annotation using CV to detect blinks and head movements, reinforcing the potential of automated approaches for the identification of motion-related artifacts in brain signals.

In parallel, another line of research has focused on a theoretical characterization of motion artifacts. These studies aim to model the statistical properties of artifacts and develop robust statistical frameworks capable of estimating brain responses even in the presence of noise (Aarabi & Huppert, 2016; Barker et al., 2013; Huppert, 2016; Santosa et al., 2017). The main advantage of this approach is that it reduces the need for extensive pre-processing, as it typically requires only the conversion of raw optical data into oxy- and deoxyhemoglobin concentration changes. The resulting statistical models are designed to be inherently resilient to motion artifacts and other noise sources.

2.6 Scope of the Project

Given the methodological challenges posed by the absence of ground-truth movement information, this Chapter presents two experimental studies aimed at developing a valid and reliable framework for obtaining

objective movement annotations during fNIRS experiments and assessing their relationship with noise patterns in fNIRS data.

Building on advances in electrocardiogram (ECG) signal processing (Duraj et al., 2022; Moskalenko et al., 2020), we framed head-movement detection as a semantic segmentation problem, training a 1D-UNet model to identify movement instances from head orientation signals extracted with a pre-trained SynergyNet model (C.-Y. Wu et al., 2021). This framework aims to automate head-movement annotation, potentially providing an efficient, scalable, and low-cost method for generating ground-truth movement data in naturalistic neuroimaging experiments.

Subsequently, we investigated how distinct head-movement patterns affect fNIRS signal quality, identifying the ways in which different types of movement compromise data integrity. These insights can support the development of improved motion artifact detection and correction algorithms, enhancing the reliability fNIRS data, especially in naturalistic scenarios.

Accordingly, the remainder of this Chapter is organized into two complementary studies:

1. **Study 1 – Validation of the CV-based movement detection framework:** This study focuses on developing and validating the proposed CV–based approach for obtaining objective annotations of head movements during fNIRS experiments. Using SynergyNet-derived head orientation signals and a 1D-UNet segmentation model, we aim to generate accurate and reliable ground-truth information about movement events, providing an efficient and scalable alternative to manual labeling.

2. **Study 2 – Impact of head movement on fNIRS signal quality:** Building on the ground-truth movement data from Study 1, this study examines the relationship between head movement patterns and motion artifacts in fNIRS signals. The goal is to characterize how different movement types and magnitudes affect data quality and to inform the design of more robust motion artifact detection and correction methods.

2.7 Study 1 – Validation of the CV-Based Movement Detection Framework

2.7.1 Methods

Study Design

Data collection procedures for the project were approved by the Ethics Committee of the University of Trento (protocol number 2023-054) and conducted in accordance with the Declaration of Helsinki. Informed consent was obtained from all participants before their inclusion in the study.

Participants took part in an experiment in which they were instructed to reproduce a series of experimentally controlled movements displayed in a video on a monitor. During each session, brain activity was recorded using fNIRS, and a webcam simultaneously captured the participants' behavior. For the purposes of this first study, only the webcam recordings were analyzed, while the fNIRS data were not used. Movement information was subsequently extracted from the videos using two approaches: *i)* a CV–based method and *ii)* manual annotations.

Participants

Fifteen participants (8 females; $M = 22.27$ years, $SD = 2.62$) were recruited through convenience and snowball sampling, using social media advertisements and the University of Trento's participant management and recruitment system. Eligibility criteria included being at least 18 years old and having no reported or diagnosed neurological or health-related conditions.

The chosen sample size is consistent with previous methodological studies investigating motion artifacts in fNIRS data (e.g., Aarabi and Huppert, 2016; Barker et al., 2013; Lanka et al., 2022; Santosa et al., 2020).

Experimental Procedure

The experimental procedure is illustrated in Figure 2.2. Participants were instructed to reproduce a series of head movements shown in a video displayed on a monitor. Each experimental video began with a short instructional phase, during which participants were prompted to "Please, imitate the movements represented in the video". Following this, an avatar demonstrated the target movement accompanied by a descriptive caption at the bottom of the screen (e.g., "Move your head backward slowly"). A three-second countdown was then presented, after which participants had seven seconds to execute the instructed movement.

In the experimental video, the avatar performed two main categories of movements: *(i)* head movements and *(ii)* facial expressions. For the purpose of the present study, only head movements were analyzed. These movements consisted of head rotations along the three principal axes: vertical, frontal, and sagittal. For clarity, the following descriptive terms

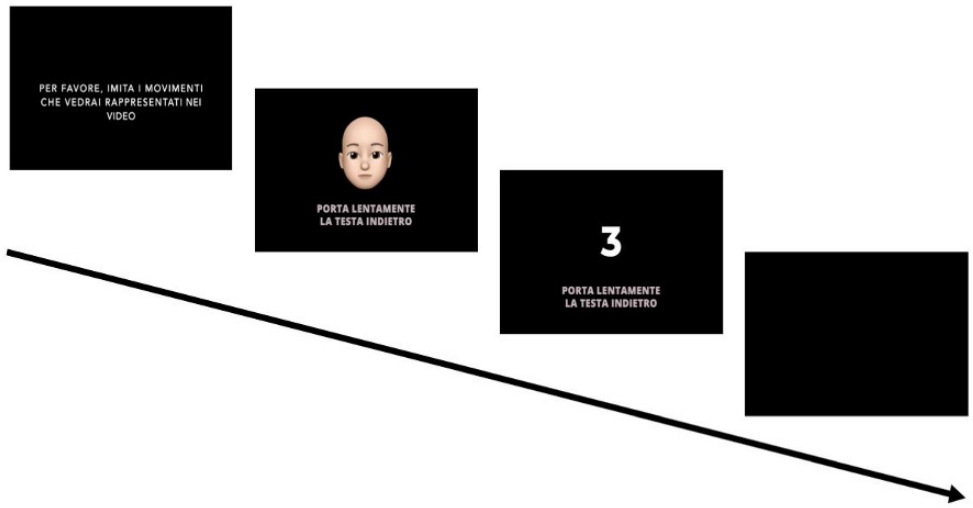

Figure 2.2: Experimental paradigm. Participants were instructed to reproduce head movements displayed in a series of video stimuli. Each video began with a prompt inviting participants to imitate the upcoming movements. An avatar then demonstrated the action while a descriptive text appeared below the video. This was followed by a three-second countdown, after which participants had seven seconds to perform the instructed head movement. Image from Bizzego, Carollo, Senay, et al. (2024).

are used instead of the anatomical labels: "Left/Right" axis for the vertical (yaw) rotations, "Up/Down" axis for the frontal (pitch) rotations, and "bendLeft/bendRight" axis for the sagittal (roll) rotations.

Four rotation types were included: half rotation (both directions, i.e., left and right), full rotation, and repeated rotation (three consecutive movements). Participants were instructed to complete each movement by returning their head to a neutral, forward-facing position. Movements along the Left/Right and Up/Down axes were executed at two speeds—slow and fast. In total, the experimental design comprised 20 distinct head movements: 16 derived from the combination of 4 rotation types, 2 speeds, and 2 axes ($4 \times 2 \times 2 = 16$), plus 4 additional slow movements for the bendLeft/bendRight axis.

The sequence of movements was identical for all participants and

was repeated three times, resulting in a total of 60 head movements per experimental session.

During task performance, three data streams were collected simultaneously: brain activity using an fNIRS system (NIRSport2, NIRx; 10.2 Hz), physiological signals (AIM Physiological Monitor, CGX; 500 Hz), and video recordings of the participants (C310 Webcam, Logitech; 30 Hz). Synchronization across all devices was achieved through the Lab Streaming Layer framework. Physiological data were recorded but not analyzed in both studies. Neural data were recorded but used only in Study 2. Stimulus presentation was managed with *PsychoPy*, and all on-screen instructions were provided in Italian.

fNIRS Data Acquisition

Participants' brain activity was recorded using fNIRS. Each fNIRS cap included 16 LED light sources emitting near-infrared light at 760 nm and 850 nm, paired with 16 light detectors. One detector was specifically used to capture data from eight short-separation channels. The optodes were positioned according to the standard international 10–20 EEG system, ensuring broad cortical coverage (see Figure 2.3). This setup produced a total of 32 fNIRS channels.

To maintain optimal data quality, optode holders were employed to keep the source–detector distance consistent (not exceeding 3 cm) and to improve the signal-to-noise ratio (Strangman et al., 2013). Before the recording, each participant's head circumference was measured to select the most suitable cap size. Data acquisition was carried out using a NIRSport2 system (NIRx Medical Technologies LLC) at a sampling frequency of 10.17 Hz.

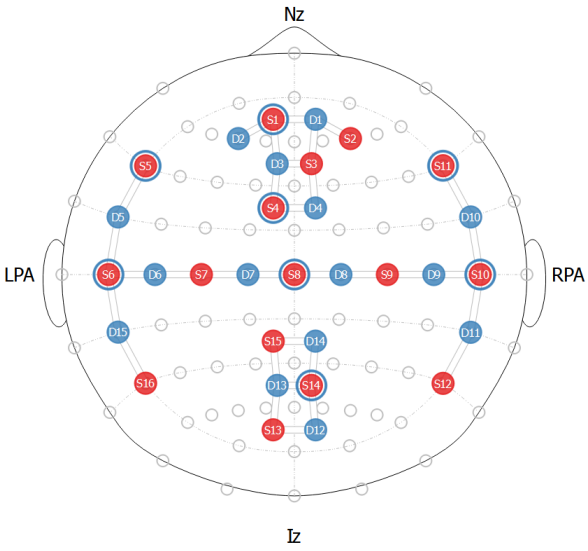

Figure 2.3: Illustration of the functional near-infrared spectroscopy (fNIRS) cap configuration used in the experiment. Red markers represent the light sources, and blue markers indicate the detectors. Blue circles around the sources denote the short-separation channels. Image from Bizzego, Carollo, Senay, et al. (2024).

Deep Learning Approach

Two deep learning architectures were employed in this work in order to extract movement information from videos: SynergyNet (C.-Y. Wu et al., 2021) and a one-dimensional UNet model (1D-UNet).

SynergyNet

SynergyNet is a pre-trained deep learning model designed to estimate head position (three axes) and head orientation (three axes) from video frames (C.-Y. Wu et al., 2021). The network integrates 3D Morphable Models (3DMM) with 3D facial landmarks through a synergistic learning process to predict facial geometry in three dimensions. It comprises two main modules: (1) a multi-attribute feature aggregation mechanism that refines landmark detection using MobileNet-V2 as its backbone (Sandler et al., 2018), and (2) a mapping stage that converts 3D landmarks into

3DMM parameters, enabling the regression of facial geometry from sparse landmark inputs. Detailed information about the model's architecture and implementation can be found in the original publication (C.-Y. Wu et al., 2021) and its corresponding GitHub repository[1].

In this study, the pre-trained SynergyNet model was applied to individual frames from each participant's webcam recording to extract head orientation data along three axes: γ_x, γ_y, and γ_z. The orientation values from all video frames were concatenated to generate continuous head orientation signals, which were then resampled to 10 Hz. Manual annotations of movement onsets and offsets were subsequently performed based on these signals.

UNet

Building on prior work demonstrating the effectiveness of UNet convolutional neural network architectures for one-dimensional semantic segmentation of ECG signals (e.g., Moskalenko et al., 2020), we trained a 1D-UNet to perform semantic segmentation on head orientation signals to detect motion events. UNet models, originally developed for image segmentation, are well-suited for capturing both local and global features due to their characteristic U-shaped architecture (Ronneberger et al., 2015). This structure comprises two main components: a contracting path that extracts features and an expansive path that enables precise localization of the target signal. Skip connections transfer information from earlier layers to later ones, improving segmentation accuracy. UNets are particularly effective even with limited labeled data, which makes them suitable for applications in domains with scarce annotations, such

[1] https://github.com/choyingw/SynergyNet

as biomedical imaging and other areas (Moskalenko et al., 2020; Ronneberger et al., 2015).

The 1D-UNet in this study was trained using movement onset annotations extracted from video recordings of 10 randomly selected participants, while data from the remaining 5 participants were reserved for testing. Following standard machine learning practice (e.g., Carollo, Bizzego, et al., 2021), this train-test split allowed estimating the model's generalizability by assessing its performance on previously unseen data.

The 1D-UNet model used in this study was implemented in PyTorch (Paszke et al., 2019) and largely followed the architecture proposed by Moskalenko et al. (2020), ensuring the effective feature extraction and segmentation capabilities reported in previous work.

Model Evaluation

Movement instances were manually annotated from the head orientation signals by two independent raters. In the task, we did not calculate an inter-rater reliability measure because this was a segmentation problem rather than a classification or rating task. These annotations were subsequently validated against the video recordings and served as ground-truth for evaluating the performance of the 1D-UNet model.

The model's performance was quantified using the Jaccard index, a common metric for assessing semantic segmentation accuracy (Ogwok & Ehlers, 2022). The Jaccard index is defined in Equation 2.1, where $A \cap B$ denotes the intersection of sets A and B, and $A \cup B$ denotes their union:

$$J(A, B) = \frac{|A \cap B|}{|A \cup B|} \tag{2.1}$$

Here, J measures the overlap between the ground-truth movement annotations (A) and the model's predicted movements (B). A value of 1 indicates perfect agreement, representing the best achievable performance when predictions fully match the ground-truth (Ogwok & Ehlers, 2022). To provide a more robust estimate of model performance, bootstrap confidence intervals (2.5%–97.5%) were computed using the *scikits-bootstrap* Python package.

2.7.2 Results

Figure 2.4 illustrates the overall performance of the 1D-UNet model across various experimental factors as compared to manual annotations.

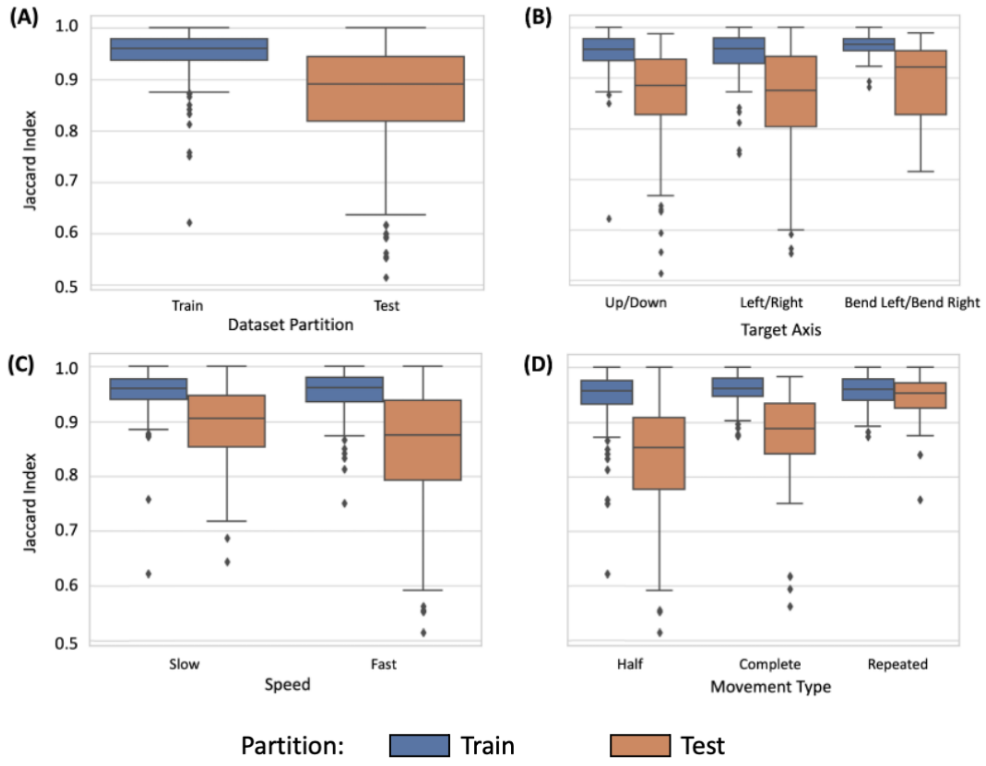

Figure 2.4: Accuracy of the 1-dimensional U-Net (1D-UNet) model across (A) dataset partition (training vs. test set), (B) head movement axis, (C) movement speed, and (D) movement type. Image from Bizzego, Carollo, Senay, et al. (2024).

Firstly, the 1D-Unet showed good and comparable performance across the train ($J = 0.954$ [0.949, 0.958]) and test set partitions ($J = 0.865$ [0.847, 0.878]; Figure 2.4A), suggesting that the model's accuracy is generalizable to new, unseen data.

Additionally, similar performance for train and test sets was observed across target movement axes (Figure 2.4B; Up/Down: Train $J = 0.951$ [0.943, 0.957], Test $J = 0.862$ [0.836, 0.883], Left/Right: Train $J = 0.952$ [0.945, 0.958], Test $J = 0.854$ [0.826, 0.878], BendLeft/BendRight: Train $J = 0.965$ [0.960, 0.970], Test $J = 0.893$ [0.868, 0.916]) and movement speeds (Figure 2.4C; Slow: Train $J = 0.953$ [0.944, 0.959], Test $J = 0.892$ [0.874, 0.908], Fast: Train $J = 0.955$ [0.949, 0.959], Test $J = 0.847$ [0.826, 0.868]).

Results suggest an influence of movement type (half, complete, repeated, Figure2.4D) on the model's performance. In particular, better performance was observed for repeated movements (Train $J = 0.956$ [0.950, 0.962], Test $J = 0.941$ [0.925, 0.953]), followed by complete (Train $J = 0.960$ [0.953, 0.965], Test $J = 0.872$ [0.839, 0.894]), and finally half movements (Train $J = 0.950$ [0.942, 0.956], Test $J = 0.826$ [0.805, 0.848]).

Overall, the CV model provided accurate information on ground-truth movements, comparable to the manual annotations. Model performance was stable across movement axes and speeds; however, we observed an effect of movement type, with greater similarity between manual and CV-based annotations during repeated movements.

2.7.3 Discussion

Although fNIRS is generally more tolerant to movement than other neuroimaging modalities, motion artifacts in fNIRS signals remain a signifi-

cant challenge. This issue is compounded by the fact that most motion artifact correction methods are developed and evaluated without access to ground-truth movement information. To fill this gap, in the present experiment, fifteen participants were instructed to perform controlled head movements—such as turning quickly or slowly to the left or to the right—while being recorded via webcam. The findings indicate that segmentation models, including the 1D-UNet, can accurately annotate movements from head orientation signals extracted from videos using the pre-trained SynergyNet (C.-Y. Wu et al., 2021). Compared to manual annotations, the 1D-UNet showed strong performance across multiple dimensions of movement detection, including dataset partitions (training vs. test sets), movement axes (up/down, left/right, bend left/bend right), and movement speeds (slow vs. fast). The model exhibited some variability in annotating different movement types (e.g., half, full, or repeated rotations), suggesting that repeated movements yielded the most accurate annotations, possibly due to their stronger and more consistent disruptive effect on brain signals.

While the current model approach proved useful in annotating head movements in controlled conditions, future studies could explore fine-tuning or re-training the model on naturalistic head movements, in which participants move their heads across multiple rotational axes. It is also important to note that head orientation signals obtained via SynergyNet are comparable to those measured with accelerometers, suggesting that the 1D-UNet could be applied to a variety of movement data sources. Expanding the model to more ecological conditions would enhance its generalizability beyond controlled laboratory settings.

Additionally, movement information could be used to better under-

stand the occurrence of motion artifacts in fNIRS signals. Incorporating such information into pre-processing pipelines may improve the robustness of fNIRS data analysis by minimizing the loss of genuine brain activity while effectively detecting and removing motion artifacts.

The ground-truth movement data obtained here provide the foundation for the subsequent analysis of the impact of head movements on fNIRS signal quality, as presented in Study 2.

2.8 Study 2 – Impact of Head Movement on fNIRS Signal Quality

2.8.1 Methods

Study Design

For the second part of the project, we combined CV techniques with neuroimaging data to examine how controlled head movements influence fNIRS signals. As outlined in Section 2.7.1, fifteen participants completed an experimental session in which they performed predefined head movements. These movements were captured on video via a webcam, while fNIRS recorded their brain activity concurrently. Using computer vision, the video data were annotated to extract movement information, and quantitative metrics of movement magnitude and speed were calculated (Figure 2.5A). Motion artifact patterns were quantitatively assessed by analyzing changes in signal baseline and spike amplitudes in the segments of fNIRS data corresponding to the movements. By using this information, the study explored the relationship between different movement types, their characteristics, and the resulting motion artifacts in

the neural recordings.

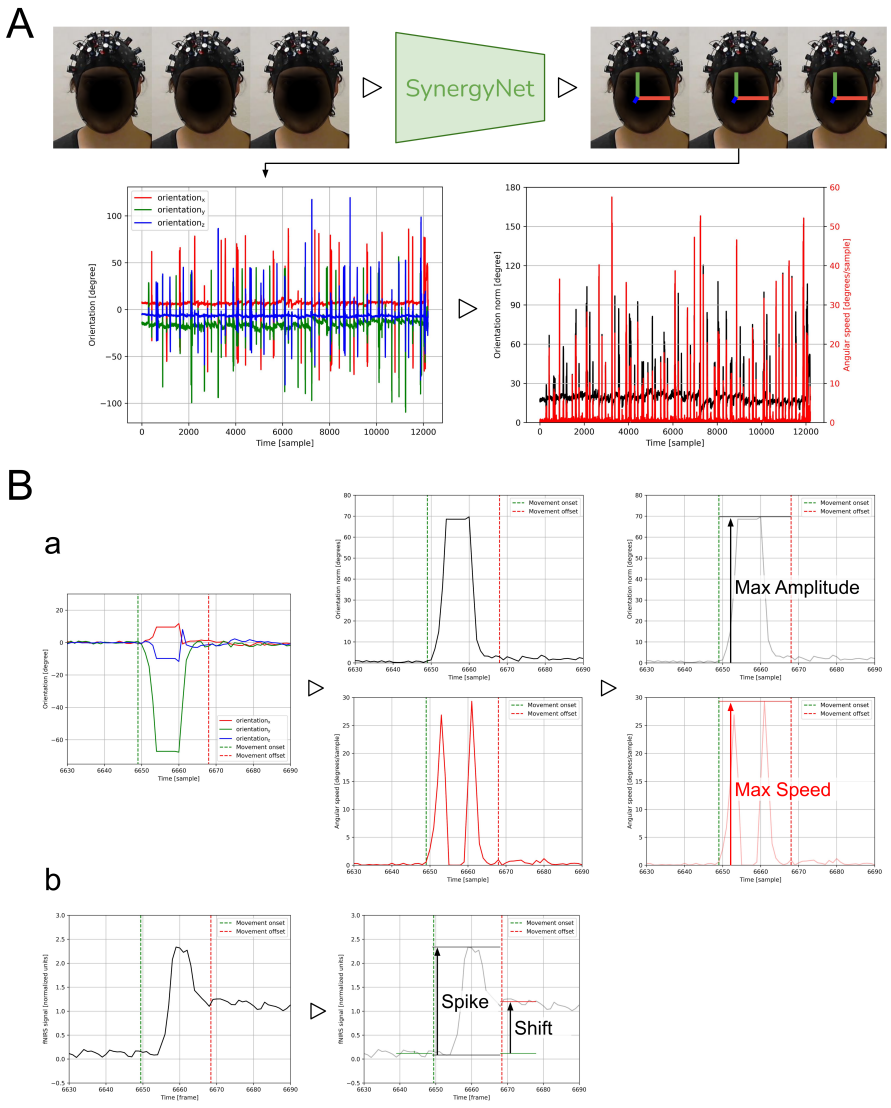

Figure 2.5: Summary of the signal processing procedures and the extracted metrics. **A)** Extraction of movement signals from video recordings. Each frame was analyzed using the SynergyNet model to obtain the three components of head orientation: γ_x (red), γ_y (green), and γ_z (blue). These values were then concatenated across all frames to create continuous orientation signals, from which the orientation vector magnitude and angular velocity (calculated as the norm of the gradient) were derived. **B)** Calculation of metrics to describe movement characteristics based on the orientation and angular velocity signals **(a)** and the motion artifacts observed in the fNIRS recordings **(b)**. Image from Bizzego et al. (2025).

fNIRS Data Pre-Processing

After collecting the fNIRS data (Section 2.7.1), the raw signals were converted into relative concentrations of oxygenated and deoxygenated hemoglobin using the modified Beer-Lambert Law (Baker et al., 2014) and resampled at 10 Hz. The 32 channels were then organized into seven regions of interest (ROIs): Left, Right, Pre-frontal, Frontal, Top, Pre-occipital, and Occipital (Figure 2.6). For each ROI, a representative brain activity signal was generated by averaging the channels within that region. All signal processing steps were performed using the *pyphysio* library (Bizzego, Battisti, et al., 2019).

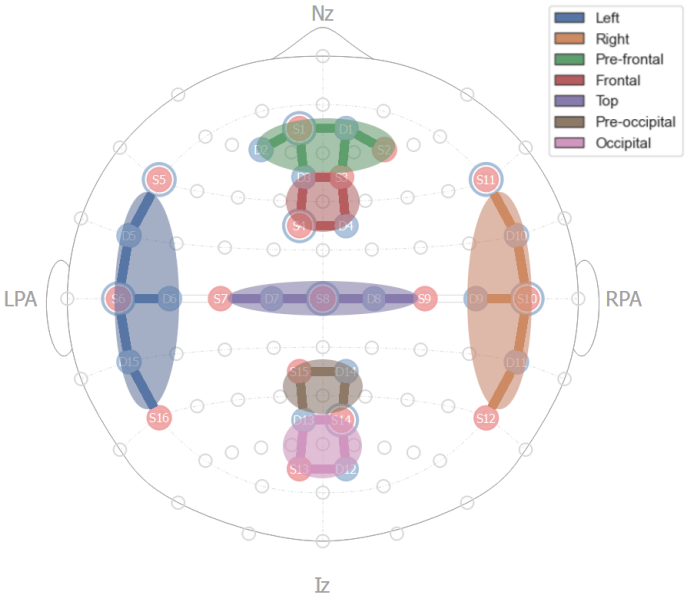

Figure 2.6: Distribution of the optodes in the functional near-infrared spectroscopy (fNIRS) cap into regions of interest. Image from Bizzego et al. (2025).

Movement and Motion Artifact Metrics

The aim of this study was to investigate how different head movements affect the quality of fNIRS data. To achieve this, two sets of quantitative

metrics were calculated (Figure 2.5B): movement metrics, which describe the characteristics of the head movements, and motion artifact metrics, which capture the impact of these movements on the fNIRS signals.

The movement metrics included the maximum speed (Max Speed) and maximum amplitude (Max Amplitude) of head rotations, both derived from the norm of the head orientation vector at each video frame:

$$\|\boldsymbol{\gamma}(n)\| = \sqrt{\gamma_x(n)^2 + \gamma_y(n)^2 + \gamma_z(n)^2}; \tag{2.2}$$

where n is the sample, and $\gamma_x(n), \gamma_y(n), \gamma_z(n)$ are the three components of the orientation vector that are computed frame-by-frame by SynergyNet.

Specifically, the Max Speed was computed as the maximal value of the norm of the orientation vector:

$$\max_{n_{on} \leq n \leq n_{off}} \left\| \frac{\partial \gamma(n)}{\partial n} \right\|. \tag{2.3}$$

The Max Amplitude was computed as the maximal value of the norm between the onset (n_{on}) and offset (n_{off}) of the movement:

$$\max_{n_{on} \leq n \leq n_{off}} \|\gamma(n))\|. \tag{2.4}$$

The motion artifacts metrics focused on two different types of motion artifacts: spikes and baseline shifts. The Spike metric was computed as the range of the fNIRS signal, considering the portion between the onset and offset of the movement:

$$\max_{n_{on} \leq n \leq n_{off}} s(n) - \min_{n_{on} \leq n \leq n_{off}} s(n); \tag{2.5}$$

where $s(n)$ is the fNIRS signal.

The Shift metric was computed as the difference in the average fNIRS signal value between the 1-second portion before the movement onset and the 1-second portion after the movement offset:

$$\mu_{n_{on-1} \leq n \leq n_{on}} - \mu_{n_{off} \leq n \leq n_{off+1}}; \tag{2.6}$$

where $\mu_{n_i \leq n \leq n_j}$ is the average of the fNIRS signal between samples n_i and n_j.

To enable comparison of motion artifact metrics across regions, which can vary in baseline levels and signal ranges, the metrics were normalized using the 5-second interval preceding each movement onset. Specifically, the Spike metric was scaled by the standard deviation of the signal within this interval, while the Shift metric was divided by the mean of the absolute signal values during the same period.

For all metrics, the values were averaged across the three repetitions of each movement.

Data Analysis

The data analysis aimed to examine how different types of head movements influence motion artifacts by comparing the movement and motion artifact metrics. The analysis proceeded as follows:

(a) Validation of head orientation and movement metrics derived from video recordings;

(b) Examination of motion artifact characteristics across different movement types;

(c) Assessment of the relationship between movement metrics and motion artifact metrics.

The study focused on providing both descriptive and statistical insights into the relationship between head movements and motion artifacts. In particular, we addressed the following research questions:

1. Which types of head movements are most likely to induce motion artifacts?

2. Are motion artifacts more prominent in specific brain regions? If so, which regions are most affected, and which movements have the greatest impact?

3. How does the magnitude of motion artifacts vary with the speed or amplitude of the movement?

4. Can experimental guidelines be derived to minimize the occurrence of motion artifacts?

Linear mixed-effects models were applied to account for both fixed and random effects (Brown, 2021). Random effects—such as participant ID or movement axis—were included to capture variability related to individual participants and specific movement contexts.

The dataset and analysis scripts are publicly available at https://gitlab.com/a.bizzego/computer-vision-fnirs.

2.8.2 Results

Movement Specificity

As the first step of our analysis, two linear mixed-effects models were fitted using the movement metrics—Max Speed and Max Amplitude—as

dependent variables. Fixed effects in both models included the target axis (target vs. non-target), movement speed (slow vs. fast), and movement type (half vs. complete vs. repeated). Participant ID and movement axis were included as random effects to account for individual and axis-specific variability.

Overall, the results indicate that the movement metrics derived from the SynergyNet model closely aligned with the ground-truth movement instructions. Movements predominantly occurred along the main rotational axis specified in the experimental design. Significantly higher Max Speed was observed along the target axis — the axis along which the movement was intended — compared to the other two axes (β = 8.25, Standard Error (SE) = 0.49, $t(653.99) = 16.72$, $p < .001$; Figure 2.7A). Similarly, Max Amplitude was significantly greater on the target axis compared to the other axes (β = 36.51, SE = 0.94, $t(654.00) = 38.94$, $p < .001$; Figure 2.7B).

Moreover, participants executed movements at two distinct speeds as instructed. Figure 2.7C shows that increased speed along the target axis occurred only in accordance with the experimental instructions. Specifically, Max Speed on the target axis was significantly lower when participants were instructed to move slowly, compared to when they were instructed to move fast (β = -4.39, SE = 0.52, $t(655.74) = -8.46$, $p < .001$). However, instructing participants to perform movements at both fast and slow speeds had no effect on the amplitude of their movements on the target axis (β = -1.81, SE = 0.99, $t(655.97) = -1.83$, $p = .067$; Figure 2.7D).

The type of movement (half, complete, or repeated) also influenced movement speed (Figure 2.7E). Specifically, Max Speed was significantly

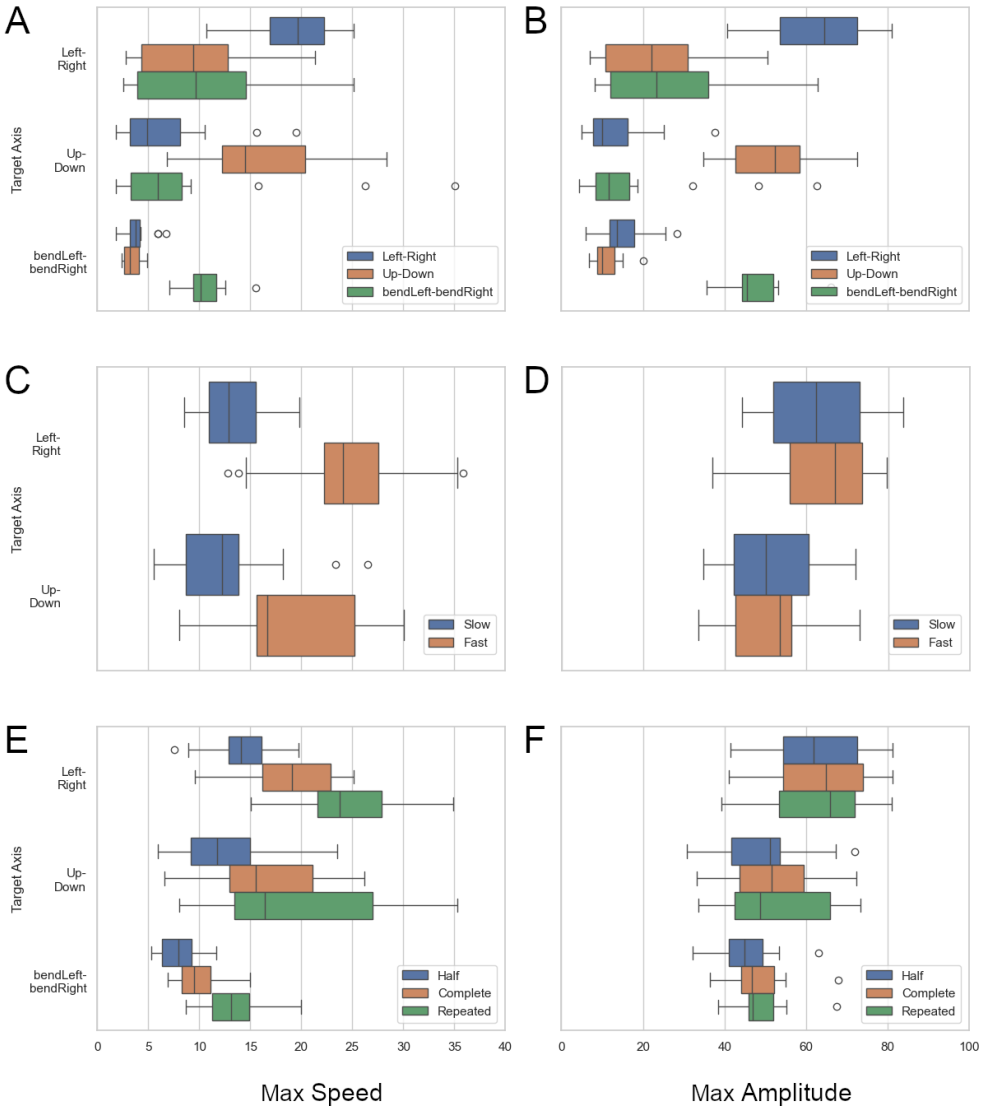

Figure 2.7: Validation of movement metrics extracted from video recordings using the SynergyNet deep neural network model (Bizzego, Carollo, Senay, et al., 2024; C.-Y. Wu et al., 2021). The x-axis shows the values of Max Speed and Max Amplitude, while the y-axis indicates the movement axes along which participants were instructed to move their heads. **A)** Max Speed across the three movement axes. **B)** Max Amplitude across the three movement axes. **C)** Max Speed along the target axis for fast versus slow movements. **D)** Max Amplitude along the target axis for fast versus slow movements. **E)** Max Speed along the target axis by movement type (half, complete, repeated). **F)** Max Amplitude along the target axis by movement type (half, complete, repeated). Image from Bizzego et al. (2025).

lower during half movements compared to complete movements (β = -1.96, SE = 0.57, $t(653.99)$ = -3.45, $p < .001$). Conversely, Max Speed was significantly higher during repeated movements compared to complete movements (β = 2.14, SE = 0.57, $t(653.99)$ = 3.76, $p < .001$). Therefore, faster movements were observed when participants performed repeated movements, followed by complete movements, and then half movements. The type of movement also influenced movement amplitude (Figure 2.7F), although the effects were less pronounced than those observed for speed. Specifically, Max Amplitude was significantly lower during half movements compared to complete movements (β = -3.07, SE = 1.08, $t(654.00)$ = -2.83, $p = .005$). No significant difference in Max Amplitude was observed between repeated and complete movements (β = 1.47, SE = 1.08, $t(654.00)$ = 1.36, $p = .174$). Therefore, reduced movement amplitude was primarily associated with half movements, while repeated and complete movements showed comparable amplitude values.

Finally, we observed a positive association between movement amplitude and speed along the target axis across movement speeds (Figure 2.8). To assess the overall relationship between Max Speed and Max Amplitude, we performed a linear mixed model with Max Amplitude as the dependent variable, and Max Speed, target speed, and their interaction as fixed effects. Participant ID, movement axis, and movement type were included as random effects. The analysis revealed a statistically significant positive relationship between Max Amplitude and Max Speed (β = 1.03, SE = 0.10, $t(186.66)$ = 9.84, $p < .001$). Although no significant main effect of target speed on Max Amplitude was found, a significant interaction emerged: the relationship between Max Speed and Max Amplitude was more strongly positive during slow movements

compared to fast movements ($\beta = 0.39$, SE $= 0.14$, $t(207.67) = 2.79$, $p = .006$).

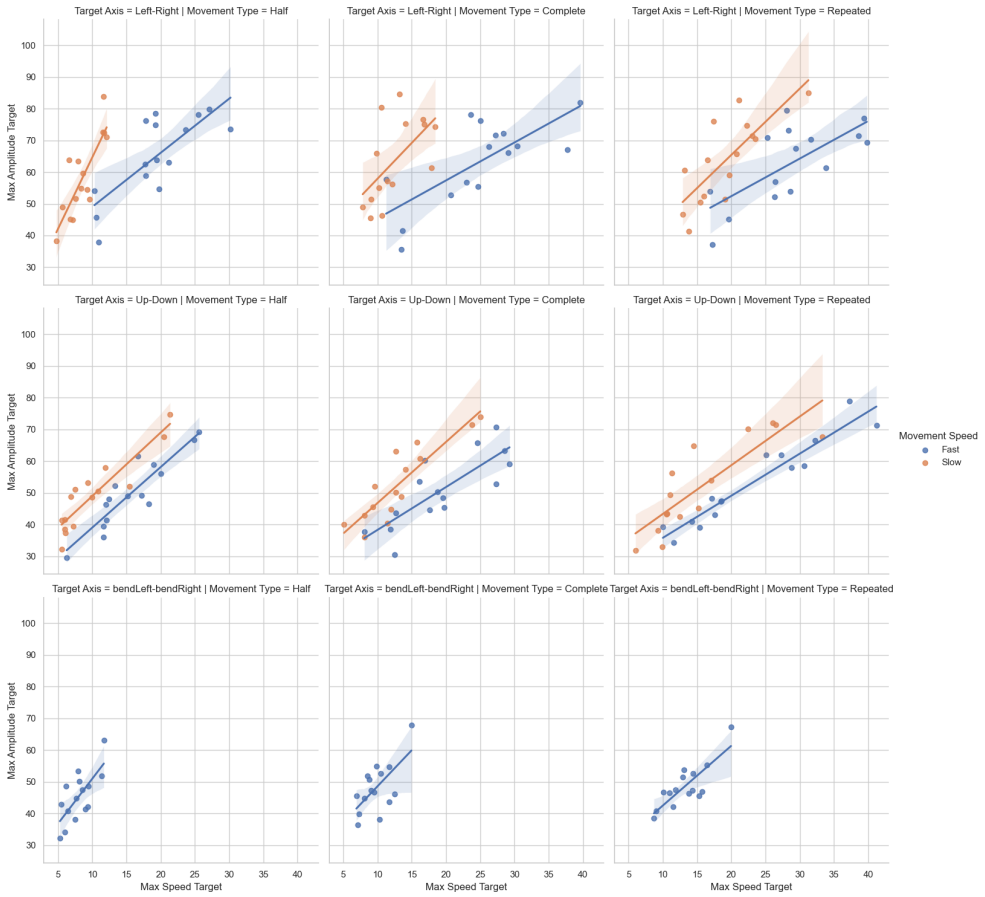

Figure 2.8: Relationship between Max Amplitude and Max Speed of movements on the target axis across all movements performed in the experiment. Image from Bizzego et al. (2025).

Overall, the movement patterns derived from the SynergyNet model align closely with the controlled head movements participants were instructed to perform, indicating that movement metrics obtained from CV-annotated head movements are potentially useful to characterize motion artifact patterns in fNIRS data.

Shifts and Spikes in fNIRS Signals

To investigate the distribution and properties of motion artifacts patterns

across movements, we implemented two linear mixed models with motion artifacts metrics (i.e., Shift and Spike) as the dependent variables. Both models included the rotational axis (i.e., Left/Right *vs.* Up/Down *vs.* bendLeft/bendRight), speed (i.e., slow *vs.* fast), and movement type (i.e., half *vs.* complete *vs.* repeated) as fixed effects. Participant ID and region of interest were included as random effects. Overall, significantly higher Shift values were observed during Up-Down movements compared to movements along the other two rotational axes ($\beta = 0.09$, SE = 0.01, $t(1549.00) = 6.21$, $p < .001$; Figure 2.9A). Similarly, Spike values were significantly higher during Up-Down movements compared to the other axes ($\beta = 1.02$, SE = 0.07, $t(1549.00) = 14.17$, $p < .001$; Figure 2.9B).

Moreover, no statistically significant differences in Shift or Spike values were observed across different movement speeds. In particular, slow movements did not generate a significantly different amount of Shift (β = -0.01, SE = 0.01, $t(1549.00)$ = -0.68, $p = .498$; Figure 2.9C) or Spike (β = -0.08, SE = 0.07, $t(1549.00)$ = -1.17, $p = .244$; Figure 2.9D) compared to fast movements.

Generally, the type of movement (i.e., half, complete, or repeated) had a slight impact on Shift and Spike values detected in the signals. Specifically, repeated movements generated significantly higher Shift values as compared to other movement type ($\beta = 0.04$, SE = 0.02, $t(1549.00) = 2.23$, $p = .026$; Figure 2.9E), while half movements produced significantly lower Spike values (β = -0.34, SE = 0.08, $t(1549.00)$ = -4.24, $p < .001$; Figure 2.9F).

In summary, movements along the Up/Down axis appear to have the greatest impact in terms of shifts and spikes, especially for repeated movements. Interestingly, movement speed does not seem to influence

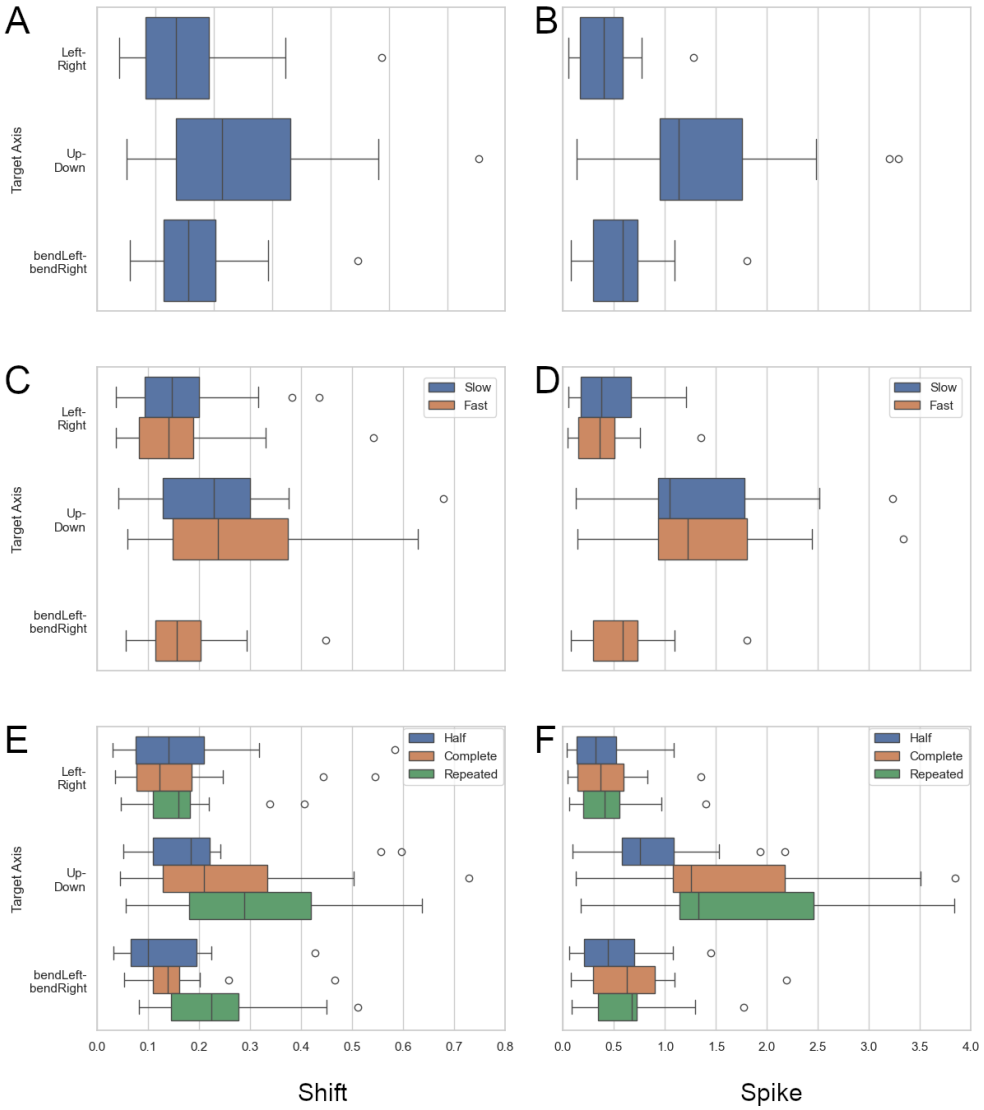

Figure 2.9: Motion artifact metrics (i.e., Shift and Spike values) across movements. **A)** Shift values after movements on the three main rotational axes. **B)** Spike values after movements on the three main rotational axes. **C)** Shift values after movements on the target axis across fast and slow movements. **D)** Spike values after movements on the target axis across fast and slow movements. **E)** Shift values after movements on the target axis across types of movement (i.e., half, complete, repeated). **F)** Spike values after movements on the target axis across types of movement (i.e., half, complete, repeated). Image from Bizzego et al. (2025).

the motion artifacts metrics.

To examine how head movements relate to motion artifacts across different regions of interest, we conducted eight linear mixed-effects models.

Two models were specified with either Shift or Spike as the dependent variable and region of interest as the sole fixed effect, while movement axis, participant ID, target speed, and movement type were included as random effects. The remaining six models focused on individual regions of interest: three models (one per movement axis) used Shift as the dependent variable, and the other three used Spike. In all six models, region of interest was treated as a fixed effect, and participant ID, target speed, and movement type were included as random effects.

Overall, the results indicated that, across movement axes, significantly higher Shift values were observed in the right ($\beta = 0.05$, SE = 0.02, $t(1550.00) = 2.28$, $p = .023$), top ($\beta = 0.05$, SE = 0.02, $t(1550.00) = 2.07$, $p = .039$), pre-occipital ($\beta = 0.37$, SE = 0.02, $t(1550.00) = 15.22$, $p < .001$), and occipital brain regions ($\beta = 0.20$, SE = 0.02, $t(1550.00) = 8.22$, $p < .001$). Similarly, significantly higher Spike values were found in the top ($\beta = 0.61$, SE = 0.12, $t(1548.91) = 5.04$, $p < .001$), pre-occipital ($\beta = 2.04$, SE = 0.12, $t(1548.91) = 16.91$, $p < .001$), and occipital regions ($\beta = 1.39$, SE = 0.12, $t(1548.91) = 11.51$, $p < .001$).

The models conducted on individual regions of interest revealed distinct patterns of motion artifacts depending on the movement performed. Specifically, the pre-occipital and occipital brain regions showed significantly higher Shift values compared to other regions during Left/Right (pre-occipital: $\beta = 0.24$, SE = 0.04, $t(292.00) = 5.87$, $p < .001$; occipital: $\beta = 0.15$, SE = 0.04, $t(292.00) = 3.65$, $p < .001$), Up/Down (pre-occipital: $\beta = 0.50$, SE = 0.04, $t(606.00) = 11.86$, $p < .001$; occipital: $\beta = 0.31$, SE = 0.04, $t(606.00) = 7.32$, $p < .001$), and bendLeft/bendRight movements (pre-occipital: $\beta = 0.24$, SE = 0.04, $t(292.00) = 5.87$, $p < .001$; occipital: $\beta = 0.15$, SE = 0.04, $t(292.00) = 3.65$, $p < .001$). Signif-

icantly higher Shift values were observed in brain regions at the top of the brain during Up/Down movements ($\beta = 0.09$, SE = 0.04, $t(606.00) = 2.16$, $p = .032$).

With regard to Spike values, the right ($\beta = 0.20$, SE = 0.09, $t(606.00) = 2.38$, $p = .018$), pre-occipital ($\beta = 0.89$, SE = 0.09, $t(606.00) = 10.41$, $p < .001$), and occipital brain regions ($\beta = 0.36$, SE = 0.09, $t(606.00) = 4.23$, $p < .001$) were the most significantly affected regions of interest during Left/Right movements. Similarly, top ($\beta = 1.17$, SE = 0.24, $t(606.00) = 4.98$, $p < .001$), pre-occipital ($\beta = 3.73$, SE = 0.24, $t(606.00) = 15.84$, $p < .001$), and occipital brain regions ($\beta = 2.81$, SE = 0.24, $t(606.00) = 11.95$, $p < .001$) were the most significantly affected regions of interest during Up/Down movements. Finally, during bendLeft/bendRight movements, we observed significantly higher Spike values in left ($\beta = 0.38$, SE = 0.14, $t(292.00) = 2.75$, $p = .006$), right ($\beta = 0.51$, SE = 0.14, $t(292.00) = 3.70$, $p < .001$), top ($\beta = 0.39$, SE = 0.14, $t(292.00) = 2.80$, $p = .006$), pre-occipital ($\beta = 0.99$, SE = 0.14, $t(292.00) = 7.12$, $p < .001$), and occipital ($\beta = 0.61$, SE = 0.14, $t(292.00) = 4.40$, $p < .001$) brain regions of interest.

Overall, channels situated in the occipital and pre-occipital regions of the cap exhibited greater sensitivity to motion artifacts, both in terms of Shift and Spike values, particularly during Up/Down movements (Figure 2.10A and Figure 2.10B). Additionally, after bendLeft/bendRight and Left/Right movements, we noted a difference in Shift and Spike values between the left and right regions of interest (Figure 2.10A and Figure 2.10B).

These results indicate that motion artifacts are primarily driven by alterations in the fit and contact of the fNIRS cap with the participant's

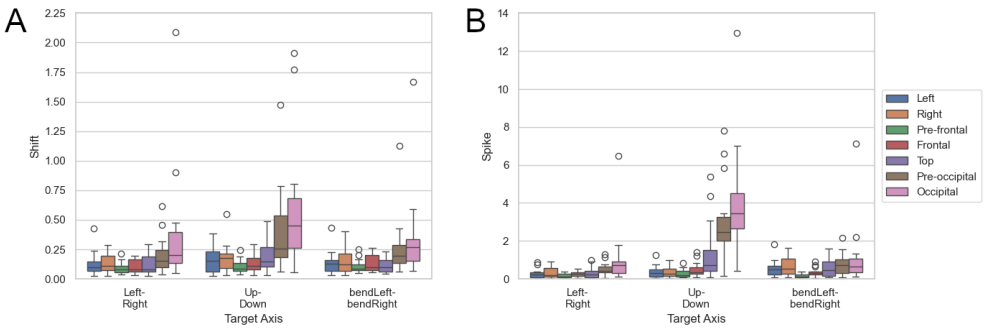

Figure 2.10: Metrics of motion artifacts (i.e., Shift and Spike) across movement conditions and regions of interest. **A)** Distribution of Shift values across regions of interest as a function of the target movement axis. **B)** Distribution of Spike values across regions of interest as a function of the target movement axis. Image from Bizzego et al. (2025).

scalp, rather than by the head movement itself. Specifically, during Up-/Down movements, the occipital and pre-occipital areas of the cap are most affected, as they are compressed between the head and the neck. Likewise, during bendLeft/bendRight movements, the lateral regions of the cap experience greater tension. These aspects are further elaborated in the Discussion section.

Finally, we estimated the relationship between motion artifacts metrics using a linear mixed model. In the model, Spike values were used as the dependent variable while Shift values, target speed, and their interaction were used as fixed effects. In the model, participant ID, movement axis, movement type, and region of interest were included as random effects. Overall, a statistically significant positive correlation between shifts and spikes across movements was observed in the experiment (β = 2.99, SE = 0.13, $t(1547.41) = 23.92$, $p < .001$; Figure 2.11). Conversely, no significant main effect of speed (β = 0.02, SE = 0.07, $t(1546.51)$ = 0.22, $p = .828$) and no interaction effect (β = -0.33, SE = 0.18, $t(1549.58)$ = -1.85, $p = .064$) were observed.

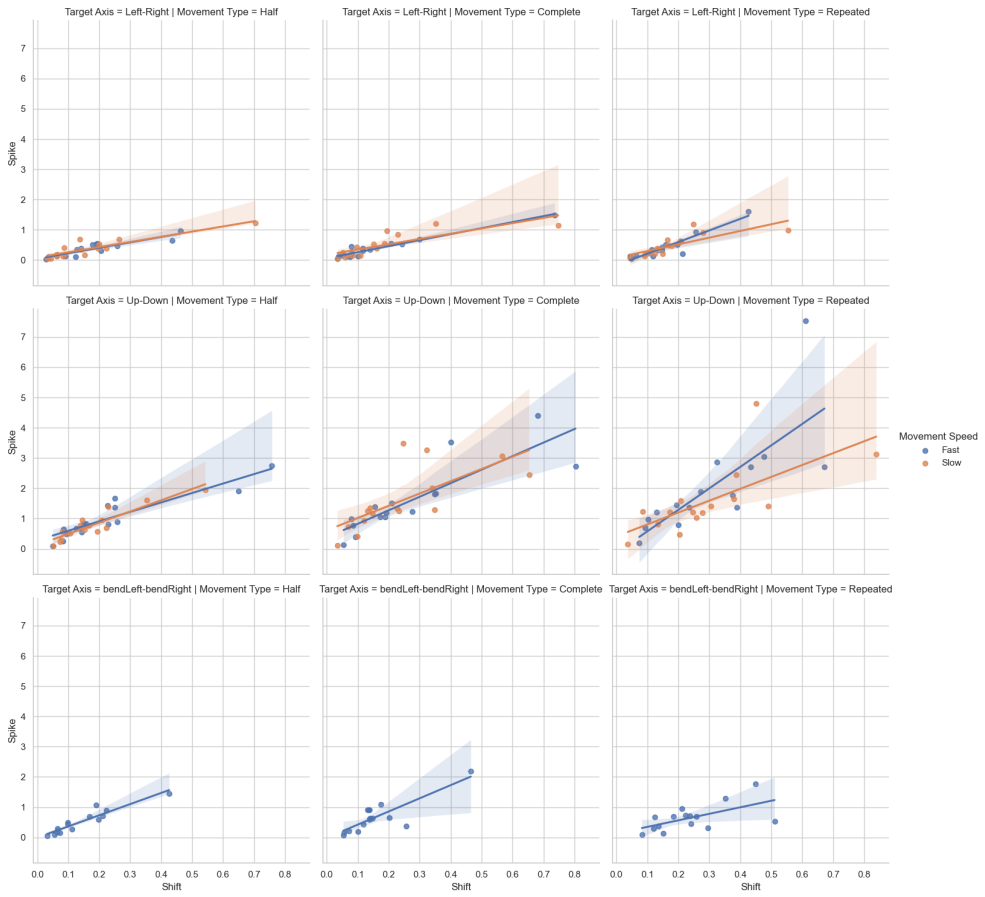

Figure 2.11: Relationship between motion artifact metrics (Shift and Spike values) across all movements performed in the experiment. Image from Bizzego et al. (2025).

Movements and Motion Artifacts

The analysis examining the relationship between movement and motion artifact metrics across different movements did not reveal any consistent pattern. Specifically, four linear mixed models were employed to assess the association between movement characteristics (i.e., Max Speed and Max Amplitude) and motion artifact measures (i.e., Shift and Spike). In each model, one of the two motion artifact metrics served as the dependent variable, while one of the movement metrics was included as a fixed effect. Target speed, participant ID, movement axis, movement

type, and region of interest were incorporated as random effects.

No statistically significant effect was observed between Max Speed and Shift values (β = 0.001, SE = 0.001, $t(483.80)$ = 0.681, p = .497; Figure 2.12). Conversely, we observed a statistically significant negative relationship between Max Speed and Spike values (β = -0.015, SE = 0.007, $t(117.63)$ = -2.099, p = .038; Figure 2.13).

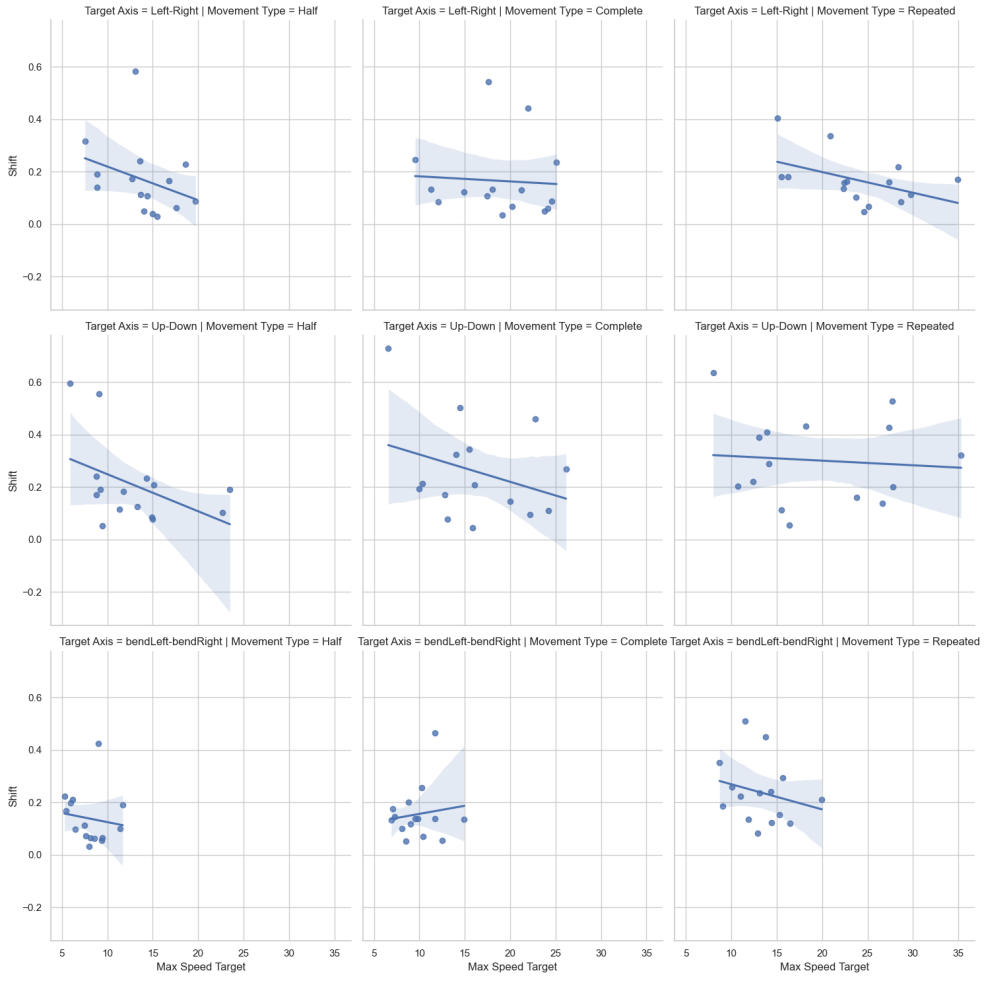

Figure 2.12: Relationship between Max Speed of movements on the target axis and Shift values across all movements performed in the experiment. Image from Bizzego et al. (2025).

Concerning the maximum amplitude of movements and motion artifacts metrics, no statistically significant pattern emerged. In particular,

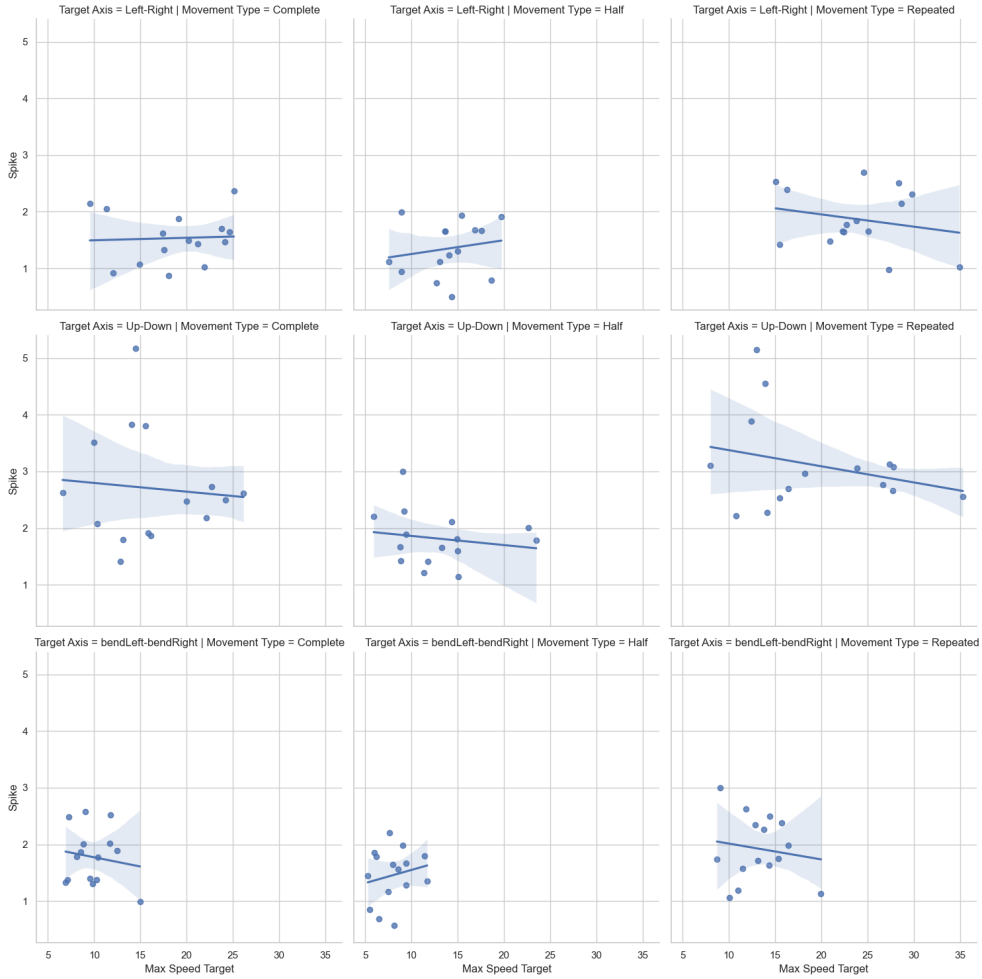

Figure 2.13: Relationship between Max Speed of movements on the target axis and Spike values across all movements performed in the experiment. Image from Bizzego et al. (2025).

the relationship between Max Amplitude and Shift values was not statistically significant across movements ($\beta = 0.001$, SE = 0.001, $t(911.30) = 1.545$, $p = .123$). Moreover, there is no discernible trend regarding the relation between Max Amplitude of movements and Spike values ($\beta =$ -0.002, SE = 0.004, $t(1224.00) =$ -0.471, $p = .638$; Figure 2.15).

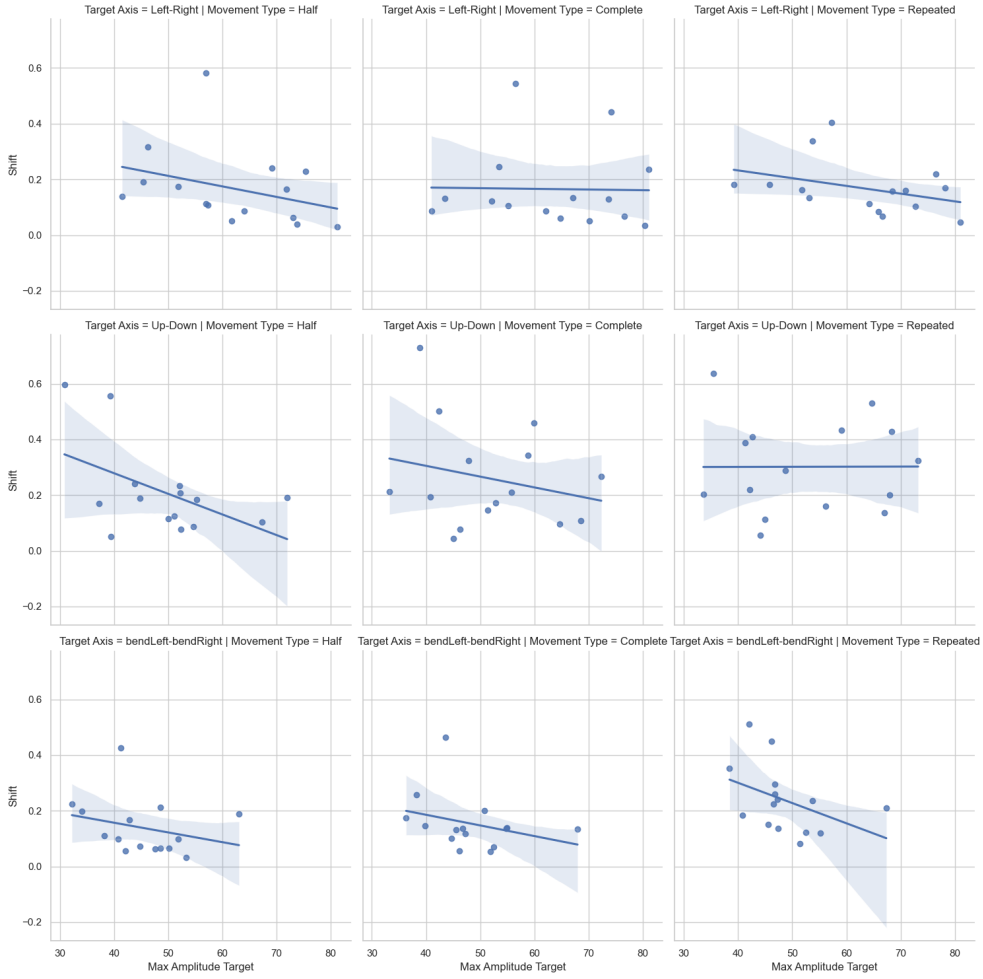

Figure 2.14: Relationship between Max Amplitude of movements on the target axis and Shift values across all movements performed in the experiment. Image from Bizzego et al. (2025).

2.8.3 Discussion

A major limitation in assessing the effectiveness of existing motion artifact identification and correction methods is the absence of reliable ground-truth movement information. In this study, we addressed this issue by integrating ground-truth movement data obtained with previously validated CV techniques (Bizzego, Carollo, Senay, et al., 2024) to examine their association with motion artifacts in fNIRS signals.

Our findings revealed a strong correlation between the movement met-

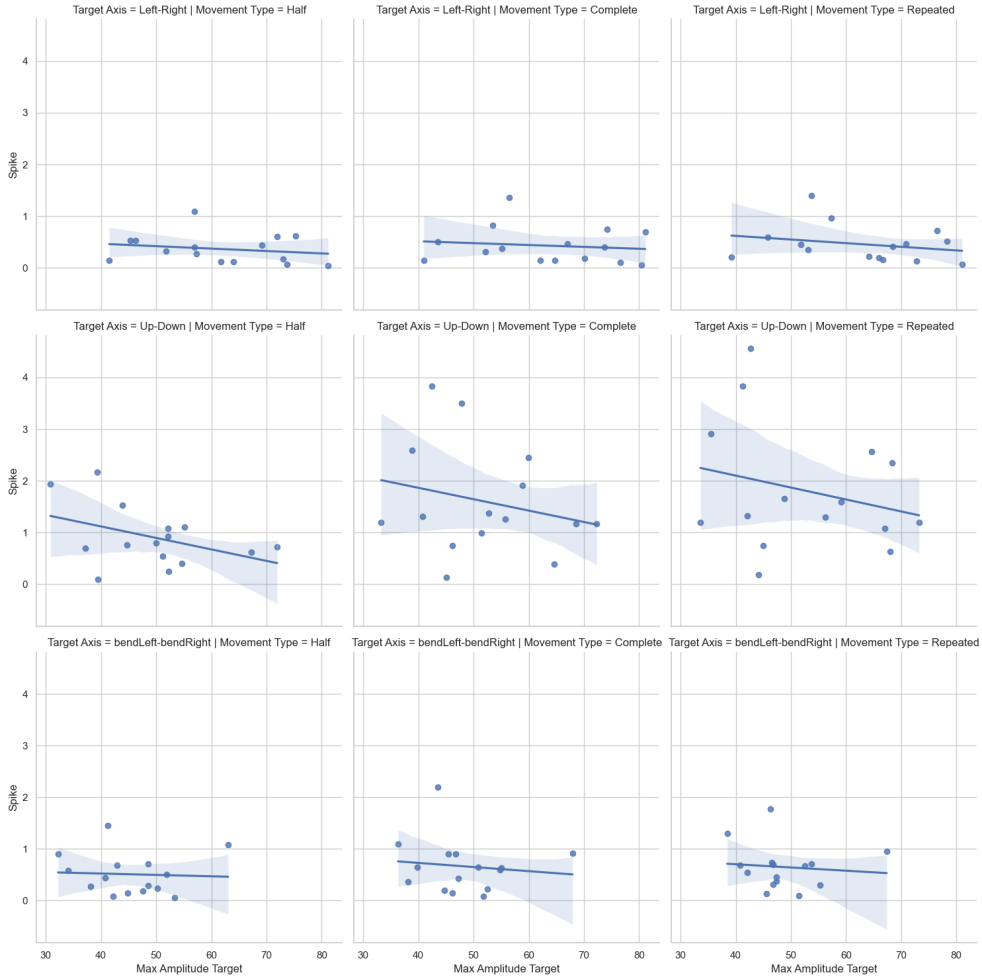

Figure 2.15: Relationship between Max Amplitude of movements on the target axis and Spike values across all movements performed in the experiment. Image from Bizzego et al. (2025).

rics (i.e., Max Speed and Max Amplitude) obtained through CV and the ground-truth movement information defined by the experimental instructions. This outcome validates the accuracy of AI-derived metrics in capturing the intended experimental movements. Additionally, unlike previous approaches that primarily examined the statistical characteristics of motion artifacts (e.g., Aarabi and Huppert 2016; Barker et al. 2013; Huppert 2016; Santosa et al. 2017), the present study established a direct link between the occurrence of motion artifacts and

specific, measurable head movement patterns. By integrating CV with neuroimaging data, we identified clear associations between motion artifacts—quantified through Shift and Spike metrics—and distinct head movement types. In particular, complete and repeated Up/Down movements produced higher Shift and Spike values, especially in the occipital and pre-occipital regions. Similarly, Left/Right movements primarily influenced the corresponding lateral regions, with movement amplitude and speed showing a relationship to the magnitude of the Shift metric. These findings suggest that motion artifacts are largely driven by changes in the stability and contact of the fNIRS cap with the scalp, rather than by the motion itself (Noponen et al., 2010; Virtanen et al., 2011). This result emphasizes the importance of maintaining a proper cap fit to ensure high-quality fNIRS recordings. During Up/Down movements, for example, the occipital section of the cap tends to be compressed between the head and neck, while during Left/Right movements, the inertia of the hair can cause slippage, loosening the cap's adherence. Such displacements can distort signal readings and compromise data accuracy. Therefore, we recommend that researchers thoroughly check and adjust the cap's fit prior to and throughout each experimental session. This precaution can substantially reduce artifacts caused by cap movement, ultimately enhancing the reliability of fNIRS measurements. Several other strategies may enhance optode–scalp contact stability. These include the use of adjustable chin straps or additional fixation bands to reduce vertical displacement, particularly in occipital regions susceptible to compression during Up/Down movements. Cap designs incorporating structured or spring-loaded optode holders may further maintain consistent pressure across measurement sites. Standardized hair management protocols, in-

cluding systematic hair separation prior to optode placement, may mitigate lateral slippage observed during Left/Right movements. Finally, integrating real-time monitoring procedures could allow early detection of cap displacement and facilitate timely intervention. Collectively, these approaches may substantially reduce motion-related artifacts and improve the robustness of fNIRS recordings.

Moreover, this study provides important insights into how different types of head movements influence fNIRS signal quality and which cortical areas are most susceptible to motion-induced artifacts. Such evidence can guide the development of future experimental protocols by helping researchers identify and limit specific movement patterns that compromise data integrity. For example, when investigating occipital or pre-occipital regions, reducing Up/Down head movements may be particularly beneficial, whereas minimizing Left/Right rotations is advisable in studies targeting temporal areas. To support this, subtle procedural or visual cues can be incorporated into the experimental design to encourage participants to keep a stable head posture, thereby mitigating unwanted motion. Implementing these measures can ultimately enhance experimental rigor and improve the overall quality of fNIRS recordings.

2.9 Limitations

For both studies, the relatively small sample size, despite being in line with previous works (e.g., Lanka et al., 2022; Santosa et al., 2020), represents a limitation that may restrict the generalizability of the findings both for the reliability of the CV approach and for the association between movement metrics and motion artifact patterns in fNIRS data.

Nevertheless, the CV–based approach employed here is inherently scalable and can be easily extended to larger datasets, as it relies solely on video recordings of participants' movements. Future research could build upon this framework by applying it to studies with larger and more diverse samples, as well as to experimental contexts featuring more naturalistic or less constrained movements, thereby broadening the understanding of how motion artifacts arise under varied conditions.

2.10 Conclusion

In these studies, we introduced an AI-based framework to automatically annotate head movements during controlled fNIRS sessions and to examine how specific motion characteristics affect signal quality. Using CV models, we successfully extracted real-time head orientation and movement data from video recordings, offering a valid, low-cost, and scalable alternative to manual annotation or external sensors.

When assessing the relationship between movement and artifact metrics, our results indicate that repeated and Up/Down head rotations substantially degrade fNIRS signals, largely independent of movement speed. Occipital and pre-occipital regions were particularly sensitive to these movements, whereas temporal regions were mainly affected by lateral bends and rotations. These effects appear to result primarily from changes in cap–scalp contact rather than the movements themselves, underscoring the importance of maintaining stable and well-fitted caps to minimize artifacts (Noponen et al., 2010; Virtanen et al., 2011).

By combining CV and neuroimaging data, this work lays the groundwork for AI-driven methods to identify and correct motion artifacts, ul-

timately enhancing data quality, reproducibility, and cross-study comparability in fNIRS research—especially in naturalistic settings (Bizzego, Carollo, Lim, & Esposito, 2024).

While the present chapter focused on methodological challenges related to movement and signal quality in fNIRS data, the following chapter shifts attention to the neural mechanisms underlying real-life social interactions. Specifically, it introduces two complementary studies, based on the same dataset, that examine how the structural and emotional characteristics of dialogues relate to distinct patterns of interpersonal neural synchrony and functional connectivity.

Chapter 3

Imaging Naturalistic Social Interactions During Active Verbal Exchanges

The content of this chapter is based on one publication and one preprint currently under review:

Carollo, A., Stella, M., Lim, M., Bizzego, A., & Esposito, G. (2025). Emotional content and semantic structure of dialogues are associated with interpersonal neural synchrony in the prefrontal cortex. *NeuroImage, 309*, 121087. https://doi.org/10.1016/j.neuroimage.2025.121087.

Carollo, A., Bizzego, A., Lim, M., Stella, M., Doderovic, G., & Esposito, G. (2025). Emotional and Linguistic Features Predict Prefrontal Functional Connectivity during Ongoing Dialogues: An fNIRS Investigation. *bioRxiv*, 2025-08. https://doi.org/10.1101/2025.08.04.668428.

In some parts, the text has been modified for consistency with the dissertation style and to avoid repetitions in the text.

Alongside methodological efforts aimed at standardizing and improv-

ing pre-processing pipelines for fNIRS data, there has been a growing interest in leveraging hyperscanning approaches to investigate the neural mechanisms underlying naturalistic social interactions. Hyperscanning offers a unique opportunity to examine both interpersonal and intra-personal neural dynamics as they unfold in real time.

Building on these conceptual frameworks, the present chapter presents two complementary studies conducted on the same dataset. The first study focuses on how structural and emotional patterns in dialogic exchanges—core components of naturalistic social interactions—relate to interpersonal neural synchrony between interacting individuals. The second study explores how these same interactions are associated with functional connectivity patterns within each participant's brain, shedding light on the intra-personal neural mechanisms supporting social communication in active social interactions.

3.1 Dialogues' Emotional and Linguistic Properties and Interpersonal Neural Synchrony

Human development and well-being are profoundly shaped by social interactions. From early childhood, people participate in social exchanges that transmit cognitive, emotional, and social skills (Ferjan Ramírez et al., 2020; Saint-Georges et al., 2013). Since birth, individuals are biologically predisposed to engage in these exchanges, supported by innate mechanisms that allow them to attend to and respond effectively to social stimuli in their environment (Johnson et al., 1991). The importance of

social interactions extends well into adulthood, where the quality of interpersonal relationships is a significant predictor of mental health outcomes and even mortality risk (Bolis et al., 2023; Holt-Lunstad et al., 2010).

Given the central role of social interactions in human life, a substantial body of research has examined the features of effective and adaptive exchanges (Bojczyk et al., 2016). A key concept emerging from this work is *bio-behavioral synchrony*, defined as the dynamic alignment of behavioral and physiological signals between interacting partners (Atzil & Gendron, 2017; Feldman, 2007, 2012a). Traditionally, studies on synchrony have focused on behaviors, hormonal levels, and physiological responses, showing that attunement can occur across multiple domains during social exchanges (Feldman, 2017).

More recently, hyperscanning approaches have extended this framework to the neural level, enabling the simultaneous recording of brain activity from two or more individuals (Carollo, Lim, et al., 2021; Montague et al., 2002). Leveraging the methodological advantages of fNIRS, recent studies have examined interpersonal neural synchrony during increasingly naturalistic social interactions, highlighting its potential as a neural marker of relationship quality and social attunement (Carollo & Esposito, 2024; Lim et al., 2024a; Morgan et al., 2023; Nguyen, Schleihauf, Kayhan, et al., 2020; Nguyen et al., 2024). Yet, the affective dimension—central to everyday social interactions—remains relatively underexplored in relation to interpersonal neural synchrony (Balconi & Vanutelli, 2017; Cornejo et al., 2017; Czeszumski et al., 2020). Emotions play a crucial role in social interactions, influencing social cohesion and individuals' propensity to engage in prosocial behavior (Lopes et al., 2005; Twenge et al., 2007).

Some pioneering studies have investigated how emotional states relate to social coordination and interpersonal neural synchrony. These studies often relied on the circumplex model of affect (Russell, 1980), which represents emotions along two axes: valence (pleasantness *vs.* unpleasantness) and arousal (activation *vs.* inhibition). For instance, Azhari et al. (2019), Nummenmaa et al. (2012), and Santamaria et al. (2020) reported that passive and active social interactions with stronger emotional valence tend to produce higher levels of neural synchrony between interacting individuals. In other words, emotionally intense experiences—whether positive or negative—appear to enhance synchrony in brain activity of interacting individuals. However, findings regarding the direction of this effect are mixed: some studies observed stronger synchrony for negatively-valenced stimuli (Nummenmaa et al., 2012), whereas others found the same effect for positively-valenced content (Santamaria et al., 2020; Zhu et al., 2018). According to a recent theoretical account by Hoehl et al. (2021), emotional stimulation plays a central role in enhancing neural synchrony. Emotions may promote synchrony by modulating time perception and increasing the alignment of internal rhythms with external events. In particular, positive emotions might facilitate the anticipation and representation of others' thoughts, feelings, and behaviors during interactions. Importantly, the findings on the association between emotional characteristics of the interaction and interpersonal neural synchrony primarily relied on self-reported emotional states or emotions induced by external stimuli.

Language serves as a fundamental medium through which emotions are conveyed in social interaction (Aitchison, 2012). As one of the major outcomes of human evolution, it enables individuals to communi-

cate intentions that encompass both cognitive and affective information, whether spoken or written. Speech, in particular, represents a highly complex system (Chan & Vitevitch, 2010; Vitevitch et al., 2024) that allows for the combination of words into structured expressions, capable of transmitting not only ideas and concepts but also emotional states (Stella, 2022). The communicative impact of speech extends beyond the literal meaning of words (Tausczik & Pennebaker, 2010); it also depends on the relationships between them—syntactic, semantic, and associative—which shape how meaning and emotion are constructed and understood (Ferrer-i-Cancho et al., 2022; Stella, 2022; Stella et al., 2019). The effectiveness of a conversation therefore varies according to how conceptual relations and emotional content are organized throughout dialogue. Interactions, for instance, may be broad and fragmented—covering many topics superficially—or narrow and cohesive, exploring a single theme in depth (Polkinghorne, 2005; Vitevitch et al., 2024). Drawing on Plutchik's theory of basic emotions (Plutchik, 1980), which conceptualizes complex affective states as combinations of eight core emotions, recent work in cognitive science (Castro et al., 2020; Ferrer-i-Cancho et al., 2022; Mohammad, 2016) and neuroscience (Atzil & Gendron, 2017; Ciampelli et al., 2023) has highlighted three key linguistic dimensions that may influence both social communication and interpersonal neural synchrony: *(i)* emotional content (e.g., linguistic segments evoking feelings such as anger or trust); *(ii)* syntactic and semantic structure, reflecting how ideas and concepts are organized within the mental lexicon (Stella et al., 2024); and *(iii)* temporal dynamics, such as the rhythm and frequency of conversational turn-taking. Regarding the latter, previous studies have shown that the timing of speech exchanges—particularly

turn-taking frequency—correlates with neural synchrony in mother–child interactions, even in preverbal stages (Nguyen, Schleihauf, Kayhan, et al., 2021; Nguyen et al., 2023). In contrast, how emotional and structural aspects of language contribute to interpersonal neural alignment remains largely unexplored.

This work addressed a current gap in the literature by introducing a quantitative approach to examine how two key aspects of dialogue—emotional content and syntactic/semantic organization—relate to interpersonal neural synchrony during naturalistic social interactions. By doing so, our study integrated cutting-edge cognitive neuroscience findings (Lim et al., 2023, 2024a) with frameworks from affective computing and cognitive data science (Stella, 2022). Specifically, we employed the *Textual Forma Mentis Networks* (TFMNs) framework, which allows the representation of conceptual associations extracted from text using artificial intelligence and psychologically validated data (Semeraro et al., 2022; Stella et al., 2019). TFMNs enable the modeling of associated mindsets, capturing the ways in which concepts are connected for an individual.

We formulated the following hypotheses:

1. The emotional content conveyed in dialogues is associated with interpersonal neural synchrony, such that interactions with more intense emotional expression are expected to show higher neural alignment between participants.

2. The syntactic and semantic organization of concepts within dialogues is related to interpersonal neural synchrony, with more structured or coherent exchanges potentially fostering greater neural coupling.

To investigate the interaction between linguistic and neural dimensions, we analyzed data from our recent fNIRS hyperscanning study, which included three interaction conditions (natural conversation, role-play, and role reversal) (Lim et al., 2023, 2024a, 2024b). While prior research has already examined how these conditions influence interpersonal neural synchrony (Lim et al., 2024a, 2024b), the current study focused specifically on dialogue characteristics. Therefore, we did not formulate predictions regarding the experimental conditions nor test their effects on synchrony, instead leveraging the dataset for its rich and varied dialogue interactions.

3.1.1 Methods

Study Design

All data analyzed in the present work originated from a cross-cultural project investigating the neural substrates of role-play—a therapeutic approach designed to reduce psychopathological symptoms (Lim et al., 2023, 2024a, 2024b). fNIRS hyperscanning was employed while participants took part in three five-minute interactive conditions: spontaneous conversation, role-play, and role reversal. While the broader study encompassed samples from both Italy and Singapore, the present analysis is restricted to the Italian participants. This decision aimed to control for potential confounds associated with linguistic variability in the Singaporean cohort, where participants often alternated among several languages, including Singlish, a creole language not compatible with the computational models used for dialogue feature extraction. Inclusion of these data could have introduced unwanted noise, thereby compromis-

ing the reliability of dialogue-related measures and inflating the risk of spurious findings.

All conversational exchanges were audio-recorded and subsequently transcribed verbatim. To assess both the emotional dimension and the syntactic–semantic organization of the dialogues, we employed automated computational approaches—specifically, EmoAtlas for quantifying emotional valence and TFMNs for modeling conceptual as well as syntactic–semantic relations. These analyses yielded emotional z-scores and a set of network-based metrics, which were subsequently entered as predictors of interpersonal neural synchrony within subregions of the prefrontal cortex.

All data collection procedures were approved by the University of Trento (2022-059) and Nanyang Technological University (NTU-IRB-2021-03-013). Experiments were conducted in accordance with the Declaration of Helsinki, and all participants provided informed consent.

Participants

The present investigation was conducted exclusively on the Italian sample ($N = 84$; 42 dyads; age range: 18–35 years). Participants were recruited through a combination of convenience and snowball sampling strategies implemented via social media channels. Each dyad comprised two friends who shared an established peer relationship. None of the participants reported any diagnosed medical or neurological conditions, particularly those that could interfere with cerebral oxygenation. Additionally, no individual was under pharmacological treatment known to affect blood flow or arterial pressure.

Experimental Protocol

The experimental procedure consisted of four distinct phases, during which neural activity was recorded using fNIRS (Lim et al., 2023, 2024a, 2024b). The study began with a two-minute resting state to capture baseline neural activity. During this period, participants were instructed to sit quietly facing each other and minimize any limb movements (see Figure 3.1A for the experimental setup).

Subsequently, participants engaged in three five-minute interactive conditions: (1) natural conversation, (2) role-play, and (3) role reversal. During the natural conversation phase, dyads conversed freely, replicating the dynamics of an ordinary social exchange. In the role-play condition, each participant was instructed to embody the persona of another pair of mutual friends from their social network. The role reversal phase required participants to exchange perspectives, such that participant A assumed participant B's role and vice versa. To ensure a consistent conversational context across all conditions, participants were provided with an identical prompt inviting them to imagine meeting one another in a shopping mall while searching for gifts for each other.

To control for potential primacy effects, the sequence of interactive conditions was randomized across dyads. For each condition, data from the initial and final minutes were discarded, as conversational dynamics typically differ at the onset and closure of interactions (Levinson, 2012; Lim et al., 2023). The resting-state period was excluded from the current analyses, given that the primary focus was on active dialogue and how its emotional features and syntactic–semantic structures associate with interpersonal neural synchrony. Moreover, since previous studies have already investigated the impact of experimental conditions on neural syn-

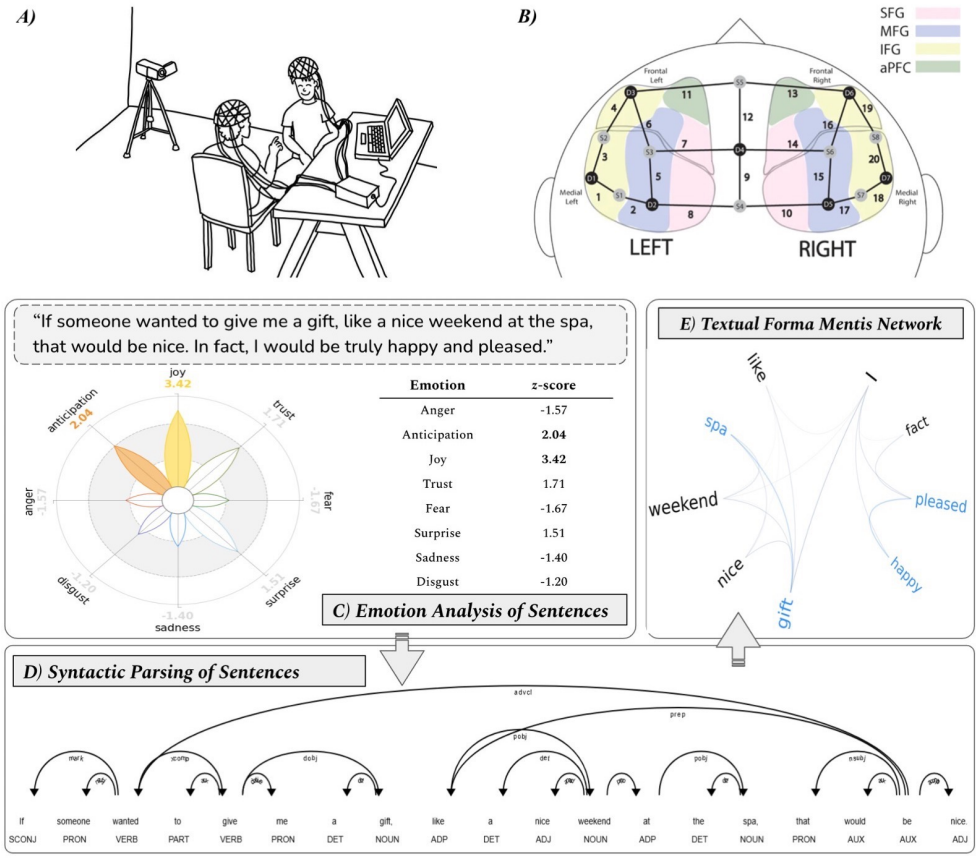

Figure 3.1: Schematic overview of the experimental procedure. **A)** Arrangement of participants and placement of devices during the sessions. **B)** Adapted from (Azhari et al., 2019): diagram illustrating the positions of 20 fNIRS channels, corresponding to the superior frontal gyrus (SFG), middle frontal gyrus (MFG), inferior frontal gyrus (IFG), and anterior prefrontal cortex (aPFC). **C)** Computation of the emotional content of sentences using EmoAtlas (Semeraro et al., 2025). **D)** Syntactic parsing of sentences. **E)** Visualization of the syntactic and semantic structure of sentences through *Textual Forma Mentis Networks* (Stella et al., 2019). Image from Carollo, Stella, et al. (2025).

chrony (Lim et al., 2024a, 2024b), these effects were not re-examined here. Instead, the conditions were modeled as random effects within the statistical framework.

Acquisition of Neural Data

fNIRS hyperscanning was used throughout all experimental conditions to monitor participants' cortical activity. Each participant wore a cap equipped with eight LED emitters (wavelengths: 760 nm and 850 nm) and seven photodetectors, arranged according to a standard prefrontal cortex configuration (Azhari et al., 2019; Bizzego, Gabrieli, et al., 2022). This setup yielded a total of 20 fNIRS channels per participant, covering the prefrontal cortical surface. The channels were organized into six ROIs: the anterior prefrontal cortex, the superior frontal gyrus, and the left and right portions of both the middle and inferior frontal gyri (see Figure 3.1B). Because of their central location and the spatial constraints inherent to fNIRS technology, the anterior prefrontal cortex and superior frontal gyrus were not further subdivided into hemispheric subregions. Channel positioning followed the international 10–20 EEG system (Homan et al., 1987), and optode holders were employed to maintain a source–detector distance below 3 cm, thereby ensuring adequate signal quality and minimizing noise (Pinti et al., 2020). Data acquisition was performed with a NIRSport2 system (NIRx Medical Technologies LLC) at a sampling frequency of 10.17 Hz.

Processing of Neural Data

Neural data pre-processing was carried out using the *pyphysio* library (Bizzego, Battisti, et al., 2019). Signal quality was assessed through a deep learning–based procedure (Bizzego, Gabrieli, & Esposito, 2021; Bizzego, Neoh, et al., 2022), employing a convolutional neural network specifically trained to evaluate the quality of individual fNIRS signal segments. Motion-related artifacts were corrected through a combined ap-

proach using spline interpolation (Scholkmann et al., 2010) and wavelet filtering (Molavi & Dumont, 2012). The cleaned optical signals were then converted into concentrations of oxygenated (HbO) and deoxygenated hemoglobin (HbR) according to the modified Beer–Lambert law (D. Delpy & Cope, 1997). In line with previous studies (e.g., Nguyen, Schleihauf, Kayhan, et al. (2020) and Reindl et al. (2018)), subsequent analyses focused primarily on HbO signals, given their higher sensitivity to task-related cortical activity.

For each ROI, neural activity was derived by averaging the normalized fNIRS signals across all channels constituting that ROI (Bizzego, Azhari, & Esposito, 2022). A regional signal was retained for analysis only when at least two constituent channels satisfied the quality criteria, thereby ensuring the reliability of the ROI-level measurements (Bizzego, Azhari, & Esposito, 2022).

Interpersonal Neural Synchrony

Interpersonal neural synchrony between the two members of each dyad was quantified using Wavelet Transform Coherence (WTC) across homologous ROIs (Chang & Glover, 2010; Grinsted et al., 2004; Nguyen, Schleihauf, Kayhan, et al., 2020). This approach enabled the assessment of coherence between the fNIRS time series of each dyad and region as a joint function of frequency and time. WTC is particularly advantageous in this context, as it captures both synchronous (in-phase) and lagged (out-of-phase) fluctuations, thereby offering a comprehensive index of global neural coupling (Nguyen, Schleihauf, Kayhan, et al., 2020).

For each dyad, a total of eighteen WTC values were extracted, corresponding to each region of interest across the three interactive conditions

(spontaneous conversation, role-play, and role reversal). Coherence was computed over frequencies ranging from 0.01 to 0.20 Hz, with a resolution of 0.01 Hz (Holper et al., 2012; Lim et al., 2024a). The final coherence value for each region and condition was obtained by averaging across the entire frequency spectrum, thus avoiding potential biases stemming from *a priori* assumptions regarding specific frequency bands.

As a control procedure, surrogate dyads were generated by randomly re-pairing participants from different real dyads, allowing the estimation of baseline coherence in the absence of interpersonal interaction and co-presence. This permutation-based approach yielded the same number of surrogate pairs as true dyads (i.e., 42), ensuring balanced comparisons.

Emotional Content of Dialogues

To quantify the emotional content of the transcribed dialogues, we applied EmoAtlas (Semeraro et al., 2025), a framework that constructs TFMNs and performs emotion profiling based on Plutchik's theory of basic emotions (Plutchik, 1980) (Figure 3.1C). EmoAtlas evaluates the presence of eight distinct emotions—anger, anticipation, disgust, fear, joy, sadness, surprise, and trust—within text. For each emotion, a z-score is computed to indicate its relative intensity in the dialogue compared to what would be expected by chance from the underlying emotional lexicon.

Specifically, given a text containing m emotional words, EmoAtlas generates 1000 random word assemblies of size m by sampling uniformly from the lexicon. This procedure accounts for the baseline frequency of each emotion in the lexicon (e.g., more words are associated with trust than disgust). For each sampling iteration i, the number of words k_e^i

corresponding to emotion e is recorded, forming a reference distribution. The observed count m_e of words eliciting emotion e in the text is then converted into a z-score as:

$$z_e = \frac{m_e - \langle k_e^{(i)} \rangle}{\sigma_e}$$

where $\langle k_e^{(i)} \rangle$ is the mean count from the random samplings and σ_e is the standard deviation across iterations.

EmoAtlas was selected for this study because it has been shown to perform comparably or better than state-of-the-art natural language processing methods (Semeraro et al., 2025). To obtain a dyad-level measure, we summed the z-scores of each emotion across the two participants within the dyad.

In a few cases ($n = 2$), EmoAtlas could not provide reliable z-scores due to an insufficient number of words in the text; these instances were treated as missing data.

Syntactic/Semantic Structure of Dialogues

To examine the syntactic and semantic structure of the dialogues, we utilized TFMNs (Latin for "mindset") (Stella et al., 2019), constructed via EmoAtlas (Semeraro et al., 2025) (Figures 3.1D–E). TFMNs represent the associative knowledge embedded in text through network theory, where nodes correspond to words or concepts and links capture either syntactic dependencies (specifications) or semantic relationships (synonyms).

The construction of TFMNs proceeds sentence by sentence. Words are linked if they are sufficiently close on the syntactic parsing tree of

the sentence, with a maximum distance of $K \leq 4$. This approach allows TFMNs to capture syntactic relationships even between non-adjacent words, an advantage over traditional word co-occurrence networks (Quispe et al., 2021). Syntactic parsing is performed using a pre-trained AI model (spaCy, see Semeraro et al., 2025). The K threshold is set to restrict links to syntactically related concepts, and the chosen value of $K \leq 4$ aligns with prior findings indicating that syntactic distances in English average around three words due to language optimization effects (i Cancho et al., 2004).

After extracting the syntactic network from non-stop words within this distance, the network is enriched with semantic and psychological information, creating a multiplex network. In this network, edges can represent either syntactic or semantic relationships, and words are annotated with emotional labels (positive, negative, or neutral) and associated with one or more emotions (Semeraro et al., 2022, 2025; Stella et al., 2019).

After constructing the semantic network for each individual in every condition, we computed several network metrics (Siew et al., 2019; Stella, 2022): the total number of nodes ($|V|$), the total number of edges ($|E|$), average local clustering, the number of connected components ($|C|$), and degree assortativity (Figure 3.2). The total number of nodes and edges reflects the size of the network: $|V|$ corresponds to the distinct words or concepts included, while $|E|$ represents the number of syntactic or semantic links connecting them. Average local clustering quantifies the tendency of a node's neighbors to be interconnected, capturing the formation of localized clusters. In a semantic network, higher clustering values indicate that concepts are more densely grouped and strongly associated

within local neighborhoods. The number of connected components $|C|$ counts the distinct subsets of nodes where each node is reachable from any other node in the same subset. For example, if the network consists of three internally connected groups of words with no links between them, $|C|$ would equal three. Degree assortativity evaluates the tendency of nodes with similar connectivity (degree) to be linked with each other. High assortativity values indicate that highly connected nodes preferentially associate with other highly connected nodes, reflecting a structured organization within the semantic network. To obtain a dyad-level measure, we summed the values of each metric across the two participants within the dyad.

Data Analysis

The analytical procedure unfolded across four consecutive stages:

1. A preliminary evaluation of interpersonal neural synchrony across all ROIs;

2. An assessment of the relationship between the emotional content of the dialogues and interpersonal neural synchrony;

3. An analysis of how the syntactic and semantic organization of dialogues relates to interpersonal neural synchrony;

4. An examination of the joint influence of emotional and syntactic–semantic features on interpersonal neural synchrony.

As an initial step, WTC values were compared between true and surrogate dyads for each ROI. To this end, six linear mixed-effects models were fitted, one per ROI (Brown, 2021). In each model, WTC served as

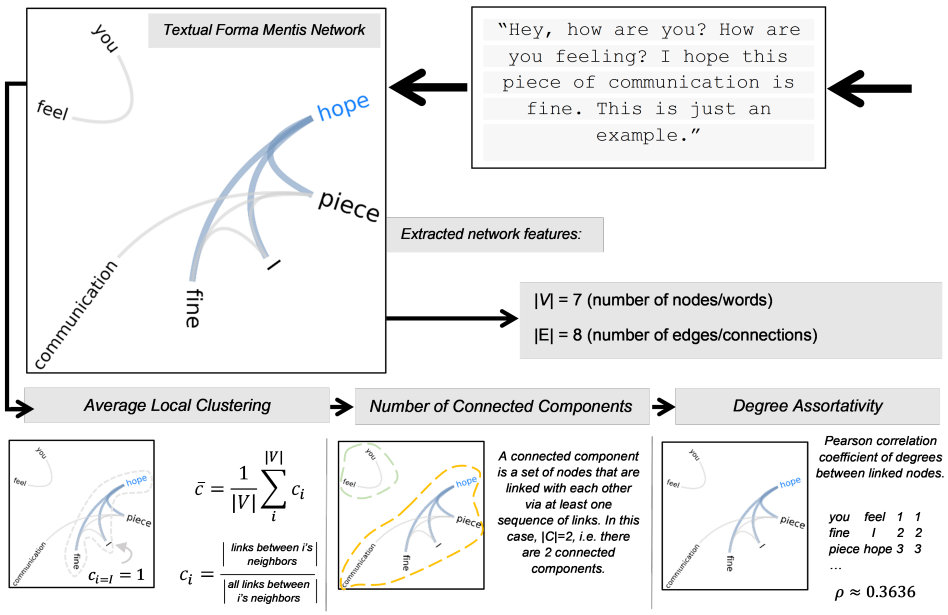

Figure 3.2: Network measures extracted from the semantic network built using *textual forma mentis* networks (TFMNs). From the semantic network, we extracted the total number of nodes $|V|$, the total number of edges $|E|$, the average local clustering, the number of connected components $|C|$, and degree assortativity. Image from Carollo, Stella, et al. (2025).

the dependent variable, dyad type (true *vs.* surrogate) was included as a fixed effect, and both experimental condition and dyad ID were modeled as random effects. Regions that exhibited significant differences in WTC between real and surrogate dyads were subsequently retained for further analyses.

To investigate the association between emotional z-scores and interpersonal neural synchrony, we employed a set of linear mixed-effects models. For each model, the WTC value corresponding to a specific ROI was entered as the dependent variable. In brain regions exhibiting synchrony levels exceeding chance, the eight aggregated emotional z-scores

were included as fixed predictors, whereas experimental condition and dyad ID were modeled as random factors. Subsequently, the analysis was expanded to encompass the entire dataset in order to predict WTC values across all prefrontal subregions based on the emotional z-scores. In this comprehensive linear mixed-effects model, WTC served as the dependent variable, while the eight aggregated emotional z-scores were entered as fixed predictors. ROI, experimental condition, and dyad ID were included as random factors to account for within-dyad and within-condition variability.

A parallel analytical approach was employed to explore the association between the syntactic–semantic organization of dialogues and interpersonal neural synchrony. In this case, the network metrics derived from the TFMNs were included as fixed predictors of WTC, first at the level of individual regions of interest and then across the entire prefrontal cortex.

Finally, emotional z-scores and the syntactic–semantic metrics derived from the TFMNs were jointly incorporated to predict interpersonal neural synchrony across the full set of prefrontal regions. In this integrative analysis, a linear mixed-effects model was fitted with WTC values as the dependent variable, while emotional and syntactic–semantic indices served as fixed predictors. ROI, experimental condition, and dyad ID were included as random factors to account for within-subject and within-condition variability.

Before fitting the linear mixed-effects models, all continuous fixed predictors were mean-centered. To correct for multiple comparisons and limit the likelihood of Type I errors, the Benjamini–Hochberg false discovery rate correction was applied.

3.1.2 Results

Interpersonal Neural Synchrony Across True and Surrogate Dyads

Before exploring the associations between the emotional and syntactic/semantic characteristics of the dialogues, we conducted a preliminary evaluation of neural synchrony scores. The purpose of this step was to identify ROIs displaying levels of interpersonal neural synchrony exceeding chance, which were subsequently included in the main analyses. To achieve this, six linear mixed-effects models were fitted—one for each ROI—with WTC values as the dependent variable. Dyad type (true *vs.* surrogate) was entered as a fixed effect, whereas experimental condition and dyad ID were modeled as random factors. To account for multiple testing and minimize the risk of false positives, the Benjamini–Hochberg false discovery rate correction was applied.

Statistically significant differences emerged between real and surrogate dyads in the WTC in their superior frontal gyrus ($\beta = 0.010$, *Standard Error (SE)* $= 0.005$, $t(207) = 2.201$, $p = .029$, $q = .038$), left middle frontal gyrus ($\beta = 0.018$, $SE = 0.004$, $t(203.50) = 4.196$, $p < .001$, $q < .001$), and right middle frontal gyrus ($\beta = 0.017$, $SE = 0.005$, $t(202.20) = 3.468$, $p < .001$, $q < .001$; see Figure 3.3). No statistically significant differences were observed in WTC values for the anterior prefrontal cortex and bilateral inferior frontal gyri ($q > .05$). Consequently, these ROIs were omitted from all further analyses, as they did not demonstrate interpersonal synchrony levels significantly exceeding those observed in surrogate dyads.

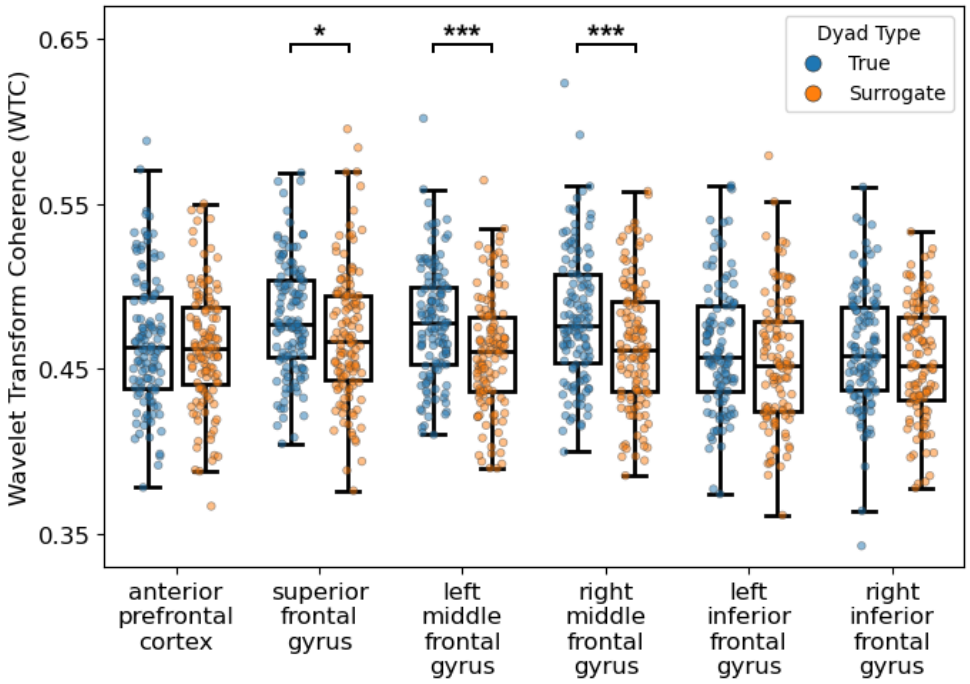

Figure 3.3: Wavelet Transform Coherence (WTC) values across regions of interest in the prefrontal cortex. For each region of interest, values of WTC in true (in blue) and surrogate (in orange) dyads are provided. (* $q < .05$; *** $q < .001$). Image from Carollo, Stella, et al. (2025).

Emotional Content of Dialogues and Interpersonal Neural Synchrony

For this analysis, we employed the emotional z-scores generated by EmoAtlas as indicators of the dialogues' emotional content. Figure 3.4 presents the distribution of aggregated emotional z-scores across the dataset. As shown, anticipation and joy emerged as the most prevalent emotions, whereas anger, disgust, and fear were the least frequently expressed.

We fitted three linear mixed-effects models to assess the relationship between the emotional content of the dialogues and interpersonal neural synchrony in the ROIs that exhibited above-chance synchrony: the superior frontal gyrus, the left middle frontal gyrus, and the right middle frontal gyrus. In each model, WTC values were treated as the dependent

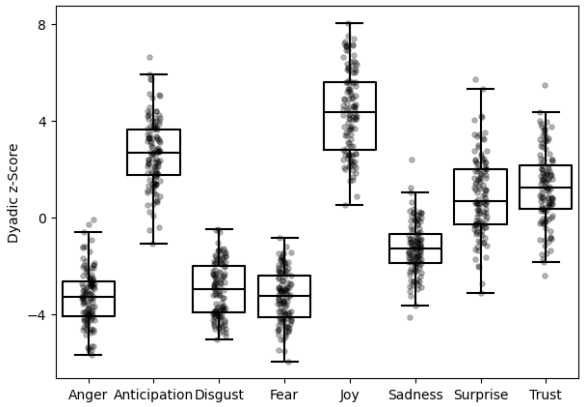

Figure 3.4: Distribution of aggregated emotional z-scores representing the emotional content of the transcribed dialogues. Image from Carollo, Stella, et al. (2025).

variable, the emotional z-scores were entered as fixed predictors, and experimental condition and dyad ID were included as random factors.

Across the three models, none of the emotional z-scores significantly predicted interpersonal neural synchrony ($q > .05$). A summary of these results is reported in Table 3.1.

To examine the relationship between overall prefrontal interpersonal neural synchrony and the emotional content of the dialogues, a linear mixed-effects model was employed. In this model, WTC values served as the dependent variable, while emotional z-scores were entered as fixed predictors. ROI, experimental condition, and dyad ID were modeled as random factors. The analysis revealed that anticipation significantly predicted interpersonal neural synchrony (β = -0.007, SE = 0.003, t(247.98) = -2.695, p = .008, q = .025; see Table 3.2 for a summary of results). The model yielded an AIC of –1223.85 and a marginal R^2 of 3.62%.

Predictor	Estimate (β)	Standard Error	t-value	p-value	q-value
Interpersonal Neural Synchrony on the Superior Frontal Gyrus					
Anger	-0.0037	0.005	-0.796	.428	.730
Anticipation	-0.0026	0.004	-0.668	.505	.744
Disgust	-0.0002	0.004	-0.039	.969	.971
Fear	0.0062	0.004	1.551	.124	.372
Joy	0.0041	0.004	1.148	.254	.684
Sadness	0.0001	0.004	0.037	.971	.971
Surprise	0.0024	0.004	0.598	.551	.744
Trust	0.0064	0.003	1.852	.067	.300
Interpersonal Neural Synchrony on the Left Middle Frontal Gyrus					
Anger	-0.0092	0.005	-1.926	.057	.300
Anticipation	-0.0080	0.004	-2.002	.048	.300
Disgust	0.0075	0.004	1.675	.097	.327
Fear	-0.0010	0.004	-0.241	.810	.875
Joy	0.0027	0.004	0.751	.454	.730
Sadness	0.0030	0.004	0.759	.450	.730
Surprise	0.0038	0.004	0.962	.338	.730
Trust	0.0033	0.004	0.935	.352	.730
Interpersonal Neural Synchrony on the Right Middle Frontal Gyrus					
Anger	-0.0042	0.006	-0.742	.460	.730
Anticipation	-0.0082	0.005	-1.677	.096	.327
Disgust	0.0024	0.005	0.453	.651	.837
Fear	-0.0014	0.005	-0.289	.773	.870
Joy	-0.0014	0.004	-0.316	.753	.870
Sadness	0.0028	0.005	0.604	.547	.744
Surprise	0.0017	0.005	0.358	.721	.870
Trust	-0.0045	0.004	-1.058	.293	.718

Table 3.1: Summary of fixed effects related to the emotion z-scores in the linear mixed models conducted to predict interpersonal neural synchrony in individual regions of interest (i.e., superior frontal gyrus, left middle frontal gyrus, right middle frontal gyrus). For each emotion, we reported the estimate, the standard error, the t-value, the p-value, and the q-value.

Syntactic/Semantic Structure of Dialogues and Interpersonal Neural Synchrony

In this analysis, we used TFMNs to capture the syntactic/semantic relationships between concepts expressed within participants' speech and examined their association with interpersonal neural synchrony.

Three separate linear mixed-effects models were fitted to investigate the ROIs that exhibited above-chance levels of synchrony: the superior

Predictor	Estimate (β)	Standard Error	t-value	p-value	q-value
Emotional z-Scores					
Anger	-0.0055	0.003	-1.794	.074	.200
Anticipation	-0.0070	0.003	-2.695	.008	**.025 ***
Disgust	0.0032	0.003	1.139	.256	.460
Fear	0.0015	0.003	0.576	.565	.587
Joy	0.0019	0.002	0.834	.405	.518
Sadness	0.0026	0.002	1.045	.297	.485
Surprise	0.0036	0.003	1.427	.154	.328
Trust	0.0016	0.002	0.738	.461	.518
Syntactic/Semantic Properties					
Nodes	0.0017	0.002	0.765	.452	.518
Average Local Clustering	-0.0022	0.002	-1.026	.306	.485
Connected Components	0.0076	0.003	2.948	.004	**.014 ***
Degree Assortativity	-0.0085	0.003	-3.350	<.001	**.006 ****
Emotional z-Scores and Syntactic/Semantic Properties					
Anger	-0.0052	0.003	-1.704	.090	.220
Anticipation	-0.0061	0.003	-2.365	.019	.056
Disgust	0.0021	0.002	0.748	.455	.518
Fear	0.0033	0.003	1.277	.202	.390
Joy	0.0014	0.002	0.604	.547	.587
Sadness	-0.0001	0.003	-0.024	.981	.981
Surprise	0.0035	0.002	1.416	.158	.328
Trust	0.0019	0.002	0.869	.385	.518
Nodes	0.0021	0.002	0.954	.341	.512
Average Local Clustering	-0.0017	0.002	-0.777	.438	.518
Connected Components	0.0082	0.003	2.950	.004	**.014 ***
Degree Assortativity	-0.0086	0.003	-3.181	.002	**.009 ****

Table 3.2: Summary of fixed effects in the linear mixed models conducted to predict interpersonal neural synchrony using data from all regions of interest (i.e., superior frontal gyrus, left middle frontal gyrus, right middle frontal gyrus). For each predictor, we reported the estimate, the standard error, the t-value, the p-value, and the q-value. Statistically significant q-values are noted in bold. (* $q < .05$; ** $q < .01$).

frontal gyrus, the left middle frontal gyrus, and the right middle frontal gyrus. In each model, WTC values were entered as the dependent variable, syntactic/semantic network metrics were included as fixed predictors, and experimental condition and dyad ID were modeled as random factors.

Of the three models tested, one revealed a significant association between the syntactic/semantic features of dialogues and interpersonal neural synchrony (see Table 3.3 for a summary of results). Specifically, the

model based on data from the right middle frontal gyrus showed that lower degree assortativity significantly predicted higher WTC values (β = -0.015, SE = 0.006, $t(106.25)$ = -3.361, p = .001, q = .004). The model yielded an AIC of –365.83 and a marginal R^2 of 9.97%. In contrast, syntactic/semantic network measures did not emerge as significant predictors of interpersonal neural synchrony in the models for the superior frontal gyrus and the left middle frontal gyrus ($q > .05$).

Overall, the findings suggest that the emotional characteristics of the dialogues do not reliably predict interpersonal neural synchrony within specific prefrontal regions. In contrast, the syntactic and semantic features of conversation appear to play a more prominent role, emerging as significant predictors of localized neural synchrony—particularly within certain prefrontal areas.

To investigate how the syntactic and semantic characteristics of dialogues relate to prefrontal interpersonal neural synchrony, a linear mixed-effects model was employed. In this analysis, WTC values were used as the dependent variable, while syntactic/semantic network metrics were entered as fixed predictors. ROI, experimental condition, and dyad ID were modeled as random factors. The results revealed significant effects of the number of connected components (β = 0.008, SE = 0.003, $t(218.30)$ = 2.948, p = .004, q = .014) and degree assortativity (β = -0.009, SE = 0.003, $t(247.88)$ = -3.350, $p < .001$, q = .006) on neural synchrony (see Table 3.2 for a summary of results). The model yielded an AIC of –1275.416 and a marginal R^2 of 4.44%.

Two key observations can be drawn from these findings. First, the explanatory strength of models based on syntactic/semantic metrics appears to decrease when extended to the entire prefrontal cortex, as op-

Predictor	Estimate (β)	Standard Error	t-value	p-value	q-value
Interpersonal Neural Synchrony on the Superior Frontal Gyrus					
Nodes	-0.0012	0.003	-0.370	.712	.801
Average Local Clustering	0.0003	0.003	0.094	.925	.925
Connected Components	0.0027	0.004	0.692	.491	.669
Degree Assortativity	0.0013	0.004	0.322	.748	.801
Interpersonal Neural Synchrony on the Left Middle Frontal Gyrus					
Nodes	0.0028	0.003	0.821	.418	.627
Average Local Clustering	-0.0034	0.003	-1.007	.316	.527
Connected Components	0.0073	0.004	1.804	.074	.158
Degree Assortativity	-0.0091	0.004	-2.256	.026	.065
Interpersonal Neural Synchrony on the Right Middle Frontal Gyrus					
Nodes	0.0023	0.004	0.600	.550	.688
Average Local Clustering	-0.0041	0.004	-1.104	.272	.510
Connected Components	0.0111	0.005	2.433	.017	.050
Degree Assortativity	-0.0152	0.006	-3.361	.001	**.004****

Table 3.3: Summary of fixed effects related to the syntactic/semantic properties of dialogues in the linear mixed models conducted to predict interpersonal neural synchrony in individual regions of interest (i.e., superior frontal gyrus, left middle frontal gyrus, right middle frontal gyrus). For each syntactic/semantic metric, we reported the estimate, the standard error, the t-value, the p-value, and the q-value. Statistically significant q-values are noted in bold. (** $q < .01$).

posed to analyses targeting specific subregions. Second, models incorporating syntactic/semantic features provide slightly greater explanatory power for prefrontal neural synchrony than those relying exclusively on emotional variables.

Emotional Content, Syntactic/Semantic Structure of Dialogues, and Interpersonal Neural Synchrony

Finally, we integrated both the emotional content and the syntactic/semantic structure of dialogues to predict interpersonal neural synchrony across the entire prefrontal cortex. The analysis revealed a significant effect of the number of connected components ($\beta = 0.008$, $SE = 0.003$, $t(205.40) = 2.950$, $p = .004$, $q = 014$), and degree assortativity ($\beta =$

-0.009, $SE = 0.003$, $t(245.40)$ = -3.181, $p = .002$, $q = .009$) on WTC scores (see Table 3.2). The AIC of the model equaled to -1187.726 and the $R^2_{marginal}$ was equal to 7.60%.

We observed that, compared with models including only emotional or only syntactic/semantic predictors, the integrated model combining both dimensions yielded improved performance and greater predictive power for prefrontal neural synchrony.

3.1.3 Discussion

This study investigated how the emotional content and associative structure of dialogues relate to interpersonal neural synchrony during a hyperscanning paradigm (Lim et al., 2023, 2024a, 2024b). Prefrontal neural activity was recorded using fNIRS, while dialogues between social dyads were manually transcribed for linguistic analysis. Automated computational tools were then applied to quantify emotional valence and to model the syntactic/semantic structure of the dialogues (Semeraro et al., 2025; Stella et al., 2019). Through this integrative framework, we observed that both emotional and syntactic/semantic features of dialogue were significantly associated with interpersonal neural synchrony within specific prefrontal areas.

First, several prefrontal regions demonstrated a significant *hyperscanning effect*, with real dyads exhibiting greater interpersonal neural synchrony than surrogate pairs. This result is consistent with previous findings by Cui et al. (2012), who observed enhanced synchrony in the superior frontal cortex during cooperative activities—although their study involved computer-mediated rather than face-to-face interactions. The regions identified here may thus be implicated in higher-order socio-

cognitive functions such as active interpersonal coordination and theory of mind (Dziobek et al., 2011). In contrast, no significant differences between real and surrogate dyads were found in the anterior prefrontal cortex or the bilateral inferior frontal gyri, diverging from prior hyperscanning studies that reported above-chance synchrony in these regions (e.g., Nguyen, Schleihauf, Kayhan, et al., 2021; Pinti et al., 2021). This divergence may stem from the specific demands of the present paradigm, in which participants engaged in role-play tasks. The prefrontal cortex has been consistently associated with identity-related processes—including both identity concealment and imitation (Christ et al., 2009; Ding et al., 2012; Langleben et al., 2002; Lim et al., 2023)—with the inferior frontal gyrus typically linked to concealment and medial prefrontal areas to identity faking (Ding et al., 2012; Langleben et al., 2002). Of these, the latter process most closely resembles the identity faking component inherent in the role-play interactions used in the current study. A broader theoretical question concerns the psychological meaning of increased interpersonal neural synchrony. Previous accounts have variously interpreted synchrony as reflecting shared attention, shared interpretation, predictive alignment, interpersonal coordination, or social bonding. In the context of the present role-play paradigm, we propose that increased prefrontal synchrony may reflect ongoing mutual modeling and predictive alignment between partners, whereby each participant continuously monitors, anticipates, and adapts to the other's behavior. Such alignment may be particularly critical in role-play contexts involving identity faking, where maintaining narrative coherence requires sustained socio-cognitive coordination. Thus, in this setting, interpersonal neural synchrony may be best interpreted as a neural correlate of dynamic interpersonal alignment

rather than simple co-attention or affective bonding.

Furthermore, among interacting partners, synchrony within the superior frontal gyrus and the bilateral middle frontal gyri was found to be associated with both the emotional content and the syntactic/semantic organization of their dialogues. This pattern contrasts with the results reported by Kinreich et al. (2017), who observed no modulation of interpersonal brain synchrony by the emotional, reminiscent, or practical dimensions of conversation. However, an important methodological distinction lies in the way these features were operationalized: Kinreich and colleagues coded conversational aspects as binary variables—simply present or absent—based on human ratings. In contrast, the present study adopts an AI framework that moves beyond categorical annotations, reconstructing the rich network of emotions and associative meanings embedded in natural language. This finer-grained characterization, enabled by contemporary natural language processing techniques, may explain the divergence in findings. As highlighted by Stella (2022), spontaneous dialogue is intrinsically multifaceted, conveying not only informational content but also affective nuances and structural relations. In this sense, dialogues can be understood both in terms of the emotions they express (Plutchik, 1980) and the syntactic/semantic associations that link the concepts articulated by the speakers (Vitevitch et al., 2024).

In the current study, emotional content did not significantly predict activity within any single region of interest. However, when ROIs were considered in combination, emotions in dialogues were associated with interpersonal neural synchrony across the prefrontal cortex. These ROIs have been consistently identified in the literature as central nodes in the networks supporting emotional processing and regulation (Grecucci et

al., 2013). The superior frontal gyrus, in particular, has been shown to exhibit increased activation during the up- or down-regulation of affective states (Frank et al., 2014), whereas the rostral segment of the middle frontal gyrus—captured by our fNIRS configuration—is implicated in assigning meaning to emotional stimuli according to their salience and self-relevance (Roy et al., 2012; Waugh et al., 2014). Broadly speaking, this region contributes to evaluating the personal significance of emotional experiences and tends to sustain activity in response to affectively charged events (Waugh et al., 2010).

The syntactic and semantic organization of dialogues revealed patterns distinct from those associated with emotional content. Specifically, higher interpersonal neural synchrony in the right middle frontal gyrus was linked to negative degree assortativity values (Newman, 2018), suggesting that dyads exhibiting stronger synchrony tended to connect highly connected words with less connected ones. This pattern may suggest a link between linguistic entropy and neural coupling within this region, whereby interpersonal synchrony could arise under conditions of heightened cognitive and social demand. In line with this interpretation, previous research has demonstrated that the middle frontal gyrus plays a key role in syntactic and semantic processing, showing greater activation for semantically distant or unrelated word pairs compared to semantically related ones (Kotz et al., 2002; Lau et al., 2008; Rissman et al., 2003). Additionally, activity in the right middle frontal gyrus has been shown to vary as a function of categorical relationships among words (Laufer et al., 2011; Raposo et al., 2006; Sachs et al., 2011). Taken together, these findings support the view that the middle frontal gyrus contributes to the processing of words differing in syntactic and semantic connectivity,

and that such variability may underlie the observed patterns of neural synchrony.

When predicting interpersonal neural synchrony across the prefrontal cortex, models that integrate both emotional content and the syntactic–semantic characteristics of dialogues outperform those based on either information source alone. Interestingly, the predictive capacity of models grounded in syntactic–semantic network features decreases when extended to the entire prefrontal cortex, compared with analyses restricted to specific regions of interest. This observation aligns with prior evidence indicating that the prefrontal cortex is involved in both emotional and syntactic processing (Dixon et al., 2017; Hertrich et al., 2021), with each domain potentially contributing uniquely to neural activity and synchrony patterns. Moreover, our results suggest a distinction between global and local processing of emotional versus syntactic/semantic aspects during social interaction. Emotional content appears to influence synchrony at a more global, prefrontal level, though its predictive strength within individual subregions is modest—possibly reflecting the need for larger samples to detect localized effects. In contrast, syntactic/semantic properties exhibit stronger associations with neural synchrony at the local level, particularly within the right middle frontal gyrus, whereas including synchrony data from additional regions may introduce noise and consequently reduce model performance.

Limitations and Future Research

In interpreting these findings, several limitations should be considered. First, neural activity was recorded exclusively from prefrontal regions using fNIRS. Although these areas play a pivotal role in social and cog-

nitive processes (Forbes & Grafman, 2010), other regions—such as the temporo-parietal junction—are also known to exhibit interpersonal neural synchrony (Nguyen, Schleihauf, Kayhan, et al., 2020) and may likewise be shaped by linguistic or emotional factors. Expanding the recording coverage to include these additional areas would allow for a more comprehensive characterization of the neural mechanisms underlying social communication.

Second, the present analyses focused solely on the emotional content conveyed through speech. However, emotional information is also transmitted via non-verbal channels, including facial expressions, gestures, and vocal prosody (Plutchik, 1980). Incorporating multimodal data in future studies could thus offer a richer understanding of how emotions modulate neural synchrony across interacting individuals (Alonso-Martin et al., 2013). An additional methodological consideration concerns the operationalization of emotional valence through EmoAtlas. While lexicon-based approaches offer transparency and replicability, alternative methods may yield partially divergent estimates of emotional content. It is plausible that broad valence distinctions (e.g., positive *vs.* negative affect) would remain relatively stable across operationalizations, whereas more fine-grained emotional nuances might vary depending on the method employed. Consequently, although the present findings are unlikely to hinge on the specific tool adopted, future studies should examine the robustness of emotion–synchrony associations across multiple measurement approaches to strengthen interpretability and generalizability.

Third, the study sample consisted of a single socio-cultural group — Italian friends — and did not account for the depth or quality of the

relationship, factors that may influence the degree of neural coupling. Future research should aim to include more diverse dyads (e.g., strangers, romantic partners, or parent–child pairs) to evaluate the generalizability of these effects across different types of social bonds.

3.1.4 Conclusion

This fNIRS hyperscanning study provides valuable insights into the integration of neuroscientific, affective, and cognitive dimensions of interpersonal synchrony, extending previous works (Huth et al., 2016; Lim et al., 2023, 2024a, 2024b; Y. Yang et al., 2024). Specifically, we quantified how the emotional content and the syntactic/semantic organization of dialogues relate to interpersonal neural synchrony within the prefrontal cortex. Emotional aspects of conversation were significantly associated with neural synchrony across the prefrontal cortex as a whole, although their predictive strength diminished when analyses were restricted to individual ROIs. Conversely, the associative structure of knowledge (Stella, 2022) showed a stronger relationship with synchrony in the right middle frontal gyrus—an effect that weakened when data from all prefrontal regions were considered together. Importantly, when emotional and syntactic/semantic features were integrated into a single predictive model, performance was maximized, emphasizing the complementary contribution of affective and cognitive components to social interaction and prefrontal functioning. Overall, this transdisciplinary, data-driven framework reinforces the central role of affect in naturalistic social exchanges, consistent with the perspective of bio-behavioral synchrony (Feldman, 2012a).

While the present study examined the association between the struc-

tural and emotional properties of dialogues and interpersonal neural synchrony, the next study focuses on how patterns of functional connectivity within the prefrontal cortex relate to the linguistic and emotional characteristics of the dialogues produced during interaction. In this way, it aims to demonstrate how hyperscanning can be leveraged to uncover the neural dynamics that shape communication itself, extending insights from traditional single-brain paradigms to more naturalistic, socially interactive contexts.

3.2 Dialogues' Emotional and Linguistic Properties and Prefrontal Functional Connectivity

Language constitutes the primary medium through which humans connect, interact, and make sense of the world. It enables individuals to express emotions, share ideas, exchange knowledge, establish social relationships, and build complex cultural and institutional systems. In everyday life, language permeates activities ranging from simple interpersonal interactions to sophisticated cognitive operations (Carollo, Stella, et al., 2025; Tomasello, 2010). Because of its pervasive role in shaping both thought and behavior, elucidating the neural mechanisms that underpin language has become a central pursuit in cognitive neuroscience.

Since the earliest neurological case studies (Broca, 1861; Geschwind, 1970; Lichtheim et al., 1885; Wernicke, 1969), research in the neuroscience of language has progressively evolved toward increasingly detailed accounts of how linguistic functions are represented and sustained in the

brain (Tremblay & Dick, 2016). The classical model of language originates from the pioneering clinical observations of Paul Broca and Carl Wernicke, who first linked specific brain regions to distinct linguistic and behavioral functions. Broca associated the left posterior inferior frontal gyrus with speech production and syntactic processing, whereas Wernicke identified the superior temporal gyrus as crucial for language comprehension, noting that patients with lesions in this area retained fluent speech but exhibited profound deficits in understanding spoken words. Subsequently, Lichtheim et al. (1885) refined this framework by proposing the existence of connecting neural pathways between these specialized regions. Over time, however, the notion of language as relying on discrete, functionally isolated modules has been increasingly challenged. A growing body of evidence instead supports the view of language as emerging from a distributed and interactive neural network that integrates multiple cortical and subcortical regions (Friederici et al., 2017).

Building on this theoretical shift, contemporary research has increasingly moved beyond the strictly modular framework proposed by the classical model, reconceptualizing language as an emergent property of a distributed network of anatomically and functionally interconnected regions (Poeppel et al., 2012; Price, 2012). Within this network-based perspective, language processing is understood to rely on the dynamic interaction of multiple pathways—including fronto-temporal, parieto-temporal, occipito-temporal, and fronto-frontal connections—as well as cortico-subcortical circuits (Tremblay & Dick, 2016).

However, as highlighted by Grappe et al. (2019), much of the empirical support for large-scale network models of language arises from studies conducted in non-human primates or from human research employing

diffusion tensor imaging and resting-state fMRI to infer structural and functional connectivity. Direct investigations into how these networks operate during active language production remain comparatively scarce (e.g., Ewald et al., 2012; Grappe et al., 2019), leaving key questions unanswered regarding the real-time neural dynamics that underpin natural linguistic production processes.

In the present study, we addressed this gap by employing fNIRS to monitor brain activity and assess prefrontal functional connectivity during naturalistic, face-to-face social interactions (Carollo, Stella, et al., 2025; Lim et al., 2024a, 2024b). As discussed in the previous chapters, fNIRS provides high tolerance to movement-related artifacts, making it particularly suitable for examining neural dynamics in ecologically valid and interactive settings without compromising data quality (Bizzego, Carollo, Senay, et al., 2024; Bizzego et al., 2025). Building on these methodological advantages, the current work explored how spontaneous language production both shapes and is supported by prefrontal connectivity, with a specific focus on the interplay between emotional and linguistic dimensions of communication. To this end, we integrated recent advances in affective computing and cognitive network modeling (Carollo, Stella, et al., 2025). In line with the previous study, EmoAtlas was used to quantify the emotional content expressed in speech, whereas TFMNs were employed to reconstruct the conceptual and associative structure underlying participants' verbal exchanges (Semeraro et al., 2025; Stella et al., 2019).

3.2.1 Methods

Study design

For the present study, we relied on the same dataset described in Section 3.1.1. Here, however, the emotional z-scores and the TFMN-derived network features were employed to model functional connectivity patterns within specific subregions of the prefrontal cortex. A graphical overview of the study design is shown in Figure 3.5.

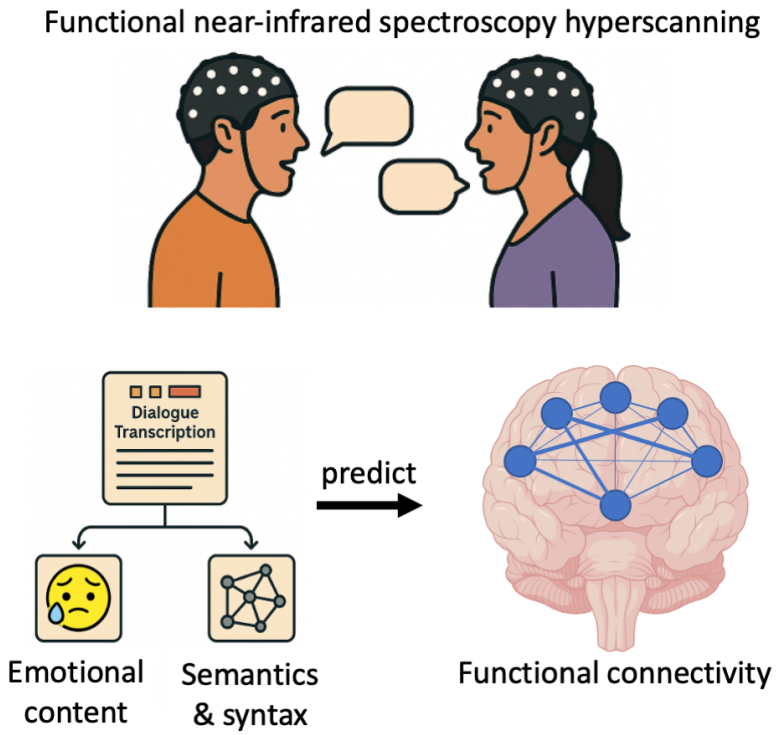

Figure 3.5: Graphical overview of the study design. Participants underwent a functional near-infrared spectroscopy (fNIRS) hyperscanning session while engaging in face-to-face verbal interactions. The recorded dialogues were manually transcribed and analyzed using computational approaches to extract emotional and syntactic/semantic features. These linguistic and affective measures were subsequently employed as predictors of prefrontal functional connectivity, estimated through wavelet transform coherence. Image from Carollo, Bizzego, Lim, et al. (2025).

Functional Connectivity

To assess functional connectivity within each participant's prefrontal cortex, WTC was calculated between the fNIRS time series of all possible pairs of regions of interest ROIs (Chang & Glover, 2010; Grinsted et al., 2004). For each participant and experimental condition (natural conversation, role-play, and role reversal), WTC was computed for every ROI pair, resulting in 15 connectivity values per participant. Coherence was analyzed across frequencies ranging from 0.01 to 0.20 Hz, with increments of 0.01 Hz (Carollo, Bizzego, Schäfer, et al., 2025; Carollo, Stella, et al., 2025). The final connectivity metric for each ROI pair and condition was obtained by averaging WTC values across the full frequency spectrum, as no *a priori* assumptions were made about the relevance of specific frequency bands (Carollo, Bizzego, Schäfer, et al., 2025; Carollo, Stella, et al., 2025).

Data Analysis

For the statistical analyses, we employed linear mixed-effects models (Bates et al., 2005), selected for their capacity to account for both fixed and random sources of variance, thereby accommodating the hierarchical structure of the dataset. The analytical plan was organized as follows.

First, we investigated the relationship between the emotional content of speech and prefrontal functional connectivity. An initial linear mixed-effects model was fitted with functional connectivity scores as the dependent variable and emotional z-scores as fixed predictors. Random effects included the combination of ROI, experimental condition, dyad ID, and participant ID. To further explore these associations at a finer spatial level, separate linear mixed-effects models were computed for each pair

of ROIs. In these models, functional connectivity served as the dependent variable, emotional z-scores were entered as fixed effects, and experimental condition, dyad ID, and participant ID were modeled as random factors. To control for multiple comparisons, the Benjamini–Hochberg false discovery rate correction was applied (Benjamini & Hochberg, 2000).

Second, we examined the association between the syntactic and semantic characteristics of speech and prefrontal functional connectivity, following the same analytical procedure described above. In this case, TFMN-derived network metrics were included as fixed predictors in the linear mixed-effects models.

3.2.2 Results

Emotional Content of Speech and Functional Connectivity

In the initial phase of our analysis, we explored how the emotional content of speech relates to functional connectivity within the prefrontal cortex.

We initially performed a linear mixed-effects model across the whole prefrontal cortex, treating functional connectivity scores as the dependent variable and emotional content of speech as the fixed effects. The model revealed that higher levels of anger ($\beta = –0.030$, $p < .001$) and anticipation ($\beta = –0.012$, $p = .002$) were significantly associated with lower prefrontal functional connectivity. In contrast, higher levels of surprise ($\beta = 0.016$, $p < .001$), disgust ($\beta = 0.009$, $p = .034$), and sadness ($\beta = 0.011$, $p = .005$) significantly predicted increased functional connectivity. Trust, joy, and fear did not emerge as significant predictors of functional connectivity (ps $> .050$). The model explained a small but meaningful portion of the variance, with a marginal R^2 of 0.03. The full results of

this model are reported in Table 3.4.

Predictor	β	***SE***	***df***	***t*-value**	***p*-value**
Emotional content of speech					
Anger	–0.030	0.005	1900	–6.48	**< .001 *** **
Anticipation	–0.012	0.004	1899	–3.05	**.002 ** **
Disgust	0.009	0.004	1882	2.12	**.034 * **
Fear	0.002	0.004	1891	0.59	> .050
Joy	0.007	0.004	1897	1.80	> .050
Sadness	0.011	0.004	1895	2.82	**.005 ** **
Surprise	0.016	0.004	1891	4.12	**< .001 *** **
Trust	–0.006	0.003	1899	–1.80	> .050
Semantic/syntactic properties					
Nodes	–0.010	0.006	1821	–1.65	> .050
Edges	–0.001	0.005	1891	–0.13	> .050
Average local clustering	–0.003	0.004	1889	–0.93	> .050
Connected components	–0.003	0.004	1899	–0.78	> .050
Degree assortativity	–0.005	0.004	1887	–1.38	> .050

Table 3.4: Results of the linear mixed-effects models predicting functional connectivity patterns across the whole prefrontal cortex. For each predictor, we report the estimate (β), the standard error (SE), the degrees of freedom (df), the t-value, and the p-value. (* $p < .05$; ** $p < .01$; *** $p < .001$).

Subsequently, we conducted separate linear mixed-effects models for each pairwise combination of regions of interest to examine functional connectivity patterns individually. After applying the Benjamini-Hochberg correction to control for multiple comparisons, we identified a statistically significant negative association between anger and functional connectivity linking the anterior prefrontal cortex and the right middle frontal gyrus ($\beta = –0.045$, $p = .006$, $q = .049$), as well as between the left middle frontal gyrus and the right inferior frontal gyrus ($\beta = –0.035$, $p = .004$, $q = .032$). These two models had a marginal R^2 of 0.08 and 0.07, respectively. None of the other emotional z-scores significantly predicted functional connectivity across regions of interest (qs $> .050$). The details regarding statistically significant predictors of these models are reported

in Table 3.5.

Regions of interest	**Predictor**	β	***SE***	***df***	***t*-value**	***p*-value**	***q*-value**
Emotional content							
aPFC – right MFG	Anger	–0.045	0.016	92.60	–2.80	.006	**.049 ***
left MFG – right IFG	Anger	–0.035	0.012	101.29	–2.97	.004	**.032 ***
Semantic/syntactic properties							
SFG – left IFG	Degree assortativity	–0.041	0.014	94.57	–2.90	.004	**.026 ***

Table 3.5: Statistically significant predictors of functional connectivity patterns across combinations of regions of interest. For each predictor, we report the estimate (β), the standard error (SE), the degrees of freedom (df), the t-value, the p-value, and the FDR-corrected q-value. Abbreviations: aPFC = anterior prefrontal cortex, IFG = inferior frontal gyrus, MFG = middle frontal gyrus, SFG = superior frontal gyri. (* $q < .05$).

Linguistic Structure of Speech and Functional Connectivity

In the second phase of the analysis, we examined whether the syntactic and semantic structure of speech was related to variations in prefrontal functional connectivity.

We first fitted a linear mixed-effects model on the entire prefrontal cortex dataset, with functional connectivity scores as the dependent variable and TFMN-derived metrics as fixed predictors. The results indicated that none of the TFMN metrics were significantly associated with functional connectivity across the prefrontal cortex (ps $> .050$). A detailed summary of the model outputs is provided in Table 3.4.

Next, we fitted separate linear mixed-effects models for each pairwise combination of regions of interest to investigate localized patterns of functional connectivity. After applying the Benjamini–Hochberg correction for multiple comparisons, a significant negative association emerged between the degree assortativity index and functional connectivity between the superior frontal gyrus and the left inferior frontal gyrus (β = –0.041, p = .004, q = .026). This finding indicates that dialogues characterized by connections between frequent and less common words

within participants' speech were associated with stronger functional connectivity between these two regions. The model yielded a marginal R^2 of 0.08. None of the other TFMN metrics significantly predicted functional connectivity across the remaining region pairs (qs $> .050$). Details on the statistically significant predictors from these models are presented in Table 3.5.

3.2.3 Discussion

In this study, we investigated how the emotional content and the syntactic/semantic properties of natural speech relate to prefrontal functional connectivity during live, face-to-face social interactions. To address this question, we adopted an integrative computational framework that combines quantitative language analysis with advanced neuroimaging techniques, enabling a fine-grained examination of the neural mechanisms underlying spontaneous language use in ecologically valid contexts.

Our findings suggest that the emotional content of speech serves as a more reliable predictor of overall prefrontal functional connectivity than the semantic or syntactic characteristics of language. The prefrontal regions monitored in this study encompass areas functionally corresponding to both the dorsolateral and ventrolateral prefrontal cortices—regions known to play a central role in emotion regulation, particularly through cognitive reappraisal processes (S. Li et al., 2022; Sanchez-Lopez et al., 2018; Tang et al., 2025). By contrast, semantic and syntactic processing is likely to depend on more localized prefrontal subregions. As a result, including all regions of interest in the connectivity analyses may introduce variability unrelated to these linguistic functions, thereby reducing their predictive power.

With regard to the emotional content of speech, expressed anger emerged as a consistent negative predictor of functional connectivity, particularly between the left middle frontal gyrus and the right inferior frontal gyrus. Our analyses showed that participants who used anger-related words more frequently exhibited reduced connectivity between these two regions. Both the right inferior frontal gyrus and the left middle frontal gyrus display atypical activation patterns in psychiatric conditions characterized by emotional dysregulation, including schizophrenia, depression, and borderline personality disorder (Engels et al., 2010; Pilon et al., 2025; Xiao et al., 2024). A meta-analysis by Sorella et al. (2021) identified the right inferior frontal gyrus as consistently involved in both the perception and the experience of anger. In contrast, the middle frontal gyrus—corresponding to the dorsolateral prefrontal cortex—plays a crucial role in the top-down regulation of emotional attention, with greater excitability in the left hemisphere associated with faster disengagement from emotional stimuli (Alizadehgoradel et al., 2024; De Raedt et al., 2010; Sanchez-Lopez et al., 2018). Taken together, these findings suggest that the verbal expression of anger may be accompanied by, and possibly facilitated through, a functional decoupling between a region implicated in the perception and experience of anger (the right inferior frontal gyrus) and a region involved in attentional disengagement from emotional stimuli (the left middle frontal gyrus). Whereas the concurrent activation of these regions may support the inhibition of anger expression and the regulation of emotional attention, their reduced coupling could enable increased attentional engagement and the overt articulation of anger-related content.

With respect to the semantic and syntactic features of language, lin-

guistic complexity—indexed by lower degree assortativity values—emerged as a significant predictor of functional connectivity between the superior frontal gyri and the left inferior frontal gyrus. In particular, higher semantic and syntactic complexity, reflected by lower assortativity (i.e., more unpredictable word associations), was associated with stronger connectivity between these regions. Both the left inferior frontal gyrus and the superior frontal gyri are known to play key roles in language processing. The left inferior frontal gyrus, commonly associated with Broca's area, is essential for the selection of semantic knowledge and the execution of syntactic operations during both speech production and comprehension (Fedorenko et al., 2024; Giglio et al., 2022; Thompson-Schill et al., 1997; Tyler et al., 2011). This region is particularly sensitive to linguistic complexity and hierarchical sentence structures (Friederici et al., 2006; Y.-H. Yang et al., 2017). The superior frontal gyri, in turn, are implicated in higher-order cognitive and motor control processes (W. Li et al., 2013), with the left superior frontal gyrus showing enhanced activation during tasks that require semantic rather than perceptual processing (Sharp et al., 2010). Structurally, these regions are interconnected via the frontal aslant tract (Bohsali et al., 2025; Catani et al., 2013; Dick et al., 2019), which facilitates the coordination of syntactic processing, grammatical morphology, and sequential motor planning. Taken together, our findings align with this body of evidence, suggesting that as linguistic output becomes more semantically and syntactically complex, functional coupling between the left inferior frontal gyrus and the superior frontal gyri intensifies to accommodate the heightened cognitive demands of language generation.

3.2.4 Limitations

Several limitations of the present study should be acknowledged, as they also highlight potential directions for future research. First, brain activity was recorded exclusively from prefrontal regions using fNIRS. Although these areas play a central role in both linguistic and emotional processing, extending the analysis to include additional cortical and subcortical regions would offer a more comprehensive understanding of how language influences functional connectivity. fNIRS was chosen for its robustness to motion artifacts, making it particularly suitable for naturalistic, face-to-face interactions. However, complementary methods such as EEG could provide higher temporal resolution and thus yield finer-grained insights into the temporal dynamics of functional connectivity.

3.2.5 Conclusion

In this study, we integrated an affective and cognitive computational framework for language analysis (Semeraro et al., 2025; Stella et al., 2019) with contemporary approaches in social and cognitive neuroscience (Carollo, Stella, et al., 2025) to investigate how the emotional and linguistic properties of spontaneous speech relate to prefrontal functional connectivity. Our results indicate that emotional content is a strong predictor of connectivity: higher levels of expressed anger were associated with reduced coupling between the left middle frontal gyrus and the right inferior frontal gyrus, suggesting transient functional disconnection during emotionally charged moments, whereas lower anger expression corresponded to more integrated prefrontal networks. Moreover, greater linguistic complexity and unpredictability were linked to stronger con-

nectivity between the superior frontal gyri and the left inferior frontal gyrus, likely reflecting increased engagement of these regions in processing complex and variable speech. Taken together, the findings reveal a functional dissociation within prefrontal connectivity: central–left connections appear more sensitive to syntactic and semantic properties, whereas central–right connections are preferentially modulated by emotional content. Overall, this study underscores the joint contribution of affective and linguistic dimensions to the neural mechanisms supporting spontaneous speech, illustrating how functional neuroimaging can elucidate the dynamic coordination of brain networks during real-world social interaction.

In summary, the two studies presented in this chapter demonstrate how the linguistic and emotional characteristics of dialogue shape neural activity during social interaction at both interpersonal and intrapersonal levels of analysis. The first study showed that emotional and syntactic/semantic features of speech predict interpersonal neural synchrony within the prefrontal cortex, revealing distinct local and global patterns of alignment. The second study extended these findings by examining functional connectivity, highlighting how emotional content and linguistic complexity modulate coupling between specific prefrontal regions during speech production. Together, these findings emphasize the intertwined influence of affective and cognitive processes in shaping brain dynamics during naturalistic social exchanges.

Building on this framework, the next chapter explores how broader relational dimensions—such as interpersonal closeness and task interactivity—further modulate interpersonal neural synchrony, offering a more comprehensive understanding of the neural mechanisms that support

real-world social interaction.

Chapter 4

Interpersonal Neural Synchrony Across Human Attachments and Interaction Contexts

The content of this chapter is based on one publication: **Carollo, A.**, Bizzego, A., Schäfer, V., Pletti, C., Hoehl, S., & Esposito, G. (2025). Interpersonal Neural Synchrony Across Levels of Interpersonal Closeness and Social Interactivity. *NeuroImage, 322*, 121532. https://doi.org/10.1016/j.neuroimage.2025.121532

In some parts, the text has been modified for consistency with the dissertation style.

4.1 Introduction

Social interactions represent a fundamental dimension of human life. From the earliest stages of development, they provide the foundation for the emergence of essential cognitive, emotional, and social capacities (Vygotsky, 1978), including language acquisition (Kuhl, 2007, 2011), emotion regulation (Bornstein & Esposito, 2023; Hollenstein et al., 2017), and the formation of expectations about the social world that support adaptive engagement with others throughout the lifespan (Bowlby & Holmes, 2012).

Given the centrality of social interaction in human life, understanding and scientifically assessing its quality has become a central objective in developmental and social research. A substantial body of work in developmental psychology identifies three core dimensions of social exchanges: rhythm, reciprocity, and synchrony (e.g., Feldman, 2007; Stern, 2009; Trevarthen, 1998).

Rhythm refers to the temporal organization and pacing of interactive behaviors—such as the alternation of vocalizations or gestures between partners—that create temporal regularities facilitating mutual coordination (De Reus et al., 2021). For instance, caregivers often engage infants in rhythmic exchanges through singing, patting, or rocking, thereby supporting physiological and emotional regulation (De Reus et al., 2021; Trehub et al., 2015). Likewise, adults tend to modulate aspects of their speech rhythm, including prosody and speech rate, to align with their conversational partners, enhancing timing precision and perceptual processing (Abney et al., 2014; De Reus et al., 2021; Haegens & Golumbic, 2018; Wilson & Wilson, 2005).

Reciprocity concerns the contingent and bidirectional responsiveness between interaction partners, whereby each individual's behavior simultaneously shapes and is shaped by that of the other (Anderson et al., 1977; Apicella et al., 2013). This mutual exchange reflects a shared motivation and capacity to engage in joint action and to align intentions, emotions, and mental states throughout the interaction (Apicella et al., 2013; Carpenter, 2009; Stern, 2009).

Synchrony broadly denotes the temporal alignment between events that gives rise to coherent states among the components of a system (Feldman, 2007; Leclère et al., 2014). In developmental contexts, synchrony has proven especially useful for capturing the moment-to-moment attunement between caregiver and child and for predicting developmental outcomes (Leclère et al., 2014). Over time, the concept has expanded beyond overt behaviors to encompass physiological and neural forms of coordination (Carollo & Esposito, 2024; Carollo, Lim, et al., 2021; Feldman, 2012b).

The emergence of second-person neuroscience and the development of hyperscanning techniques have significantly advanced the investigation of bio-behavioral synchrony, offering compelling evidence for the phenomenon of interpersonal neural coupling (Carollo & Esposito, 2024; Carollo, Lim, et al., 2021; Hakim et al., 2023; Hasson et al., 2012). By moving beyond traditional single-brain paradigms (e.g., Rizzolatti and Fabbri-Destro 2008; Van Overwalle and Baetens 2009), these approaches have allowed researchers to capture the neural dynamics that unfold during genuine social exchanges. A meta-analysis by Czeszumski et al. (2022) demonstrated that cooperative behavior is consistently associated with synchronized neural activity across frontal and temporopari-

etal regions in interacting individuals. Furthermore, both the magnitude and spatial distribution of such synchrony appear to vary depending on the nature of the cooperative task: for example, the inferior and middle frontal gyri exhibit enhanced coupling during interactive, game-like paradigms such as cooperative Jenga (Y. Li et al., 2021; N. Liu et al., 2016). A seminal study by Cui et al. (2012) marked a turning point in this field by demonstrating the potential of fNIRS hyperscanning for examining the neural bases of real-world social cooperation. In their experiment, dyads played a cooperative video game while undergoing simultaneous fNIRS recording, and results revealed greater synchrony in the right superior frontal cortex during cooperative compared to competitive or individual play—a pattern that was positively correlated with task performance.

Subsequent research has expanded these findings to the domain of caregiver–child interactions. For example, Azhari et al. (2021) reported increased left prefrontal synchrony in father–child dyads who co-viewed animated videos, compared to control pairings. Similarly, Nguyen, Schleihauf, Kayhan, et al. (2020) and Nguyen, Schleihauf, Kungl, et al. (2021) observed enhanced synchrony within the inferior frontal gyrus (IFG) and temporo-parietal junction (TPJ) during cooperative tasks performed by both mother–child and father–child dyads, relative to individual task performance. Notably, higher levels of neural synchrony were associated with greater behavioral reciprocity and improved task outcomes. In related work, Nguyen, Schleihauf, Kayhan, et al. (2021) and Nguyen et al. (2023) demonstrated that the temporal rhythm of early social exchanges modulates the degree of interpersonal neural alignment. Complementary EEG evidence from Endevelt-Shapira and Feldman (2023) further

showed that maternal sensitivity was linked to increased mother–child synchrony in the theta frequency band, whereas maternal intrusiveness predicted reduced coupling. Specifically, synchrony between the mother's right frontal and the infant's left temporal regions correlated with sensitivity, while the inverse pattern—left frontal to right temporal—was associated with intrusive caregiving behaviors. Collectively, these studies highlight interpersonal neural synchrony as a promising quantitative neural marker of interaction quality within parent–child relationships (Nguyen, Schleihauf, Kayhan, et al., 2020; Reindl et al., 2018).

Research on bio-behavioral synchrony extends far beyond the context of caregiver–child relationships. The phenomenon of interpersonal neural synchrony has been examined across a broad spectrum of social bonds—including romantic partners, friends, coworkers, and even unfamiliar individuals (Astolfi, Toppi, Borghini, et al., 2011; Carollo, Stella, et al., 2025; Feldman, 2017; Gvirts & Perlmutter, 2020; Lim et al., 2024a; Long et al., 2021; Toppi et al., 2016). Hyperscanning studies have explored this phenomenon in a wide variety of interactive settings, using tasks that differ in both their social relevance and degree of interactivity. Neural synchrony has been documented when individuals jointly attend to the same stimulus (e.g., co-viewing videos; Azhari et al., 2019; De Felice, Hakim, et al., 2024), collaborate on cooperative games or joint problem-solving tasks (e.g., Cui et al., 2012; T. Liu et al., 2021), or engage in spontaneous verbal exchanges (e.g., Carollo, Stella, et al., 2025; Nguyen, Schleihauf, Kayhan, et al., 2021). These paradigms vary considerably in the extent of mutual engagement they elicit. Contexts involving joint attention to a shared sensory input typically require minimal active participation, as partners share an environment without directly

interacting. Conversely, cooperative and conversational tasks demand continuous reciprocity and adaptive coordination. Among these, free and natural conversation represents the most interactive condition, enabling participants to dynamically regulate turn-taking, emotional tone, and linguistic complexity—thus providing the closest approximation to real-world social interaction.

In line with this perspective, De Felice, Chand, et al. (2024) highlighted two fundamental dimensions that underpin research on interpersonal neural synchrony: interpersonal closeness and interactivity. Interpersonal closeness captures the degree of social connectedness or intimacy between individuals, typically assessed through the length or depth of their relationship. Interactivity, in contrast, reflects the extent of reciprocal engagement and the complexity of multisensory exchanges that occur during social interaction. Although both factors are believed to enhance neural synchrony, empirical evidence directly comparing their distinct contributions across different types of dyads and social situations remains limited.

A growing body of research has investigated how interpersonal neural synchrony varies across different types of social dyads, including strangers, friends, romantic partners, and caregivers with their children. Using fNIRS, for example, Pan et al. (2017) reported that romantic partners exhibited greater synchrony in the right superior frontal cortex compared to both friends and strangers. Similarly, Song et al. (2024) found enhanced prefrontal synchrony—particularly within dorsolateral and medial regions—among friends relative to strangers during cooperative tasks. In a sender–receiver paradigm, Shao et al. (2023) observed higher levels of coupling in romantic couples than in stranger

dyads, especially within the frontopolar cortex and right TPJ. Comparable patterns have been documented in EEG studies: Kinreich et al. (2017) identified significant gamma-band synchrony among romantic partners, but not between strangers, predominantly in temporo-parietal areas. Likewise, Djalovski et al. (2021) reported a graded distribution of synchrony across frequency bands, strongest for romantic couples, intermediate for friends, and weakest for strangers. Interestingly, at the physiological level, Bizzego, Azhari, et al. (2019) observed the opposite pattern—physiological synchrony decreased as interpersonal closeness increased during a co-viewing task. Taken together, these findings suggest that the nature of the relationship modulates neural synchrony; however, most existing studies have focused on specific dyad types and often within a single task context, which constrains the generalizability of their conclusions.

Another line of research has focused on how the characteristics of a task influence interpersonal neural synchrony. For instance, using fNIRS, Fishburn et al. (2018) compared interpersonal neural synchrony during passive co-viewing and active cooperation, showing that interactive tasks elicited greater synchrony within the inferior and middle frontal gyri. Similarly, both Cui et al. (2012) and T. Liu et al. (2021) reported increased neural alignment during joint problem-solving relative to control conditions that involved shared attention without active coordination. Collectively, these findings highlight task interactivity as a critical determinant of interpersonal neural synchrony—likely driven by the heightened reciprocity, mutual adaptation, and predictive mechanisms that characterize real-time cooperative engagement.

Despite the significant insights offered by previous research, a com-

prehensive investigation of how interpersonal closeness and task interactivity jointly shape interpersonal neural synchrony is still missing. This limitation reduces the comparability across hyperscanning studies and constrains the development of a unified theoretical framework for understanding interpersonal coordination at the neural level. For example, in their EEG work, Djalovski et al. (2021) compared romantic couples, best friends, and strangers across both motor and empathy-based tasks, emphasizing the importance of comparative designs that integrate multiple relational and contextual factors. Building on this perspective, the present study systematically examines how interpersonal neural synchrony varies as a function of (i) the degree of interpersonal closeness and (ii) the level of interactivity required by the task.

To address this question, we employed fNIRS hyperscanning to record brain activity in three relationship types—close friends, romantic partners, and mother–child dyads—chosen because they represent core and theoretically significant models within the interpersonal synchrony and developmental neuroscience literatures. Each dyad completed three interactive tasks that differed in their degree of interactivity: joint video watching, a structured cooperative game, and an unstructured free conversation. By systematically varying both relationship closeness and task interactivity, this study aims to clarify how these dimensions interact to modulate interpersonal neural synchrony and to contribute novel evidence toward understanding the neural mechanisms supporting naturalistic social interaction. Grounded in the bio-behavioral synchrony framework (De Felice, Chand, et al., 2024; Feldman, 2017), we hypothesized that:

- Interpersonal neural synchrony was expected to increase as a func-

tion of interpersonal closeness, following the gradient: mother–child dyads showing the highest synchrony, romantic partners intermediate levels, and close friends the lowest.

- Task interactivity was also hypothesized to modulate synchrony, such that passive tasks (e.g., video co-watching) would elicit lower levels of synchrony, structured cooperative tasks would yield moderate synchrony, and free conversational interactions—involving spontaneous and reciprocal exchanges—would produce the highest levels of interpersonal neural synchrony.

4.2 Methods

4.2.1 Study Design

All data for the present study were obtained using an fNIRS hyperscanning design, whereby pairs of participants performed the experimental tasks while their neural activity was recorded simultaneously.

To examine the influence of interpersonal closeness on interpersonal neural synchrony, three dyad types were included: close friends, romantic partners, and mother–child pairs. These relationship categories were selected because they are among the most frequently investigated in the literature on interpersonal synchrony and developmental psychology, are supported by well-established theoretical models, and represent core forms of human social and emotional bonding. Data from close friends and romantic partners were collected at the University of Trento (Italy), whereas data from mother–child dyads were acquired at the University of Vienna (Austria).

Each dyad participated in three social tasks — video co-watching, a structured cooperative game, and an unstructured free conversation — designed to progressively vary in their level of interactivity, ranging from passive and rule-based exchanges to spontaneous and dynamic dialogue.

The study was approved by the Ethics Committees of the University of Trento (ref. 2022-052) and the University of Vienna (ref. 00732). All procedures conformed to the principles outlined in the Declaration of Helsinki. Written informed consent was obtained from all adult participants, and for child participants, consent was provided by their primary caregivers.

4.2.2 Participants

A total of 284 participants (142 dyads) took part in the study. The sample included 70 close-friend dyads (29 male-male dyads, 23 female-female dyads, and 18 male-female dyads; Mean age = 21.60±2.06 years), 39 heterosexual romantic partner dyads (Mean age = 23.45±3.08 years), and 33 mother-child dyads (20 female children, Mean age mother = 38.59 ± 4.66 years, Mean age children = 5 years 6 months 18 days ± 3 months 22 days). Data from two friend dyads, one romantic-partner dyad, and two mother–child dyads were excluded due to technical issues during data collection.

Eligibility criteria varied by relationship type. For close-friend dyads, participants were required to have a friendship without any current or previous romantic involvement. Romantic-partner dyads included only heterosexual couples in an ongoing relationship. Mother–child dyads were restricted to mothers with five-year-old children. All participants reported no history of neurological or medical conditions, particularly

those that could affect blood oxygenation.

Recruitment for close-friend and romantic-partner dyads was conducted through convenience and snowball sampling, using social media and the University of Trento's SONA recruitment platform. Mother–child dyads were recruited from a volunteer database at the University of Vienna. While close-friend and romantic-partner dyads participated without monetary compensation, mother–child pairs received €6 (covering the cost of two round trips on Vienna's public transport) and a small toy for the child (e.g., a €6 Lego set).

4.2.3 Experimental Tasks

For all dyads, each experimental session began with a resting-state recording that served as a baseline measure of neural activity. This period lasted two minutes for adult dyads and one minute for mother–child pairs. In addition, mother–child dyads completed an additional one-minute resting-state interval between each of the experimental tasks. The physical distance between partners was kept consistent across all conditions and dyad types, ranging from 60 to 80 cm, with each participant seated on a separate chair to maintain comparable spatial configurations.

The experimental protocol comprised three tasks: video co-exposure, a rules-based cooperative game, and a free verbal interaction. These conditions were designed to investigate how different degrees of social interactivity modulate interpersonal neural synchrony, ranging from highly structured (video co-exposure), to moderately structured (cooperative game), to fully spontaneous and unstructured forms of interaction (free verbal conversation).

In the video co-exposure condition, dyads viewed a 3-minute, language-

free animated clip presented on a monitor positioned in front of them. The video was carefully chosen to ensure cross-cultural consistency between the two data-collection sites and to avoid any potential confounds related to language processing, while remaining suitable for both adult and child participants. During this task, participants were instructed to refrain from interacting with one another, enabling the assessment of interpersonal neural synchrony driven exclusively by shared perceptual experience in a social context rather than by direct social exchange.

In the rules-based cooperative condition, dyads participated in a 5-minute session of cooperative Jenga. The tower was placed on a table between the two participants, who were instructed to adhere to the game rules: taking turns to remove one block at a time and place it on top of the structure. To ensure a comparable level of difficulty across dyads, participants were asked to remove only one block per layer, beginning from the lower sections of the tower. If the tower collapsed, they were permitted to rebuild it and continue playing, maintaining a constant total task duration. This semi-structured activity provided a controlled yet interactive setting.

In the free verbal interaction condition, participants sat facing one another and engaged in an unstructured 5-minute conversation. Unlike the cooperative Jenga task—which involves rule-based turn-taking and predictable exchanges centered on a shared objective—this condition fostered spontaneous and open-ended dialogue, allowing partners to communicate freely and flexibly in a naturalistic manner.

The order of experimental conditions was randomized across dyads to minimize potential order effects. Resting-state data were not included in the following analyses.

4.2.4 Acquisition of Neural Data

fNIRS hyperscanning was employed throughout all experimental tasks to record participants' neural activity. Each participant wore a cap fitted with eight LED sources emitting light at 760 nm and 850 nm, paired with eight detectors positioned to capture activity from the bilateral IFG and bilateral TPJ, following established protocols in prior research (e.g., Lei et al., 2025; Nguyen, Schleihauf, Kayhan, et al., 2020).

The fNIRS cap configuration differed slightly across the two data-collection sites. For the close-friend and romantic-partner dyads tested in Italy, one detector was dedicated to eight short-distance channels, resulting in a total of 14 channels per participant. In contrast, for the mother–child dyads recorded in Vienna, short-distance channels were not implemented; instead, the eighth detector was used to create two additional long-distance channels, yielding a total of 16 fNIRS channels per participant.

For analysis purposes, fNIRS channels were grouped into four regions of interest: left IFG, right IFG, left TPJ, and right TPJ. The cap configuration for the close friend and romantic partner studies was optimized using the fNIRS Optodes' Location Decider (fOLD) to maximize sensitivity in these target regions (Zimeo Morais et al., 2018) (see Figure 4.1A). In the mother-child study in Austria, due to logistical constraints, the cap arrangement was designed based on protocols from previous adult-child research (Nguyen, Schleihauf, Kayhan, et al., 2020, 2021; Nguyen, Schleihauf, Kungl, et al., 2021) (see Figure 4.1B).

During the experiment, channel placement was based on the international 10-20 EEG system. In the Italian data collection, optode stabilizers ensured that the distance between sources and detectors remained

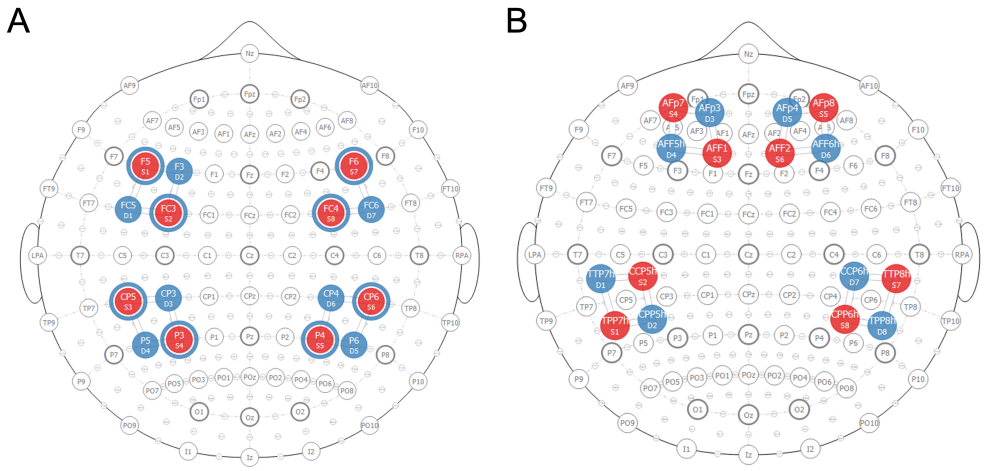

Figure 4.1: Diagram of the functional near-infrared spectroscopy (fNIRS) cap setup, illustrating the arrangement of optodes for data collection. Solid red circles represent the light sources, while solid blue circles indicate the light detectors. The blue circles surrounding the light sources represent short-separation channels. **(A)** Diagram of the cap setup used for close friends and romantic partner dyads in Italy. **(B)** Diagram of the cap setup used for mother-child dyads in Austria. Image from Carollo, Bizzego, Schäfer, et al. (2025).

below 3 cm, optimizing signal quality and minimizing noise. Different fNIRS devices were used across sites: the Italian study employed a NIRSport2 system (NIRx Medical Technologies LLC) with a sampling rate of 10.17 Hz, whereas the Austrian study used a NIRSport device (NIRx Medical Technologies LLC) operating at 7.81 Hz.

4.2.5 Processing of Neural Data

Preprocessing and synchrony analyses were conducted using the *pyphysio* library (Bizzego, Battisti, et al., 2019). Initially, raw fNIRS intensity signals were converted into changes in optical density. To ensure comparability across conditions, only the first three minutes of each experimental task were retained for analysis. Signal quality was then assessed using a convolutional neural network specifically trained to classify the quality

of fNIRS segments (Bizzego, Gabrieli, & Esposito, 2021; Bizzego, Neoh, et al., 2022). The data were subsequently resampled at 10 Hz and transformed into oxygenated (HbO) and deoxygenated (HbR) hemoglobin concentration changes using the modified Beer–Lambert law (D. T. Delpy et al., 1988). Consistent with previous work (e.g., Lim et al., 2024a, 2024b), statistical analyses focused exclusively on HbO signals. Finally, to mitigate temporal autocorrelation and physiological noise, the time series were pre-whitened using an autoregressive model (Barker et al., 2013), a step demonstrated to reduce false discovery rates in coherence estimation (Santosa et al., 2017).

4.2.6 Interpersonal Neural Synchrony

Interpersonal neural synchrony was assessed on a channel-by-channel basis between participants using WTC (Grinsted et al., 2004). For each pair of high-quality channels within each experimental task, WTC was computed across a frequency range of 0.01–0.20 Hz, with steps of 0.01 Hz, following established procedures (Carollo, Stella, et al., 2025; Lim et al., 2024a, 2024b). The final coherence value for each channel pair was obtained by averaging across the entire frequency spectrum, ensuring an unbiased analysis without relying on pre-specified frequency bands (Carollo, Stella, et al., 2025).

To estimate a baseline level of synchrony unrelated to direct interaction, we also calculated WTC for surrogate dyads—pairs of participants who performed the same experimental task but were not actual partners. These surrogate dyads were created by randomly pairing individuals from different original dyads of the same type (e.g., friend with friend, mother with child), while avoiding any cross-cohort pairings. Following Carollo,

Stella, et al. (2025), a single permutation of participants was performed, yielding the same number of data points as in the real dyads.

For each surrogate pair, data segments were matched by channel and experimental task to ensure consistency (e.g., channel X during the video co-exposure task from participant A in dyad 001 was paired with channel X from participant B in dyad 002 for the same task). Synchrony measured in these surrogate dyads reflects stimulus-driven effects alone, providing a reference to distinguish task-related synchrony from the additional neural alignment arising from co-presence in true dyads (Golland et al., 2015).

4.2.7 Data Analysis

The data analysis in this study was conducted in three main stages:

1. Identification of significant region-pair synchrony: Determine which combinations of brain regions across participants exhibit statistically significant differences in WTC between true dyads and surrogate dyads.

2. Global effects of relational factors: Assess how interpersonal closeness and task interactivity influence overall interpersonal neural synchrony across all region-pair combinations.

3. Localized effects of relational factors: Examine how interpersonal closeness and task interactivity modulate neural synchrony in specific region-to-region pairs between participants.

For all analytical steps, we employed linear mixed-effects models (Bates et al., 2005), which are particularly suitable for unbalanced datasets

as they can effectively accommodate unequal group sizes and missing data. Prior to the analyses, we generated two types of region-combination identifiers: one that treated region pairs as order-independent (e.g., region X in participant A paired with region Y in participant B considered equivalent to region Y in participant A paired with region X in participant B), and another that treated the order as distinct (e.g., the two pairings considered separately). Using these identifiers, we then conducted:

1. We ran separate linear mixed-effects models for each combination of regions of interest (treating region order as irrelevant) between participants, with WTC scores as the dependent variable and dyad type (true vs. surrogate) as a fixed effect. Random effects included dyad relationship type (close friends, romantic partners, mother-child), experimental condition (video co-exposure, rules-based cooperative game, free verbal interaction), and dyad ID. For models involving non-homologous brain region pairs, the order-dependent region combination IDs were also included as a random effect. A Bonferroni correction was applied to account for multiple comparisons, providing conservative control over false positives.

2. We implemented a single linear mixed-effects model across all brain region combinations to assess the overall influence of interpersonal closeness and task interactivity on interpersonal neural synchrony, using only true dyads. WTC scores served as the dependent variable, with dyad type and experimental task included as fixed effects. Random effects comprised both order-independent and order-dependent region combination IDs, as well as dyad IDs. *Post hoc*

pairwise comparisons of marginal means were conducted to identify significant differences between levels of each main factor, with a Bonferroni correction applied to control for multiple comparisons.

3. We ran separate linear mixed-effects models for each combination of regions of interest (regardless of order) between participants. In these models, WTC scores from true dyads served as the dependent variable, with dyad type and experimental task included as fixed effects. Random effects included dyad IDs and, for non-homologous region combinations, order-dependent region combination IDs. *Post hoc* pairwise comparisons of marginal means were conducted, with Bonferroni correction applied to control for multiple comparisons and reduce the risk of Type I errors.

4.3 Results

4.3.1 Neural Synchrony in True Versus Surrogate Dyads

In the first stage of the analysis, we used a linear mixed model to test the differences in interpersonal neural synchrony between true and surrogate dyads for each combination of brain regions between the two participants. The results revealed significant differences in synchrony across all brain region combinations, with true dyads showing higher levels of synchrony compared to surrogate dyads (i.e., left IFG–left IFG: $t = 12.48$, $p < .001$, $q < .001$, $d = 0.24$, 95% CI [0.20, 0.27]; left IFG–right IFG: $t = 18.60$, $p < .001$, $q < .001$, $d = 0.25$, 95% CI [0.22, 0.28]; left IFG–left TPJ: $t = 16.48$, $p < .001$, $q < .001$, $d = 0.22$, 95% CI [0.20, 0.25]; left IFG–

right TPJ: $t = 13.15$, $p < .001$, $q < .001$, $d = 0.23$, 95% CI [0.19, 0.26]; right IFG–right IFG: $t = 16.81$, $p < .001$, $q < .001$, $d = 0.32$, 95% CI [0.29, 0.36]; right IFG–left TPJ: $t = 19.20$, $p < .001$, $q < .001$, $d = 0.26$, 95% CI [0.23, 0.29]; right IFG–right TPJ: $t = 13.77$, $p < .001$, $q < .001$, $d = 0.24$, 95% CI [0.21, 0.28]; left TPJ–left TPJ: $t = 11.80$, $p < .001$, $q < .001$, $d = 0.23$, 95% CI [0.19, 0.27]; left TPJ–right TPJ: $t = 10.20$, $p < .001$, $q < .001$, $d = 0.18$, 95% CI [0.15, 0.21]; right TPJ–right TPJ: $t = 5.42$, $p < .001$, $q < .001$, $d = 0.17$, 95% CI [0.11, 0.23]; see Figure 4.2). These results suggest that neural synchrony in real interacting dyads differs significantly from that observed in surrogate, non-interacting pairs—particularly within the right IFG. This finding supports the idea that social interaction and co-presence promote the emergence of interpersonal neural synchrony. Based on these statistical differences, all data from true dyads across the various ROI combinations were retained for subsequent analyses.

4.3.2 Interpersonal Closeness and Social Interactivity on Neural Synchrony (All Combinations of Regions)

In the second stage of our analysis, we conducted a linear mixed model to examine the effects of interpersonal closeness and levels of social interactivity on interpersonal neural synchrony across all regions of interest. Our results indicate that both interpersonal closeness ($F(2, 131) = 10.60$, $p < .001$, partial $\eta^2 = 0.14$, 95% CI [0.05, 1.00]; see Figure 4.3A) and social interactivity ($F(2, 71{,}653) = 185.81$, $p < .001$, partial $\eta^2 = 0.01$, 95% CI [0.00, 1.00]; see Figure 4.3B) have a statistically significant effect

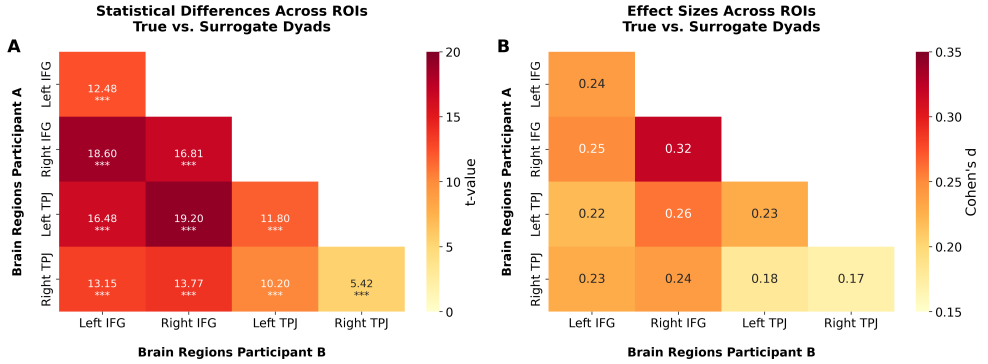

Figure 4.2: **(A)** Comparisons between true and surrogate dyads in terms of interpersonal neural synchrony. For each pairwise combination of brain regions of interest (ROIs; i.e., bilateral inferior frontal gyri (IFG) and bilateral temporo-parietal junctions (TPJ)) between the two participants, we report the corresponding t-values and their significance levels. A linear mixed-effects model was applied, with wavelet transform coherence scores as the dependent variable and dyad type (true *vs.* surrogate) as a fixed effect. Random effects included dyadic relationships, experimental conditions, and dyad IDs. For non-homologous region pairs, an order-specific region combination ID was also included as a random effect. Bonferroni correction was applied to account for multiple comparisons (*** $q < .001$). **(B)** Effect sizes (Cohen's d) corresponding to the contrasts reported in panel **A**. Image from Carollo, Bizzego, Schäfer, et al. (2025).

on interpersonal neural synchrony scores. Additionally, a statistically significant interaction effect between interpersonal closeness and social interactivity on interpersonal neural synchrony emerged ($F(4, 71{,}654) = 69.14$, $p < .001$, partial $\eta^2 = 0.01$, 95% CI [0.00, 1.00]).

Pairwise comparisons of marginal means revealed significant differences in interpersonal neural synchrony between close friend dyads and mother-child dyads (estimate = 0.00586, Standard Error (SE) = 0.00128, $z = 4.57$, $q < .001$, $d = 0.42$, 95% CI [0.24, 0.60]), as well as between romantic partners and mother-child dyads (estimate = 0.00466, SE = 0.00143, $z = 3.26$, $q = .003$, $d = 0.33$, 95% CI [0.13, 0.53]). However, no significant difference was found between close friend dyads and romantic

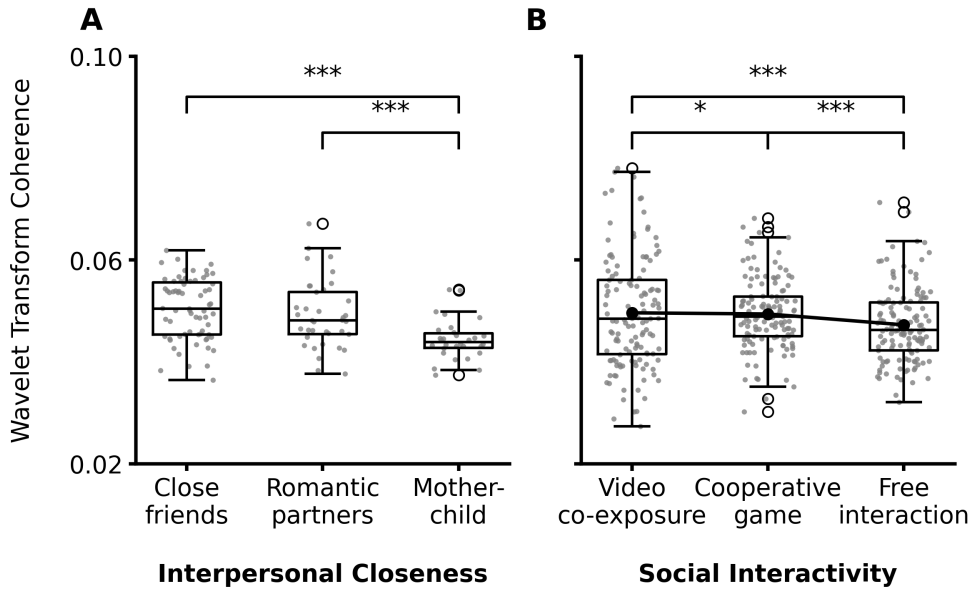

Figure 4.3: **(A)** Comparison of overall interpersonal neural synchrony scores across different levels of interpersonal closeness (i.e., close friends, romantic partners, and mother-child dyads). **(B)** Comparison of overall interpersonal neural synchrony scores across varying levels of social interactivity (i.e., video co-exposure, rules-based cooperative game, and free verbal interaction). (* $q < .05$; *** $q < .001$). Image from Carollo, Bizzego, Schäfer, et al. (2025).

partner dyads ($q > .05$).

Further *post hoc* analyses showed significant differences in interpersonal neural synchrony between video co-exposure and rules-based cooperative game (estimate = 0.000353, SE = 0.000136, $z = 2.59$, $q = .029$, $d = 0.03$, 95% CI [0.01, 0.04]), video co-exposure and free verbal interaction (estimate = 0.002411, SE = 0.000135, $z = 17.82$, $q < .001$, $d = 0.17$, 95% CI [0.15, 0.19]), and rules-based cooperative game and free verbal interaction (estimate = 0.002058, SE = 0.000136, $z = 15.18$, $q < .001$, $d = 0.15$, 95% CI [0.13, 0.17]).

Post hoc analyses examining the interaction between interpersonal closeness and social interactivity on interpersonal neural synchrony revealed distinct patterns across dyad types and tasks. Within each dyad

type, close friends and romantic partners exhibited a consistent trend: synchrony was highest during video co-exposure, intermediate during the cooperative game, and lowest during free interaction, reflecting the pattern observed in the main effects. In contrast, mother–child dyads showed no statistically significant differences in interpersonal neural synchrony across levels of social interactivity. Table 4.1 provides the full set of comparisons and associated statistics for these effects.

Contrast	Estimate	Standard Error	z-ratio	q	Cohen's d 95% CI
Close friends					
Video–Cooperative game	0.00061	0.0002	3.28	.038 *	0.04 [0.02, 0.07]
Video–Free interaction	0.00216	0.0002	11.94	< .001 ***	0.15 [0.13, 0.18]
Cooperative game–Free interaction	0.00155	0.0002	8.35	< .001 ***	0.11 [0.08, 0.14]
Romantic partners					
Video–Cooperative game	0.00090	0.0003	3.60	.011 *	0.06 [0.03, 0.10]
Video–Free interaction	0.00537	0.0002	21.53	< .001 ***	0.38 [0.35, 0.42]
Cooperative game–Free interaction	0.00447	0.0003	17.68	< .001 ***	0.32 [0.28, 0.35]
Mother-child					
Video–Cooperative game	-0.00045	0.0003	-1.71	> .05	/
Video–Free interaction	-0.00030	0.0003	-1.12	> .05	/
Cooperative game–Free interaction	0.00016	0.0003	0.61	> .05	/
Video co-exposure					
Close friends–Romantic partners	0.00003	0.0012	0.02	> .05	/
Close friends–Mother-child	0.00703	0.0013	5.43	< .001 ***	0.50 [0.32, 0.68]
Romantic partners–Mother-child	0.00700	0.0014	4.84	< .001 ***	0.50 [0.30, 0.70]
Cooperative game					
Close friends–Romantic partners	0.00032	0.0012	0.26	> .05	/
Close friends–Mother-child	0.00597	0.0013	4.61	< .001 ***	0.43 [0.25, 0.61]
Romantic partners–Mother-child	0.00565	0.0014	3.90	.004 **	0.40 [0.20, 0.61]
Free interaction					
Close friends–Romantic partners	0.00324	0.0012	2.68	> .05	/
Close friends–Mother-child	0.00458	0.0013	3.54	.015 *	0.33 [0.15, 0.51]
Romantic partners–Mother-child	0.00134	0.0014	0.92	> .05	/

Table 4.1: Results from the *post hoc* pairwise comparisons of the interaction between interpersonal closeness and social interactivity on interpersonal neural synchrony (across all brain region combinations). For each level of one factor, the table reports the estimated contrasts between two levels of the other factor, together with the standard error, z-ratio, corrected q-value, and Cohen's d. (* $q < .05$; ** $q < .01$; *** $q < .001$).

Additionally, in both the video co-exposure and cooperative game conditions, mother–child dyads exhibited the lowest levels of synchrony compared to close friends and romantic partners, with no statistically significant differences between the latter two groups. In the free interaction condition, only close friends showed higher synchrony than mother–child dyads, while no significant differences were observed between close friends and romantic partners, or between romantic partners and mother–child

dyads. The complete set of comparisons and statistics for these effects is provided in Table 4.1.

These results indicate that both the nature of the relationship between individuals and the type of social interaction they engage in are important factors influencing interpersonal neural synchrony. Furthermore, examination of effect sizes suggests that interpersonal closeness may have a stronger impact on neural synchrony than the level of social interactivity.

4.3.3 Interpersonal Closeness and Social Interactivity on Neural Synchrony (Individual Combinations of Regions)

In the third stage of our analysis, we applied linear mixed-effects models to investigate the influence of interpersonal closeness and social interactivity on interpersonal neural synchrony across individual pairs of ROIs. The results revealed that both interpersonal closeness and social interactivity had statistically significant effects on synchrony scores for the following brain region pairs: left IFG–left IFG, left IFG–right IFG, left IFG–left TPJ, right IFG–right IFG, right IFG–left TPJ, and right IFG–right TPJ.

In contrast, social interactivity—but not interpersonal closeness—exerted a statistically significant effect on synchrony in the following brain region pairs: left IFG–right TPJ, left TPJ–left TPJ, left TPJ–right TPJ, and right TPJ–right TPJ. Table 4.2 reports the results of the analysis investigating the effect of interpersonal closeness and social interactivity levels on interpersonal neural synchrony across combinations of ROIs.

Factor	Sum Sq	Mean Sq	NumDf	DenDf	*F*	*p*	*q*	partial η^2 95% CI
Left inferior frontal gyrus – left inferior frontal gyrus								
Interpersonal closeness	0.003	0.001	2	130.2	8.31	< .001	.008 **	0.11 [0.04, 1.00]
Social interactivity	0.013	0.006	2	5581.1	37.42	< .001	< .001 ***	0.01[0.01, 1.00]
Left inferior frontal gyrus – right inferior frontal gyrus								
Interpersonal closeness	0.008	0.004	2	132.4	20.98	< .001	< .001 ***	0.24 [0.14, 1.00]
Social interactivity	0.020	0.010	2	11,072.3	51.95	< .001	< .001 ***	0.01 [0.01, 1.00]
Left inferior frontal gyrus – left temporoparietal junction								
Interpersonal closeness	0.003	0.001	2	131.8	7.54	< .001	.016 *	0.10 [0.03, 1.00]
Social interactivity	0.008	0.004	2	11,012.8	22.45	< .001	< .001 ***	0.004 [0.00, 1.00]
Left inferior frontal gyrus – right temporoparietal junction								
Interpersonal closeness	0.002	0.001	2	128.3	4.86	.009	.185	/
Social interactivity	0.010	0.005	2	6603.0	29.80	< .001	< .001 ***	0.01 [0.01, 1.00]
Right inferior frontal gyrus – right inferior frontal gyrus								
Interpersonal closeness	0.008	0.004	2	131.2	20.44	< .001	< .001 ***	0.24 [0.13, 1.00]
Social interactivity	0.021	0.011	2	5390.5	55.16	< .001	< .001 ***	0.02 [0.01, 1.00]
Right inferior frontal gyrus – left temporoparietal junction								
Interpersonal closeness	0.006	0.003	2	132.2	14.51	< .001	< .001 ***	0.18 [0.09, 1.00]
Social interactivity	0.027	0.014	2	10,838.9	66.97	< .001	< .001 ***	0.01 [0.01, 1.00]
Right inferior frontal gyrus – right temporoparietal junction								
Interpersonal closeness	0.004	0.002	2	127.5	9.75	< .001	.002 **	0.13 [0.05, 1.00]
Social interactivity	0.003	0.001	2	6451.6	7.66	< .001	.010 *	0.002 [0.00, 1.00]
Left temporoparietal junction – left temporoparietal junction								
Interpersonal closeness	0.0003	0.0002	2	128.7	0.84	.434	.999	/
Social interactivity	0.013	0.007	2	5337.3	36.71	< .001	< .001 ***	0.01 [0.00, 1.00]
Left temporoparietal junction – right temporoparietal junction								
Interpersonal closeness	0.0005	0.0002	2	128.8	1.11	0.33	.999	/
Social interactivity	0.005	0.002	2	6435.1	13.50	< .001	< .001 ***	0.004 [0.00, 1.00]
Right temporoparietal junction – right temporoparietal junction								
Interpersonal closeness	0.0001	0.0001	2	119.14	0.35	.705	.999	/
Social interactivity	0.004	0.002	2	2014.71	13.06	< .001	< .001 ***	0.01 [0.00, 1.00]

Table 4.2: Results of the analysis examining the main effects of interpersonal closeness and social interactivity on interpersonal neural synchrony across different combinations of brain regions. For each combination, we report the Sum of Squares (Sum Sq), Mean Square (Mean Sq), numerator and denominator degrees of freedom (NumDf, DenDf), F-value, p-value, corrected q-value, and partial η^2. (* $q < .05$; ** $q < .01$; *** $q < .001$).

Pairwise comparisons of marginal means revealed that close friends exhibited significantly higher interpersonal neural synchrony than mother-child dyads in the left IFG–left IFG, left IFG–right IFG, left IFG–left TPJ, right IFG–right IFG, right IFG–left TPJ, and right IFG–right TPJ. Moreover, romantic partners showed significantly higher brain synchrony than mother-child dyads in the left IFG–right IFG, right IFG–right IFG, right IFG–left TPJ, and right IFG–right TPJ. The complete results of these analyses are presented in Table 4.3 and represented in Figure 4.4. These findings suggest that interpersonal neural synchrony is generally stronger among close friends and romantic partners compared to mother-child dyads, as found in the analysis presented in Section 4.3.2.

Contrast	Estimate	Standard Error	z-ratio	q	Cohen's d 95% CI
Left inferior frontal gyrus – left inferior frontal gyrus					
Close friends–Romantic partners	0.00222	0.0013	1.68	> .05	/
Close friends–Mother-child	0.00579	0.0014	4.06	< .001 ***	0.45 [0.23, 0.66]
Romantic partners–Mother-child	0.00357	0.0016	2.25	> .05	/
Left inferior frontal gyrus – right inferior frontal gyrus					
Close friends–Romantic partners	0.00147	0.0013	1.16	> .05	/
Close friends–Mother-child	0.00878	0.0014	6.40	< .001 ***	0.63 [0.44, 0.83]
Romantic partners–Mother-child	0.00730	0.0015	4.77	< .001 ***	0.53 [0.31, 0.75]
Left inferior frontal gyrus – left temporoparietal junction					
Close friends–Romantic partners	0.00173	0.0013	1.39	> .05	/
Close friends–Mother-child	0.00524	0.0014	3.88	< .001 ***	0.39 [0.19, 0.59]
Romantic partners–Mother-child	0.00351	0.0015	2.33	> .05	/
Right inferior frontal gyrus – right inferior frontal gyrus					
Close friends–Romantic partners	0.00046	0.0016	0.29	> .05	/
Close friends–Mother-child	0.01080	0.0018	6.13	< .001 ***	0.78 [0.53, 1.02]
Romantic partners–Mother-child	0.01034	0.0020	5.27	< .001 ***	0.74 [0.47, 1.02]
Right inferior frontal gyrus – left temporoparietal junction					
Close friends–Romantic partners	0.00074	0.0015	0.51	> .05	/
Close friends–Mother-child	0.00825	0.0016	5.23	< .001 ***	0.58 [0.36, 0.80]
Romantic partners–Mother-child	0.00751	0.0018	4.26	< .001 ***	0.53 [0.29, 0.77]
Right inferior frontal gyrus – right temporoparietal junction					
Close friends–Romantic partners	0.00142	0.0013	1.09	> .05	/
Close friends–Mother-child	0.00618	0.0014	4.40	< .001 ***	0.44 [0.25, 0.64]
Romantic partners–Mother-child	0.00476	0.0016	3.03	.007 **	0.34 [0.12, 0.56]

Table 4.3: Results of the *post hoc* pairwise comparisons examining the effect of interpersonal closeness on interpersonal neural synchrony across different brain region combinations. For each combination, we report the estimated contrast between two levels of interpersonal closeness, along with the standard error, z-ratio, corrected q-value, and Cohen's d. (** $q < .01$; *** $q < .001$).

Furthermore, regarding the effect of social interactivity, pairwise comparisons of marginal means revealed distinct synchrony patterns across different brain region pairs. Notably, the video co-exposure condition exhibited significantly greater synchrony than the other experimental tasks in the following combinations: right IFG–right IFG, right IFG–left TPJ, left TPJ–left TPJ, and left TPJ–right TPJ. In contrast, the rules-based cooperative game condition demonstrated the highest synchrony for left IFG–left IFG and left IFG–right TPJ. Additionally, both the video co-exposure and rules-based cooperative game conditions showed greater synchrony than free interaction in the following region pairs: left IFG–right IFG, left IFG–left TPJ, right IFG–right TPJ, and right TPJ–right TPJ. Overall, across all experimental tasks, free interaction consistently exhibited the lowest level of interpersonal neural synchrony. The full re-

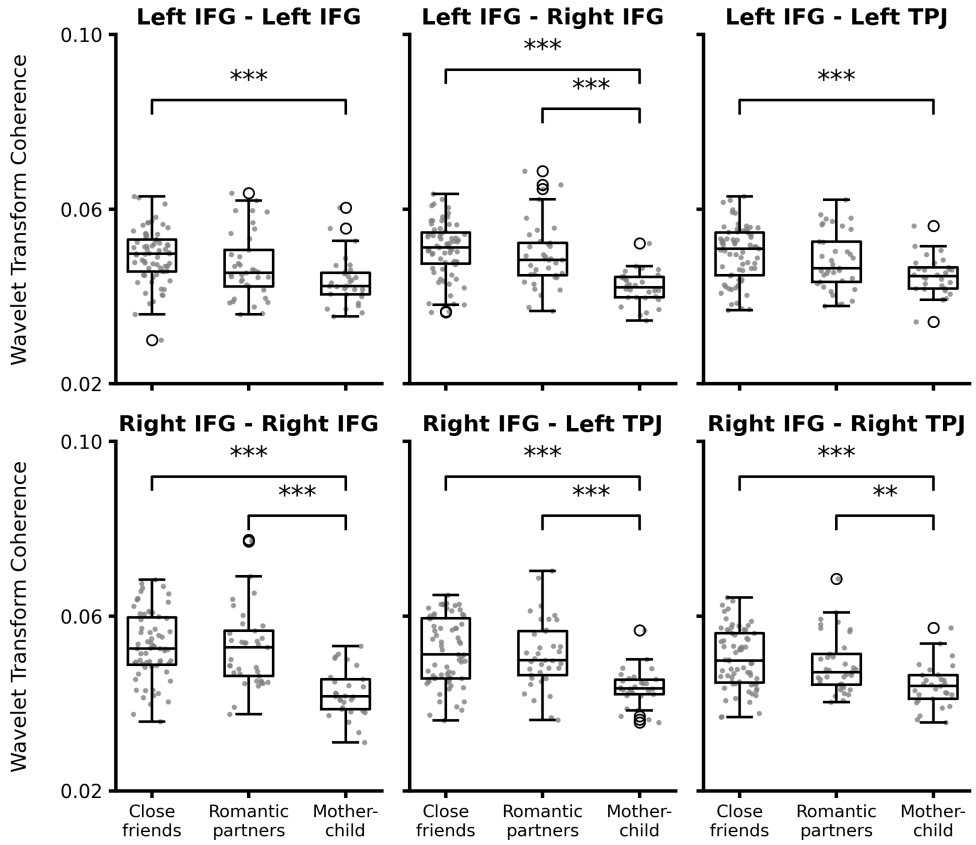

Figure 4.4: Effect of interpersonal closeness on interpersonal neural synchrony across combinations of regions of interest (i.e., bilateral inferior frontal gyri (IFG) and bilateral temporoparietal junctions (TPJ)). (** $q < .01$; *** $q < .001$). Image from Carollo, Bizzego, Schäfer, et al. (2025).

sults detailing the effect of interactivity levels on neural synchrony are provided in Table 4.4 and represented in Figure 4.5.

4.4 Discussion

In this study, we employed fNIRS hyperscanning with a total of 142 dyads to investigate how interpersonal closeness and the level of social interactivity shape interpersonal neural synchrony. Dyads were drawn from three relationship categories—close friends, romantic partners, and

Contrast	Estimate	Standard Error	z-ratio	q	Cohen's d 95% CI
Left inferior frontal gyrus – left inferior frontal gyrus					
Video–Cooperative game	-0.00203	0.0004	-4.73	< .001 ***	-0.16 [-0.22, -0.09]
Video–Free interaction	0.00166	0.0004	3.91	< .001 ***	0.13 [0.06, 0.19]
Cooperative game–Free interaction	0.00369	0.0004	8.64	< .001 ***	0.28 [0.22. 0.35]
Left inferior frontal gyrus – right inferior frontal gyrus					
Video–Cooperative game	-0.000403	0.0003	-1.23	> .05	/
Video–Free interaction	0.002624	0.0003	8.15	< .001 ***	0.19 [0.14, 0.24]
Cooperative game–Free interaction	0.003027	0.0003	9.32	< .001 ***	0.22 [0.17, 0.26]
Left inferior frontal gyrus – left temporoparietal junction					
Video–Cooperative game	-0.000124	0.0003	-0.40	> .05	/
Video–Free interaction	0.001758	0.0003	5.61	< .001 ***	0.13 [0.09, 0.18]
Cooperative game–Free interaction	0.001882	0.0003	5.94	< .001 ***	0.14 [0.09, 0.19]
Left inferior frontal gyrus – right temporoparietal junction					
Video–Cooperative game	-0.00251	0.0004	-6.25	< .001 ***	-0.19 [-0.25, -0.13]
Video–Free interaction	0.00032	0.0004	0.81	> .05	/
Cooperative game–Free interaction	0.00284	0.0004	7.09	< .001 ***	0.21 [0.15, 0.27]
Right inferior frontal gyrus – right inferior frontal gyrus					
Video–Cooperative game	0.00220	0.0005	4.70	< .001 ***	0.16 [0.09, 0.22]
Video–Free interaction	0.00484	0.0005	10.49	< .001 ***	0.35 [0.28, 0.41]
Cooperative game–Free interaction	0.00264	0.0005	5.66	< .001 ***	0.19 [0.12, 0.26]
Right inferior frontal gyrus – left temporoparietal junction					
Video–Cooperative game	0.00253	0.0003	7.47	< .001 ***	0.18 [0.13, 0.23]
Video–Free interaction	0.00379	0.0003	11.38	< .001 ***	0.27 [0.22, 0.31]
Cooperative game–Free interaction	0.00127	0.0003	3.76	< .001 ***	0.09 [0.04, 0.14]
Right inferior frontal gyrus – right temporoparietal junction					
Video–Cooperative game	-0.000583	0.0004	-1.36	> .05	/
Video–Free interaction	0.001057	0.0004	2.50	.037 *	0.08 [0.02, 0.14]
Cooperative game–Free interaction	0.001640	0.0004	3.85	< .001 ***	0.12 [0.06, 0.18]
Left temporoparietal junction – left temporoparietal junction					
Video–Cooperative game	0.003630	0.0005	7.93	< .001 ***	0.27 [0.20, 0.33]
Video–Free interaction	0.003039	0.0005	6.74	< .001 ***	0.23 [0.16, 0.29]
Cooperative game–Free interaction	-0.000591	0.0005	-1.29	> .05	/
Left temporoparietal junction – right temporoparietal junction					
Video–Cooperative game	0.001644	0.0004	3.94	< .001 ***	0.12 [0.06, 0.18]
Video–Free interaction	0.002009	0.0004	4.89	< .001 ***	0.15 [0.09, 0.21]
Cooperative game–Free interaction	0.000365	0.0004	0.88	> .05	/
Right temporoparietal junction – right temporoparietal junction					
Video–Cooperative game	-0.000603	0.0007	-0.86	> .05	/
Video–Free interaction	0.002724	0.0007	3.94	< .001 ***	0.21 [0.11, 0.31]
Cooperative game–Free interaction	0.003327	0.0007	4.77	< .001 ***	0.26 [0.15, 0.36]

Table 4.4: Results of the *post hoc* pairwise comparisons examining the effect of social interactivity levels on interpersonal neural synchrony across different brain region combinations. For each combination, we report the estimated contrast between two levels of social interactivity, along with the standard error, z-ratio, and corrected q-value, and Cohen's d. (* $q < .05$; *** $q < .001$).

mother–child pairs—chosen to represent distinct degrees of interpersonal closeness. During the experimental session, each dyad completed three types of social tasks that differed in their degree of interactivity: video co-exposure (passive, no direct interaction), a rules-based cooperative game (active, structured interaction), and free conversation (active, unstructured interaction). Drawing on prior work (De Felice, Chand, et al., 2024; Feldman, 2017), we hypothesized that greater interpersonal closeness (mother–child > romantic partners > close friends) and higher levels

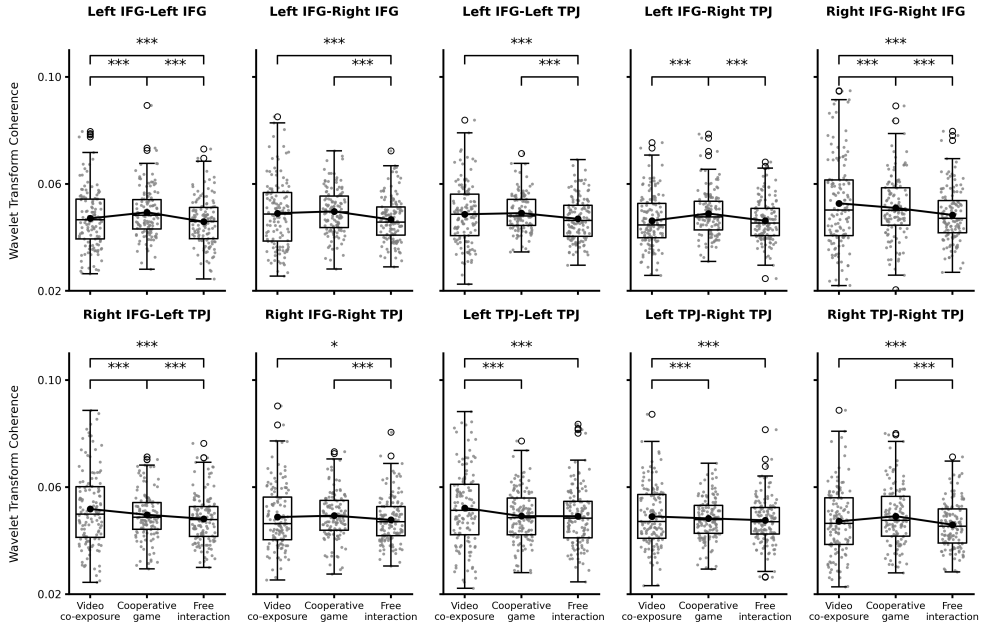

Figure 4.5: Effect of social interactivity on interpersonal neural synchrony across combinations of regions of interest (i.e., bilateral inferior frontal gyri (IFG) and bilateral temporo-parietal junctions (TPJ)). (* $q < .05$; *** $q < .001$). Image from Carollo, Bizzego, Schäfer, et al. (2025).

of social interactivity (free conversation > cooperative game > video co-exposure) would be associated with increased interpersonal neural synchrony.

To test these hypotheses, we first examined neural synchrony patterns across different brain regions, comparing true dyads to surrogate, non-interacting dyads. Our results indicated that interpersonal neural synchrony was significantly higher in true dyads compared to surrogate pairs across all combinations of the bilateral IFG and TPJ. This finding is consistent with prior fNIRS hyperscanning studies in cooperative contexts, which have reported significant interpersonal neural synchrony in frontal and temporo-parietal regions (Czeszumski et al., 2022). Notably, in the present study, the most pronounced difference between real and surrogate dyads was observed in synchrony involving the right IFG. The

IFG is a critical component of the mirror neuron system (Aziz-Zadeh et al., 2006), which supports action understanding and imitation by enabling the brain to internally simulate observed actions (Aziz-Zadeh et al., 2006; Carr et al., 2003; Iacoboni, 2005; Lyons et al., 2006). Mirror neurons are proposed to link passive action observation with the encoding of social perception (Lyons et al., 2006). Concerning the right IFG, research by Adolfi et al. (2017), Bzdok et al. (2012), and Hartwigsen et al. (2019) indicates that anterior portions are involved in higher-level social cognitive processing. Similarly, the TPJ serves as a central hub for mentalizing and perspective-taking, enabling individuals to infer others' thoughts, beliefs, and intentions (Gallagher et al., 2000; Samson et al., 2004; Van Overwalle, 2009; J. Wu et al., 2025; J. Yang et al., 2020). Overall, a plausible mechanism facilitating effective social processing is the temporal alignment of neural activity within mirroring and mentalizing networks to the ongoing dynamics of interaction. This alignment may lead to synchronization of neural signals between individuals, promoting interpersonal neural synchrony and supporting social prediction, communication, and affiliation (Hoehl et al., 2021).

Building on these findings, we further examined how interpersonal closeness and social interactivity modulate neural synchrony across different pairs of brain regions. When considering all region combinations collectively, both factors emerged as significant determinants of interpersonal neural synchrony. However, the observed patterns diverged from our initial predictions: close friends and romantic partners exhibited markedly higher synchrony than mother–child dyads. A similar, though non-significant, trend indicated that romantic partners might display slightly lower synchrony compared to close friends. Unexpectedly,

passive interactions (video co-exposure) elicited stronger neural coupling than both active structured (rules-based cooperative game) and active unstructured (free interaction) tasks, with this pattern being most pronounced in the friend and romantic partner dyads.

The effects of interpersonal closeness remained significant when analyses were restricted to specific brain region pairs, all of which involved the IFG. In line with prior findings on physiological synchrony reported by Bizzego, Azhari, et al. (2019), interpersonal closeness may sometimes show an inverse relationship with synchrony, whereby more distant—but still socially meaningful—relationships exhibit stronger bio-behavioral coupling. As argued by Bizzego, Azhari, et al. (2019), this pattern could stem from the continuous exposure and reduced novelty characterizing highly intimate relationships. Within such established dyads, partners may depend less on physiological or cortical coordination within mirroring and mentalizing networks, as rapid alignment of communicative cues becomes less essential under conditions of greater predictability and lower uncertainty. Extending this reasoning, Nguyen et al. (2024) proposed that heightened neural synchrony may, in some cases, reflect compensatory processes that facilitate behavioral coordination under more demanding or less familiar interactional contexts. An additional, potentially complementary interpretation concerns the functional meaning of positive versus negative synchrony. Rather than solely reflecting degrees of interpersonal closeness or novelty, distinct synchrony profiles may index asymmetric interaction dynamics, such as leader–follower configurations or regulatory scaffolding. In caregiver–child dyads, for example, neural synchrony may reflect complementary rather than parallel activation patterns, consistent with processes of dyadic regulation

and support. Under this view, lower or differently signed synchrony in mother–child pairs would not necessarily indicate reduced alignment, but instead a qualitatively distinct form of coordination shaped by developmental asymmetry.

Beyond interpersonal closeness, developmental factors likely contribute to the observed effects (Hoehl et al., 2025). Neural oscillations and functional dynamics in children differ substantially from those in adults (Meng et al., 2022), and regions supporting social cognition continue to mature throughout adolescence and early adulthood (Gweon et al., 2012; Kolk & Rakic, 2022; J. Wang et al., 2020). Ongoing neurodevelopmental processes, including myelination, synaptic pruning, and the refinement of large-scale network connectivity, influence both the efficiency and coordination of neural activity during social exchanges. Consequently, the lower levels of neural synchrony observed in mother–child dyads in this study may also reflect developmental differences in the maturation of neural systems underlying shared attention, perspective-taking, and interpersonal attunement, rather than differences in relational closeness alone.

Finally, distinct patterns emerged across brain region pairs in relation to the effects of social interactivity on interpersonal neural synchrony. Several region combinations (i.e., right IFG–right IFG, right IFG–left TPJ, left TPJ–left TPJ, and left TPJ–right TPJ) followed the trend described above, showing the strongest synchrony during video co-exposure, intermediate levels during the cooperative game, and the weakest synchrony during free interaction. In contrast, other region pairs (i.e., left IFG–left IFG and left IFG–right TPJ) exhibited the opposite pattern, with the cooperative game eliciting the highest synchrony, followed by

video co-exposure and free interaction. These divergent patterns suggest that distinct neural mechanisms are recruited depending on the type of social engagement. In regions where synchrony peaked during video co-exposure—mainly those involving the right IFG and left TPJ—neural alignment is likely driven by shared perceptual processing in co-presence contexts, as both participants passively experience identical audiovisual stimuli. Conversely, region pairs showing maximal synchrony during the cooperative game—predominantly those connecting the left IFG and right TPJ—may underpin processes related to joint action coordination and shared goal pursuit, which demand active engagement and real-time behavioral coordination. This interpretation aligns with prior studies of cooperative tasks such as Jenga, which reported significant interpersonal synchrony in the IFG (e.g., Y. Li et al. 2021; N. Liu et al. 2016), as well as with intracranial recording evidence demonstrating TPJ involvement in coordination-related activity during cooperative behavior (J. Wang et al., 2025). The present findings extend this literature by revealing lateralized effects, with particularly pronounced synchrony between the left IFG and right TPJ during structured cooperative interaction.

4.5 Limitations

A first consideration concerns the slight methodological and contextual differences across participant groups. Adult–adult dyads and mother–child pairs were tested in different countries (Italy and Austria, respectively) and with two fNIRS systems from the same manufacturer. Although both regions are culturally comparable and methodological consistency was carefully maintained, minor variability related to contextual or device-

specific factors cannot be entirely ruled out (Bizzego, Carollo, Lim, & Esposito, 2024). To mitigate these potential sources of noise, all sessions were conducted by the same researcher (AC) following identical procedures, and a conservative preprocessing pipeline was applied to minimize device-related variance.

A further limitation involves the absence of fine-grained behavioral annotation. While task interactivity provided control at a macro-behavioral level, neural synchrony was not examined in relation to specific moment-to-moment actions. Future studies integrating detailed behavioral coding could help clarify how micro-level interactional dynamics shape interpersonal neural coupling, despite the theoretical and methodological complexity this entails.

Another limitation is that the present study focused exclusively on the bilateral IFG and TPJ, omitting other regions—such as the medial prefrontal cortex—that play key roles in social cognition. Expanding brain coverage in future work would allow a more comprehensive characterization of the neural systems underlying interpersonal synchrony.

Finally, although developmental factors likely contributed to the observed patterns, the inclusion of additional dyad types—such as non-parental adult–child or child–child pairs—would enable a clearer dissociation between effects of neural maturation and those of relationship type. Extending the design to such groups could provide deeper insight into how developmental stage and interpersonal closeness jointly shape the dynamics of neural synchrony.

4.6 Conclusion

In this study, we used fNIRS hyperscanning to examine how interpersonal closeness and social interactivity influence interpersonal neural synchrony, analyzing data from 284 participants. To manipulate interpersonal closeness, we recruited close friends, romantic partners, and mother-child dyads, while social interactivity was varied across three conditions: video co-exposure, a rules-based cooperative game, and free interaction. Our results revealed that the strongest hyperscanning effect emerged between one participant's right IFG and the other's fronto-temporal regions. Across multiple analyses, we observed a general trend indicating that neural synchrony decreases with interpersonal closeness and may also vary with developmental stage. Social interactivity showed a smaller effect overall, though video co-exposure produced the highest synchrony across regions, whereas the cooperative game specifically enhanced synchrony between the left IFG and the other participant's left IFG and right TPJ.

These findings contribute to the growing body of evidence indicating that interpersonal neural synchrony captures the dynamic nature of social relationships and shared experiences (Carollo, Stella, et al., 2025; Lim et al., 2024a, 2024b), with important implications for both developmental and social neuroscience. Understanding how different relationship types and interaction contexts shape neural coupling offers valuable insights into the mechanisms of social cognition, cooperative behavior, and the potential development of therapeutic strategies for individuals with social communication and behavior difficulties, such as those on the autism spectrum. Future research should explore how individual differences in

personality, social competence, and relationship quality modulate neural alignment during real-life interactions. By systematically comparing dyads across a variety of interactive settings, the present work provides a framework for hypothesis-driven hyperscanning research, fostering more integrative models of the neural mechanisms that underpin human social behavior. Taken together, our results underscore that human connection is deeply grounded in the coordination of behavioral, physiological, and neural processes.

Chapter 5

Conclusion

In recent years, fNIRS has become a preferred technique for hyperscanning studies due to its high tolerance for participants' movements (Carollo & Esposito, 2024). This advantage has enabled researchers to explore how the brain supports behavior in naturalistic and interactive contexts, allowing participants to move more freely while their neural activity is recorded. The shift toward ecologically valid paradigms has fostered two parallel developments in the literature: a methodological one, focused on improving data quality and pre-processing pipelines (e.g., Bizzego, Carollo, Lim, and Esposito, 2024; Yücel et al., 2025), and a conceptual one, aimed at understanding how the brain supports social interaction at both interpersonal and intra-personal levels (e.g., Azhari et al., 2019; Lim et al., 2024a; Nguyen, Schleihauf, Kayhan, et al., 2020).

On the methodological side, recent work has concentrated on identifying and correcting motion artifacts in fNIRS signals. Most studies have relied on simulated data or theoretical models of neural activity, often lacking ground-truth information about movement. In this thesis, I contributed to this line of research by: *(i)* demonstrating the feasibility

of extracting reliable movement information during fNIRS experiments using CV approaches (Bizzego, Carollo, Senay, et al., 2024), and *(ii)* leveraging CV-derived movement data to characterize how specific motion patterns relate to fNIRS artifacts (Bizzego et al., 2025). Together, these contributions lay the groundwork for developing and evaluating artifact detection—and eventually correction—algorithms informed by ground-truth movement metrics.

Conceptually, fNIRS hyperscanning has traditionally focused on interpersonal neural synchrony (Feldman, 2012a), often interpreted as a neural marker of interaction quality (Endevelt-Shapira & Feldman, 2023; Nguyen, Schleihauf, Kayhan, et al., 2020). In this thesis, I extended this framework by examining how the brain supports interacting individuals at both interpersonal and intra-personal levels of analysis. Specifically, I found that patterns of interpersonal neural synchrony and functional connectivity are modulated by the linguistic and emotional characteristics of natural dialogues.

With respect to interpersonal neural synchrony, the emotional content of dialogues predicted synchrony at the global (whole-prefrontal) level, whereas syntactic and semantic properties were predictive already at the local level—particularly in the right middle frontal gyrus. Higher linguistic complexity was associated with stronger interpersonal synchrony both locally and globally, suggesting that more cognitively demanding exchanges might require greater cortical coordination between interacting individuals (Carollo, Stella, et al., 2025).

Regarding prefrontal functional connectivity — the intra-personal coupling between brain regions — findings were consistent with previous single-brain studies conducted during controlled experimental tasks

(Carollo, Bizzego, Lim, et al., 2025). Emotional content was primarily linked to connectivity between central and right prefrontal regions, whereas linguistic complexity was associated with enhanced connectivity in left-lateralized networks. Higher levels of expressed anger were related to transient functional segregation within the right hemisphere, while greater linguistic complexity predicted stronger connectivity between the superior and inferior frontal regions in the left hemisphere.

Beyond emotional and linguistic factors, social interactions are also shaped by two broader dimensions: social interactivity and interpersonal closeness. While prior hyperscanning studies have examined their effects separately, few have tested how these dimensions jointly modulate neural synchrony (e.g., Djalovski et al., 2021). To address this gap, the final study in this thesis (Carollo, Bizzego, Schäfer, et al., 2025) tested 284 participants (142 dyads) across three relationship types — close friends, romantic partners, and mother–child pairs — and three levels of interactivity. Contrary to initial expectations, both interpersonal closeness and task interactivity were negatively associated with neural synchrony. Close friends and romantic partners displayed higher synchrony than mother–child dyads, particularly in the bilateral IFG. These results may reflect both developmental factors — since children's neural systems for social cognition are still maturing — and compensatory mechanisms in less established dyads, which may require greater neural alignment to sustain social coordination (Bizzego, Azhari, et al., 2019; Nguyen et al., 2024). Furthermore, passive social contexts, such as joint video watching, elicited the strongest synchrony, likely reflecting alignment driven by shared sensory input in a co-presence context. This pattern was most pronounced in the right IFG and left TPJ, whereas structured cooper-

ative games induced maximal synchrony in the left IFG and right TPJ, suggesting a lateralized effect of task interactivity on neural synchrony.

Overall, this thesis demonstrates the interdependence of methodological and conceptual advances in studying brain activity during naturalistic social interaction. Future research could build on these findings by integrating CV-derived movement data into motion artifact detection and correction algorithms, thereby improving comparability across studies and promoting standardized fNIRS pre-processing pipelines. Applying these approaches to increasingly naturalistic scenarios will further enhance ecological validity and result cross-comparability. Moreover, future work should explore whether elevated interpersonal synchrony — as measured cortically via fNIRS — sometimes reflects over-compensatory coordination in less established dyads or during cognitively demanding exchanges. Taken together, these perspectives have both theoretical and applied significance, contributing to a more integrative understanding of human social neuroscience and informing interventions in educational, clinical, and everyday social contexts.

Bibliography

Aarabi, A., & Huppert, T. J. (2016). Characterization of the relative contributions from systemic physiological noise to whole-brain resting-state functional near-infrared spectroscopy data using single-channel independent component analysis. *Neurophotonics*, *3*(2), 025004–025004.

Abe, M. O., Koike, T., Okazaki, S., Sugawara, S. K., Takahashi, K., Watanabe, K., & Sadato, N. (2019). Neural correlates of online cooperation during joint force production. *NeuroImage*, *191*, 150–161.

Abney, D. H., Paxton, A., Dale, R., & Kello, C. T. (2014). Complexity matching in dyadic conversation. *Journal of Experimental Psychology: General*, *143*(6), 2304.

Acquadro, M. A., Congedo, M., & De Riddeer, D. (2016). Music performance as an experimental approach to hyperscanning studies. *Frontiers in human neuroscience*, *10*, 242.

Adolfi, F., Couto, B., Richter, F., Decety, J., Lopez, J., Sigman, M., Manes, F., & Ibáñez, A. (2017). Convergence of interoception, emotion, and social cognition: A twofold fmri meta-analysis and lesion approach. *Cortex*, *88*, 124–142.

Aitchison, J. (2012). *Words in the mind: An introduction to the mental lexicon*. John Wiley & Sons.

Alizadehgoradel, J., Razavi, S. D., Shirani, Z., Barati, M., Taherifard, M., Nejati, V., & Nitsche, M. A. (2024). Targeting the left dlpfc and right vlpfc in unmarried romantic relationship breakup (love trauma syndrome) with intensified electrical stimulation: A randomized, single-blind, parallel-group, sham-controlled study. *Journal of psychiatric research*, *175*, 170–182.

Alonso-Martin, F., Malfaz, M., Sequeira, J., Gorostiza, J. F., & Salichs, M. A. (2013). A multimodal emotion detection system during human–robot interaction. *Sensors*, *13*(11), 15549–15581.

Anderson, B. J., Vietze, P., & Dokecki, P. R. (1977). Reciprocity in vocal interactions of mothers and infants. *Child Development*, *48*, 1676–1681.

Apicella, F., Chericoni, N., Costanzo, V., Baldini, S., Billeci, L., Cohen, D., & Muratori, F. (2013). Reciprocity in interaction: A window on the first year of life in autism. *Autism Research and Treatment*, *2013*(1), 705895.

Aria, M., & Cuccurullo, C. (2017). Bibliometrix: An r-tool for comprehensive science mapping analysis. *Journal of informetrics*, *11*(4), 959–975.

Ashton–James, C., Van Baaren, R. B., Chartrand, T. L., Decety, J., & Karremans, J. (2007). Mimicry and me: The impact of mimicry on self–construal. *Social cognition*, *25*(4), 518–535.

Astolfi, L., Cincotti, F., Mattia, D., Babiloni, C., Carducci, F., Basilisco, A., Rossini, P., Salinari, S., Ding, L., Ni, Y., et al. (2005). Assessing cortical functional connectivity by linear inverse estimation

and directed transfer function: Simulations and application to real data. *Clinical neurophysiology*, *116*(4), 920–932.

Astolfi, L., Toppi, J., Borghini, G., Vecchiato, G., Isabella, R., Fallani, F. D. V., Cincotti, F., Salinari, S., Mattia, D., He, B., et al. (2011). Study of the functional hyperconnectivity between couples of pilots during flight simulation: An eeg hyperscanning study. *2011 Annual International Conference of the IEEE Engineering in Medicine and Biology Society*, 2338–2341.

Astolfi, L., Toppi, J., Casper, C., Freitag, C., Mattia, D., Babiloni, F., Ciaramidaro, A., & Siniatchkin, M. (2015). Investigating the neural basis of empathy by eeg hyperscanning during a third party punishment. *2015 37th Annual International Conference of the IEEE Engineering in Medicine and Biology Society (EMBC)*, 5384–5387.

Astolfi, L., Toppi, J., De Vico Fallani, F., Vecchiato, G., Salinari, S., Mattia, D., Cincotti, F., & Babiloni, F. (2010). Neuroelectrical hyperscanning measures simultaneous brain activity in humans. *Brain topography*, *23*, 243–256.

Astolfi, L., Toppi, J., Fallani, F. D. V., Vecchiato, G., Cincotti, F., Wilke, C. T., Yuan, H., Mattia, D., Salinari, S., He, B., et al. (2011). Imaging the social brain by simultaneous hyperscanning during subject interaction. *IEEE intelligent systems*, *26*(5), 38.

Atzil, S., & Gendron, M. (2017). Bio-behavioral synchrony promotes the development of conceptualized emotions. *Current opinion in psychology*, *17*, 162–169.

Azhari, A., Bizzego, A., Balagtas, J. P. M., Leng, K. S. H., & Esposito, G. (2022). Asymmetric prefrontal cortex activation associated with

mutual gaze of mothers and children during shared play. *Symmetry*, *14*(5), 998.

Azhari, A., Bizzego, A., & Esposito, G. (2021). Father-child dyads exhibit unique inter-subject synchronization during co-viewing of animation video stimuli. *Social Neuroscience*, *16*(5), 522–533.

Azhari, A., Leck, W. Q., Gabrieli, G., Bizzego, A., Rigo, P., Setoh, P., Bornstein, M. H., & Esposito, G. (2019). Parenting stress undermines mother-child brain-to-brain synchrony: A hyperscanning study. *Scientific reports*, *9*(1), 1–9.

Aziz-Zadeh, L., Koski, L., Zaidel, E., Mazziotta, J., & Iacoboni, M. (2006). Lateralization of the human mirror neuron system. *Journal of Neuroscience*, *26*(11), 2964–2970.

Babiloni, C., Buffo, P., Vecchio, F., Marzano, N., Del Percio, C., Spada, D., Rossi, S., Bruni, I., Rossini, P. M., & Perani, D. (2012). Brains "in concert": Frontal oscillatory alpha rhythms and empathy in professional musicians. *Neuroimage*, *60*(1), 105–116.

Babiloni, C., Vecchio, F., Infarinato, F., Buffo, P., Marzano, N., Spada, D., Rossi, S., Bruni, I., Rossini, P. M., & Perani, D. (2011). Simultaneous recording of electroencephalographic data in musicians playing in ensemble. *cortex*, *47*(9), 1082–1090.

Babiloni, F., & Astolfi, L. (2014). Social neuroscience and hyperscanning techniques: Past, present and future. *Neuroscience & Biobehavioral Reviews*, *44*, 76–93.

Babiloni, F., Cincotti, F., Babiloni, C., Carducci, F., Mattia, D., Astolfi, L., Basilisco, A., Rossini, P. M., Ding, L., Ni, Y., et al. (2005). Estimation of the cortical functional connectivity with the multi-

modal integration of high-resolution eeg and fmri data by directed transfer function. *Neuroimage*, *24*(1), 118–131.

Babiloni, F., Cincotti, F., Mattia, D., de Vico Fallani, F., Tocci, A., Bianchi, L., Salinari, S., Marciani, M., Colosimo, A., & Astolfi, L. (2007). High resolution eeg hyperscanning during a card game. *2007 29th annual international conference of the IEEE engineering in medicine and biology society*, 4957–4960.

Babiloni, F., Cincotti, F., Mattia, D., Mattiocco, M., Fallani, F. D. V., Tocci, A., Bianchi, L., Marciani, M. G., & Astolfi, L. (2006). Hypermethods for eeg hyperscanning. *2006 International Conference of the IEEE Engineering in Medicine and Biology Society*, 3666–3669.

Baess, P., Zhdanov, A., Mandel, A., Parkkonen, L., Hirvenkari, L., Mäkelä, J. P., Jousmäki, V., & Hari, R. (2012). Meg dual scanning: A procedure to study real-time auditory interaction between two persons. *Frontiers in human neuroscience*, *6*, 83.

Baker, W. B., Parthasarathy, A. B., Busch, D. R., Mesquita, R. C., Greenberg, J. H., & Yodh, A. (2014). Modified beer-lambert law for blood flow. *Biomedical optics express*, *5*(11), 4053–4075.

Balconi, M., & Vanutelli, M. E. (2017). Cooperation and competition with hyperscanning methods: Review and future application to emotion domain. *Frontiers in computational neuroscience*, *11*, 86.

Balconi, M., Vanutelli, M. E., & Gatti, L. (2018). Functional brain connectivity when cooperation fails. *Brain and cognition*, *123*, 65–73.

Balters, S., Baker, J. M., Hawthorne, G., & Reiss, A. L. (2020). Capturing human interaction in the virtual age: A perspective on the

future of fnirs hyperscanning. *Frontiers in Human Neuroscience*, *14*, 588494.

Barde, A., Gumilar, I., Hayati, A. F., Dey, A., Lee, G., & Billinghurst, M. (2020). A review of hyperscanning and its use in virtual environments. *Informatics*, *7*(4), 55.

Barker, J. W., Aarabi, A., & Huppert, T. J. (2013). Autoregressive model based algorithm for correcting motion and serially correlated errors in fnirs. *Biomedical Optics Express*, *4*(8), 1366–1379.

Bates, D., et al. (2005). Fitting linear mixed models in r. *R news*, *5*(1), 27–30.

Benjamini, Y., & Hochberg, Y. (2000). On the adaptive control of the false discovery rate in multiple testing with independent statistics. *Journal of Educational and Behavioral Statistics*, *25*(1), 60–83.

Bizzego, A., Azhari, A., Campostrini, N., Truzzi, A., Ng, L. Y., Gabrieli, G., Bornstein, M. H., Setoh, P., & Esposito, G. (2019). Strangers, friends, and lovers show different physiological synchrony in different emotional states. *Behavioral Sciences*, *10*(1), 11.

Bizzego, A., Azhari, A., & Esposito, G. (2021). Assessing computational methods to quantify mother-child brain synchrony in naturalistic settings based on fnirs signals. *Neuroinformatics*, *20*, 1–10.

Bizzego, A., Azhari, A., & Esposito, G. (2022). Correction to: Reproducible inter-personal brain coupling measurements in hyperscanning settings with functional near infra-red spectroscopy. *Neuroinformatics*, *20*(3), 677–677.

Bizzego, A., Balagtas, J. P. M., & Esposito, G. (2020). Commentary: Current status and issues regarding pre-processing of fnirs neuroimaging data: An investigation of diverse signal filtering meth-

ods within a general linear model framework. *Frontiers in Human Neuroscience*, *14*, 247.

Bizzego, A., Battisti, A., Gabrieli, G., Esposito, G., & Furlanello, C. (2019). Pyphysio: A physiological signal processing library for data science approaches in physiology. *SoftwareX*, *10*, 100287.

Bizzego, A., Carollo, A., Fong, S., Furlanello, C., & Esposito, G. (2025). Characterizing motion artifacts in functional near-infrared spectroscopy signals using ground-truth movement information and computer vision. *Biomedical Signal Processing and Control*, *110*, 108256.

Bizzego, A., Carollo, A., Lim, M., & Esposito, G. (2024). Effects of individual research practices on fnirs signal quality and latent characteristics. *IEEE Transactions on Neural Systems & Rehabilitation Engineering*, *32*, 3515–3521.

Bizzego, A., Carollo, A., Senay, B., Fong, S., Furlanello, C., & Esposito, G. (2024). Computer vision-driven movement annotations to advance fnirs pre-processing algorithms. *Sensors*, *24*(21), 6821.

Bizzego, A., Gabrieli, G., Azhari, A., Lim, M., & Esposito, G. (2022). Dataset of parent-child hyperscanning functional near-infrared spectroscopy recordings. *Scientific Data*, *9*(1), 625.

Bizzego, A., Gabrieli, G., & Esposito, G. (2021). Deep neural networks and transfer learning on a multivariate physiological signal dataset. *Bioengineering*, *8*(3), 35.

Bizzego, A., Neoh, M., Gabrieli, G., & Esposito, G. (2022). A machine learning perspective on fnirs signal quality control approaches. *IEEE Transactions on Neural Systems and Rehabilitation Engineering*, *30*, 2292–2300.

Bohsali, A. A., Gullett, J. M., FitzGerald, D. B., Mareci, T., Crosson, B., White, K., & Nadeau, S. E. (2025). Neural connectivity underlying core language functions. *Brain and Language*, *262*, 105535.

Bojczyk, K. E., Davis, A. E., & Rana, V. (2016). Mother–child interaction quality in shared book reading: Relation to child vocabulary and readiness to read. *Early childhood research quarterly*, *36*, 404–414.

Bolis, D., Dumas, G., & Schilbach, L. (2023). Interpersonal attunement in social interactions: From collective psychophysiology to interpersonalized psychiatry and beyond. *Philosophical Transactions of the Royal Society B*, *378*(1870), 20210365.

Bornstein, M. H., & Esposito, G. (2023). Coregulation: A multilevel approach via biology and behavior. *Children*, *10*(8), 1323.

Bowlby, J., & Holmes, J. (2012). *A secure base*. Routledge: London.

Brigadoi, S., Ceccherini, L., Cutini, S., Scarpa, F., Scatturin, P., Selb, J., Gagnon, L., Boas, D. A., & Cooper, R. J. (2014). Motion artifacts in functional near-infrared spectroscopy: A comparison of motion correction techniques applied to real cognitive data. *Neuroimage*, *85*, 181–191.

Broca, P. (1861). Remarques sur le siège de la faculté du langage articulé, suivies d'une observation d'aphémie (perte de la parole). *Bulletin et Memoires de la Societe anatomique de Paris*, *6*, 330–357.

Brown, V. A. (2021). An introduction to linear mixed-effects modeling in r. *Advances in Methods and Practices in Psychological Science*, *4*(1), 2515245920960351.

Bzdok, D., Schilbach, L., Vogeley, K., Schneider, K., Laird, A. R., Langner, R., & Eickhoff, S. B. (2012). Parsing the neural correlates of moral

cognition: Ale meta-analysis on morality, theory of mind, and empathy. *Brain Structure and Function*, *217*, 783–796.

Carollo, A., Bizzego, A., Gabrieli, G., Wong, K. K.-Y., Raine, A., & Esposito, G. (2021). I'm alone but not lonely. u-shaped pattern of self-perceived loneliness during the covid-19 pandemic in the uk and greece. *Public Health in Practice*, *2*, 100219.

Carollo, A., Bizzego, A., Lim, M., Stella, M., Doderovic, G., & Esposito, G. (2025). Emotional and linguistic features predict prefrontal functional connectivity during ongoing dialogues: An fnirs investigation. *bioRxiv*, 2025–08.

Carollo, A., Bizzego, A., Schäfer, V., Pletti, C., Hoehl, S., & Esposito, G. (2025). Interpersonal neural synchrony across levels of interpersonal closeness and social interactivity. *NeuroImage*, *322*.

Carollo, A., Cataldo, I., Fong, S., Corazza, O., & Esposito, G. (2022). Unfolding the real-time neural mechanisms in addiction: Functional near-infrared spectroscopy (fnirs) as a resourceful tool for research and clinical practice. *Addiction Neuroscience*, *4*, 100048.

Carollo, A., & Esposito, G. (2024). Hyperscanning literature after two decades of neuroscientific research: A scientometric review. *Neuroscience*, *551*, 345–354.

Carollo, A., Lim, M., Aryadoust, V., & Esposito, G. (2021). Interpersonal synchrony in the context of caregiver-child interactions: A document co-citation analysis. *Frontiers in psychology*, *12*, 701824.

Carollo, A., Stella, M., Lim, M., Bizzego, A., & Esposito, G. (2025). Emotional content and semantic structure of dialogues are associated with interpersonal neural synchrony in the prefrontal cortex. *NeuroImage*, *309*, 121087.

Carpenter, M. (2009). Just how joint is joint action in infancy? *Topics in Cognitive Science*, *1*(2), 380–392.

Carr, L., Iacoboni, M., Dubeau, M.-C., Mazziotta, J. C., & Lenzi, G. L. (2003). Neural mechanisms of empathy in humans: A relay from neural systems for imitation to limbic areas. *Proceedings of the National Academy of Sciences*, *100*(9), 5497–5502.

Castro, N., Stella, M., & Siew, C. S. (2020). Quantifying the interplay of semantics and phonology during failures of word retrieval by people with aphasia using a multiplex lexical network. *Cognitive science*, *44*(9), e12881.

Catani, M., Mesulam, M. M., Jakobsen, E., Malik, F., Martersteck, A., Wieneke, C., Thompson, C. K., Thiebaut de Schotten, M., Dell'Acqua, F., Weintraub, S., et al. (2013). A novel frontal pathway underlies verbal fluency in primary progressive aphasia. *Brain*, *136*(8), 2619–2628.

Chan, K. Y., & Vitevitch, M. S. (2010). Network structure influences speech production. *Cognitive science*, *34*(4), 685–697.

Chang, C., & Glover, G. H. (2010). Time–frequency dynamics of resting-state brain connectivity measured with fmri. *Neuroimage*, *50*(1), 81–98.

Chen, C. (2006). Citespace ii: Detecting and visualizing emerging trends and transient patterns in scientific literature. *Journal of the American Society for information Science and Technology*, *57*(3), 359–377.

Chen, J., Leong, Y. C., Honey, C. J., Yong, C. H., Norman, K. A., & Hasson, U. (2017). Shared memories reveal shared structure in neural activity across individuals. *Nature neuroscience*, *20*(1), 115–125.

Christ, S. E., Van Essen, D. C., Watson, J. M., Brubaker, L. E., & McDermott, K. B. (2009). The contributions of prefrontal cortex and executive control to deception: Evidence from activation likelihood estimate meta-analyses. *Cerebral cortex*, *19*(7), 1557–1566.

Ciampelli, S., de Boer, J. N., Voppel, A. E., Corona Hernandez, H., Brederoo, S. G., van Dellen, E., Mota, N. B., & Sommer, I. E. (2023). Syntactic network analysis in schizophrenia-spectrum disorders. *Schizophrenia Bulletin*, *49*(Supplement_2), S172–S182.

Cornejo, C., Cuadros, Z., Morales, R., & Paredes, J. (2017). Interpersonal coordination: Methods, achievements, and challenges. *Frontiers in psychology*, *8*, 1685.

Cui, X., Bryant, D. M., & Reiss, A. L. (2012). Nirs-based hyperscanning reveals increased interpersonal coherence in superior frontal cortex during cooperation. *Neuroimage*, *59*(3), 2430–2437.

Czeszumski, A., Eustergerling, S., Lang, A., Menrath, D., Gerstenberger, M., Schuberth, S., Schreiber, F., Rendon, Z. Z., & König, P. (2020). Hyperscanning: A valid method to study neural inter-brain underpinnings of social interaction. *Frontiers in Human Neuroscience*, *14*, 39.

Czeszumski, A., Liang, S. H.-Y., Dikker, S., König, P., Lee, C.-P., Koole, S. L., & Kelsen, B. (2022). Cooperative behavior evokes interbrain synchrony in the prefrontal and temporoparietal cortex: A systematic review and meta-analysis of fnirs hyperscanning studies. *eNeuro*, *9*(2).

De Felice, S., Hakim, U., Gunasekara, N., Pinti, P., Tachtsidis, I., & Hamilton, A. (2024). Having a chat and then watching a movie:

How social interaction synchronises our brains during co-watching. *Oxford Open Neuroscience*, *3*, kvae006.

De Felice, S., Chand, T., Croy, I., Engert, V., Goldstein, P., Holroyd, C. B., Kirsch, P., Krach, S., Ma, Y., Scheele, D., et al. (2024). Relational neuroscience: Insights from hyperscanning research. *Neuroscience & Biobehavioral Reviews*, *169*, 105979.

De Raedt, R., Leyman, L., Baeken, C., Van Schuerbeek, P., Luypaert, R., Vanderhasselt, M.-A., & Dannlowski, U. (2010). Neurocognitive effects of hf-rtms over the dorsolateral prefrontal cortex on the attentional processing of emotional information in healthy women: An event-related fmri study. *Biological psychology*, *85*(3), 487–495.

De Reus, K., Soma, M., Anichini, M., Gamba, M., de Heer Kloots, M., Lense, M., Bruno, J. H., Trainor, L., & Ravignani, A. (2021). Rhythm in dyadic interactions. *Philosophical Transactions of the Royal Society B*, *376*(1835), 20200337.

Delpy, D. T., Cope, M., van der Zee, P., Arridge, S., Wray, S., & Wyatt, J. (1988). Estimation of optical pathlength through tissue from direct time of flight measurement. *Physics in Medicine & Biology*, *33*(12), 1433.

Delpy, D., & Cope, M. (1997). Quantification in tissue near–infrared spectroscopy. *Philosophical Transactions of the Royal Society of London. Series B: Biological Sciences*, *352*(1354), 649–659.

Dick, A. S., Garic, D., Graziano, P., & Tremblay, P. (2019). The frontal aslant tract (fat) and its role in speech, language and executive function. *Cortex*, *111*, 148–163.

Ding, X. P., Du, X., Lei, D., Hu, C. S., Fu, G., & Chen, G. (2012). The neural correlates of identity faking and concealment: An fmri study. *PLoS One*, *7*(11), e48639.

Dixon, M. L., Thiruchselvam, R., Todd, R., & Christoff, K. (2017). Emotion and the prefrontal cortex: An integrative review. *Psychological bulletin*, *143*(10), 1033.

Djalovski, A., Dumas, G., Kinreich, S., & Feldman, R. (2021). Human attachments shape interbrain synchrony toward efficient performance of social goals. *NeuroImage*, *226*, 117600.

Dumas, G., Lachat, F., Martinerie, J., Nadel, J., & George, N. (2011). From social behaviour to brain synchronization: Review and perspectives in hyperscanning. *Irbm*, *32*(1), 48–53.

Dumas, G., Martinerie, J., Soussignan, R., & Nadel, J. (2012). Does the brain know who is at the origin of what in an imitative interaction? *Frontiers in human neuroscience*, *6*, 128.

Dumas, G., Nadel, J., Soussignan, R., Martinerie, J., & Garnero, L. (2010). Inter-brain synchronization during social interaction. *PloS one*, *5*(8), e12166.

Duraj, K., Piaseczna, N., Kostka, P., & Tkacz, E. (2022). Semantic segmentation of 12-lead ecg using 1d residual u-net with squeeze-excitation blocks. *Applied sciences*, *12*(7), 3332.

Dziobek, I., Preißler, S., Grozdanovic, Z., Heuser, I., Heekeren, H. R., & Roepke, S. (2011). Neuronal correlates of altered empathy and social cognition in borderline personality disorder. *Neuroimage*, *57*(2), 539–548.

Endevelt-Shapira, Y., & Feldman, R. (2023). Mother–infant brain-to-brain synchrony patterns reflect caregiving profiles. *Biology*, *12*(2), 284.

Engels, A. S., Heller, W., Spielberg, J. M., Warren, S. L., Sutton, B. P., Banich, M. T., & Miller, G. A. (2010). Co-occurring anxiety influences patterns of brain activity in depression. *Cognitive, Affective, & Behavioral Neuroscience*, *10*(1), 141–156.

Ewald, A., Aristei, S., Nolte, G., & Rahman, R. A. (2012). Brain oscillations and functional connectivity during overt language production. *Frontiers in psychology*, *3*, 166.

Fedorenko, E., Ivanova, A. A., & Regev, T. I. (2024). The language network as a natural kind within the broader landscape of the human brain. *Nature Reviews Neuroscience*, *25*(5), 289–312.

Feldman, R. (2007). Parent–infant synchrony: Biological foundations and developmental outcomes. *Current Directions in Psychological Science*, *16*(6), 340–345.

Feldman, R. (2012a). Bio-behavioral synchrony: A model for integrating biological and microsocial behavioral processes in the study of parenting. *Parenting*, *12*(2-3), 154–164.

Feldman, R. (2012b). Parent-infant synchrony: A biobehavioral model of mutual influences in the formation of affiliative bonds. *Monographs of the Society for Research in Child Development*, *77*(2), 42–51.

Feldman, R. (2017). The neurobiology of human attachments. *Trends in cognitive sciences*, *21*(2), 80–99.

Ferjan Ramírez, N., Lytle, S. R., & Kuhl, P. K. (2020). Parent coaching increases conversational turns and advances infant language

development. *Proceedings of the National Academy of Sciences*, *117*(7), 3484–3491.

Ferrer-i-Cancho, R., Gómez-Rodríguez, C., Esteban, J. L., & Alemany-Puig, L. (2022). Optimality of syntactic dependency distances. *Physical Review E*, *105*(1), 014308.

Fishburn, F. A., Ludlum, R. S., Vaidya, C. J., & Medvedev, A. V. (2019). Temporal derivative distribution repair (tddr): A motion correction method for fnirs. *Neuroimage*, *184*, 171–179.

Fishburn, F. A., Murty, V. P., Hlutkowsky, C. O., MacGillivray, C. E., Bemis, L. M., Murphy, M. E., Huppert, T. J., & Perlman, S. B. (2018). Putting our heads together: Interpersonal neural synchronization as a biological mechanism for shared intentionality. *Social Cognitive and Affective Neuroscience*, *13*(8), 841–849.

Forbes, C. E., & Grafman, J. (2010). The role of the human prefrontal cortex in social cognition and moral judgment. *Annual review of neuroscience*, *33*, 299–324.

Frank, D., Dewitt, M., Hudgens-Haney, M., Schaeffer, D., Ball, B., Schwarz, N., Hussein, A., Smart, L., & Sabatinelli, D. (2014). Emotion regulation: Quantitative meta-analysis of functional activation and deactivation. *Neuroscience & Biobehavioral Reviews*, *45*, 202–211.

Friederici, A. D., Chomsky, N., Berwick, R. C., Moro, A., & Bolhuis, J. J. (2017). Language, mind and brain. *Nature human behaviour*, *1*(10), 713–722.

Friederici, A. D., Fiebach, C. J., Schlesewsky, M., Bornkessel, I. D., & Von Cramon, D. Y. (2006). Processing linguistic complexity and grammaticality in the left frontal cortex. *Cerebral cortex*, *16*(12), 1709–1717.

Funane, T., Kiguchi, M., Atsumori, H., Sato, H., Kubota, K., & Koizumi, H. (2011). Synchronous activity of two people's prefrontal cortices during a cooperative task measured by simultaneous near-infrared spectroscopy. *Journal of biomedical optics*, *16*(7), 077011–077011.

Gallagher, H. L., Happé, F., Brunswick, N., Fletcher, P. C., Frith, U., & Frith, C. D. (2000). Reading the mind in cartoons and stories: An fmri study of 'theory of mind'in verbal and nonverbal tasks. *Neuropsychologia*, *38*(1), 11–21.

Gao, Y., Chao, H., Cavuoto, L., Yan, P., Kruger, U., Norfleet, J. E., Makled, B. A., Schwaitzberg, S., De, S., & Intes, X. (2022). Deep learning-based motion artifact removal in functional near-infrared spectroscopy. *Neurophotonics*, *9*(4), 041406–041406.

Geschwind, N. (1970). The organization of language and the brain: Language disorders after brain damage help in elucidating the neural basis of verbal behavior. *Science*, *170*(3961), 940–944.

Giglio, L., Ostarek, M., Weber, K., & Hagoort, P. (2022). Commonalities and asymmetries in the neurobiological infrastructure for language production and comprehension. *Cerebral Cortex*, *32*(7), 1405–1418.

Golland, Y., Arzouan, Y., & Levit-Binnun, N. (2015). The mere co-presence: Synchronization of autonomic signals and emotional responses across co-present individuals not engaged in direct interaction. *PloS one*, *10*(5), e0125804.

Grappe, A., Sarma, S. V., Sacré, P., González-Martínez, J., Liégeois-Chauvel, C., & Alario, F.-X. (2019). An intracerebral exploration of functional connectivity during word production. *Journal of Computational Neuroscience*, *46*, 125–140.

Grecucci, A., Giorgetta, C., Bonini, N., & Sanfey, A. G. (2013). Reappraising social emotions: The role of inferior frontal gyrus, temporo-parietal junction and insula in interpersonal emotion regulation. *Frontiers in human neuroscience*, *7*, 523.

Grinsted, A., Moore, J. C., & Jevrejeva, S. (2004). Application of the cross wavelet transform and wavelet coherence to geophysical time series. *Nonlinear processes in geophysics*, *11*(5/6), 561–566.

Gumilar, I., Barde, A., Hayati, A. F., Billinghurst, M., Lee, G., Momin, A., Averill, C., & Dey, A. (2021). Connecting the brains via virtual eyes: Eye-gaze directions and inter-brain synchrony in vr. *Extended Abstracts of the 2021 CHI Conference on Human Factors in Computing Systems*, 1–7.

Gvirts, H. Z., & Perlmutter, R. (2020). What guides us to neurally and behaviorally align with anyone specific? a neurobiological model based on fnirs hyperscanning studies. *The Neuroscientist*, *26*(2), 108–116.

Gweon, H., Dodell-Feder, D., Bedny, M., & Saxe, R. (2012). Theory of mind performance in children correlates with functional specialization of a brain region for thinking about thoughts. *Child Development*, *83*(6), 1853–1868.

Haegens, S., & Golumbic, E. Z. (2018). Rhythmic facilitation of sensory processing: A critical review. *Neuroscience & Biobehavioral Reviews*, *86*, 150–165.

Hakim, U., De Felice, S., Pinti, P., Zhang, X., Noah, J. A., Ono, Y., Burgess, P. W., Hamilton, A., Hirsch, J., & Tachtsidis, I. (2023). Quantification of inter-brain coupling: A review of current meth-

ods used in haemodynamic and electrophysiological hyperscanning studies. *NeuroImage*, *280*, 120354.

Hamilton, A. F. d. C. (2021). Hyperscanning: Beyond the hype. *Neuron*, *109*(3), 404–407.

Hartwigsen, G., Neef, N. E., Camilleri, J. A., Margulies, D. S., & Eickhoff, S. B. (2019). Functional segregation of the right inferior frontal gyrus: Evidence from coactivation-based parcellation. *Cerebral Cortex*, *29*(4), 1532–1546.

Hasson, U., Ghazanfar, A. A., Galantucci, B., Garrod, S., & Keysers, C. (2012). Brain-to-brain coupling: A mechanism for creating and sharing a social world. *Trends in Cognitive Sciences*, *16*(2), 114–121.

Hasson, U., Nir, Y., Levy, I., Fuhrmann, G., & Malach, R. (2004). Intersubject synchronization of cortical activity during natural vision. *science*, *303*(5664), 1634–1640.

Hertrich, I., Dietrich, S., Blum, C., & Ackermann, H. (2021). The role of the dorsolateral prefrontal cortex for speech and language processing. *Frontiers in human neuroscience*, *15*, 645209.

Hirsch, J., Zhang, X., Noah, J. A., & Ono, Y. (2017). Frontal temporal and parietal systems synchronize within and across brains during live eye-to-eye contact. *NeuroImage*, *157*, 314–330.

Hoehl, S., Bánki, A., Brzozowska, A., Carollo, A., Kostorz, K., Nguyen, T., Pletti, C., Reisner, S., Schäfer, V., Schaetz, C., et al. (2025). A developmental framework of interpersonal neural synchrony. *PsyArXiv*.

Hoehl, S., Fairhurst, M., & Schirmer, A. (2021). Interactional synchrony: Signals, mechanisms and benefits. *Social cognitive and affective neuroscience*, *16*(1-2), 5–18.

Hollenstein, T., Tighe, A. B., & Lougheed, J. P. (2017). Emotional development in the context of mother–child relationships. *Current Opinion in Psychology*, *17*, 140–144.

Holper, L., Scholkmann, F., & Wolf, M. (2012). Between-brain connectivity during imitation measured by fnirs. *Neuroimage*, *63*(1), 212–222.

Holroyd, C. B. (2022). Interbrain synchrony: On wavy ground. *Trends in Neurosciences*, *45*(5), 346–357.

Holt-Lunstad, J., Smith, T. B., & Layton, J. B. (2010). Social relationships and mortality risk: A meta-analytic review. *PLoS medicine*, *7*(7), e1000316.

Homan, R. W., Herman, J., & Purdy, P. (1987). Cerebral location of international 10–20 system electrode placement. *Electroencephalography and clinical neurophysiology*, *66*(4), 376–382.

Hu, X.-S., Wagley, N., Rioboo, A. T., DaSilva, A. F., & Kovelman, I. (2020). Photogrammetry-based stereoscopic optode registration method for functional near-infrared spectroscopy. *Journal of Biomedical Optics*, *25*(9), 095001–095001.

Huppert, T. J. (2016). Commentary on the statistical properties of noise and its implication on general linear models in functional near-infrared spectroscopy. *Neurophotonics*, *3*(1), 010401–010401.

Huth, A. G., De Heer, W. A., Griffiths, T. L., Theunissen, F. E., & Gallant, J. L. (2016). Natural speech reveals the semantic maps that tile human cerebral cortex. *Nature*, *532*(7600), 453–458.

i Cancho, R. F., Solé, R. V., & Köhler, R. (2004). Patterns in syntactic dependency networks. *Physical Review E*, *69*(5), 051915.

Iacoboni, M. (2005). Neural mechanisms of imitation. *Current Opinion in Neurobiology*, *15*(6), 632–637.

Islam, M. T., Zabir, I., Ahamed, S. T., Yasar, M. T., Shahnaz, C., & Fattah, S. A. (2017). A time-frequency domain approach of heart rate estimation from photoplethysmographic (ppg) signal. *Biomedical Signal Processing and Control*, *36*, 146–154.

Izzetoglu, M., Chitrapu, P., Bunce, S., & Onaral, B. (2010). Motion artifact cancellation in nir spectroscopy using discrete kalman filtering. *Biomedical engineering online*, *9*, 1–10.

Izzetoglu, M., Devaraj, A., Bunce, S., & Onaral, B. (2005). Motion artifact cancellation in nir spectroscopy using wiener filtering. *IEEE Transactions on Biomedical Engineering*, *52*(5), 934–938.

Jiang, J., Zheng, L., & Lu, C. (2021). A hierarchical model for interpersonal verbal communication. *Social Cognitive and Affective Neuroscience*, *16*(1-2), 246–255.

Jöbsis, F. F. (1977). Noninvasive, infrared monitoring of cerebral and myocardial oxygen sufficiency and circulatory parameters. *Science*, *198*(4323), 1264–1267.

Johnson, M. H., Dziurawiec, S., Ellis, H., & Morton, J. (1991). Newborns' preferential tracking of face-like stimuli and its subsequent decline. *Cognition*, *40*(1-2), 1–19.

Kanwisher, N., McDermott, J., & Chun, M. M. (1997). The fusiform face area: A module in human extrastriate cortex specialized for face perception. *Journal of neuroscience*, *17*(11), 4302–4311.

Kayhan, E., Matthes, D., Haresign, I. M., Bánki, A., Michel, C., Langeloh, M., Wass, S., & Hoehl, S. (2022). Deep: A dual eeg pipeline for developmental hyperscanning studies. *Developmental cognitive neuroscience*, *54*, 101104.

Kim, C.-K., Lee, S., Koh, D., & Kim, B.-M. (2011). Development of wireless nirs system with dynamic removal of motion artifacts. *Biomedical Engineering Letters*, *1*, 254–259.

Kim, M., Lee, S., Dan, I., & Tak, S. (2022). A deep convolutional neural network for estimating hemodynamic response function with reduction of motion artifacts in fnirs. *Journal of neural engineering*, *19*(1), 016017.

Kinreich, S., Djalovski, A., Kraus, L., Louzoun, Y., & Feldman, R. (2017). Brain-to-brain synchrony during naturalistic social interactions. *Scientific reports*, *7*(1), 17060.

Kolk, S. M., & Rakic, P. (2022). Development of prefrontal cortex. *Neuropsychopharmacology*, *47*(1), 41–57.

Konvalinka, I., Xygalatas, D., Bulbulia, J., Schjødt, U., Jegindø, E.-M., Wallot, S., Van Orden, G., & Roepstorff, A. (2011). Synchronized arousal between performers and related spectators in a fire-walking ritual. *Proceedings of the National Academy of Sciences*, *108*(20), 8514–8519.

Kotz, S. A., Cappa, S. F., von Cramon, D. Y., & Friederici, A. D. (2002). Modulation of the lexical–semantic network by auditory semantic priming: An event-related functional mri study. *Neuroimage*, *17*(4), 1761–1772.

Kuhl, P. K. (2007). Is speech learning 'gated'by the social brain? *Developmental Science*, *10*(1), 110–120.

Kuhl, P. K. (2011). Early language learning and literacy: Neuroscience implications for education. *Mind, Brain, and Education*, *5*(3), 128–142.

Langleben, D. D., Schroeder, L., Maldjian, J. A., Gur, R. C., McDonald, S., Ragland, J. D., O'Brien, C. P., & Childress, A. R. (2002). Brain activity during simulated deception: An event-related functional magnetic resonance study. *Neuroimage*, *15*(3), 727–732.

Lanka, P., Bortfeld, H., & Huppert, T. J. (2022). Correction of global physiology in resting-state functional near-infrared spectroscopy. *Neurophotonics*, *9*(3), 035003–035003.

Lau, E. F., Phillips, C., & Poeppel, D. (2008). A cortical network for semantics:(de) constructing the n400. *Nature reviews neuroscience*, *9*(12), 920–933.

Laufer, I., Negishi, M., Lacadie, C. M., Papademetris, X., & Constable, R. T. (2011). Dissociation between the activity of the right middle frontal gyrus and the middle temporal gyrus in processing semantic priming. *PloS one*, *6*(8), e22368.

Leclère, C., Viaux, S., Avril, M., Achard, C., Chetouani, M., Missonnier, S., & Cohen, D. (2014). Why synchrony matters during mother-child interactions: A systematic review. *PloS one*, *9*(12), e113571.

Lei, Y., Liu, S., Guo, X., Zuo, B., & Wen, F. (2025). Neural synchronization and its impact on intergroup attitudes in dynamic interactions. *Communications Biology*, *8*(1), 312.

Levinson, S. C. (2012). Action formation and ascription. *The handbook of conversation analysis*, 101–130.

Li, S., Xie, H., Zheng, Z., Chen, W., Xu, F., Hu, X., & Zhang, D. (2022). The causal role of the bilateral ventrolateral prefrontal cortices

on emotion regulation of social feedback. *Human Brain Mapping*, *43*(9), 2898–2910.

Li, W., Qin, W., Liu, H., Fan, L., Wang, J., Jiang, T., & Yu, C. (2013). Subregions of the human superior frontal gyrus and their connections. *Neuroimage*, *78*, 46–58.

Li, Y., Chen, R., Turel, O., Feng, T., Zhu, C.-Z., & He, Q. (2021). Dyad sex composition effect on inter-brain synchronization in face-to-face cooperation. *Brain Imaging and Behavior*, *15*(3), 1667–1675.

Lichtheim, L., et al. (1885). On aphasia. *Broca's Region*, 318–347.

Lim, M., Carollo, A., Bizzego, A., Chen, A. S., & Esposito, G. (2024a). Culture, sex and social context influence brain-to-brain synchrony: An fnirs hyperscanning study. *BMC psychology*, *12*(1), 350.

Lim, M., Carollo, A., Bizzego, A., Chen, A. S., & Esposito, G. (2024b). Synchrony within, synchrony without: Establishing the link between interpersonal behavioural and brain-to-brain synchrony during role-play. *Royal Society Open Science*, *11*(9), 240331.

Lim, M., Carollo, A., Bizzego, A., Chen, S. A., & Esposito, G. (2023). Decreased activation in left prefrontal cortex during role-play: An fnirs study of the psychodrama sociocognitive model. *The Arts in Psychotherapy*, 102098.

Lindenberger, U., Li, S.-C., Gruber, W., & Müller, V. (2009). Brains swinging in concert: Cortical phase synchronization while playing guitar. *BMC neuroscience*, *10*(1), 1–12.

Liu, N., Mok, C., Witt, E. E., Pradhan, A. H., Chen, J. E., & Reiss, A. L. (2016). Nirs-based hyperscanning reveals inter-brain neural synchronization during cooperative jenga game with face-to-face communication. *Frontiers in Human Neuroscience*, *10*, 82.

Liu, T., Duan, L., Dai, R., Pelowski, M., & Zhu, C. (2021). Team-work, team-brain: Exploring synchrony and team interdependence in a nine-person drumming task via multiparticipant hyperscanning and inter-brain network topology with fnirs. *NeuroImage*, *237*, 118147.

Long, Y., Zheng, L., Zhao, H., Zhou, S., Zhai, Y., & Lu, C. (2021). Interpersonal neural synchronization during interpersonal touch underlies affiliative pair bonding between romantic couples. *Cerebral Cortex*, *31*(3), 1647–1659.

Lopes, P. N., Salovey, P., Côté, S., Beers, M., & Petty, R. E. (2005). Emotion regulation abilities and the quality of social interaction. *Emotion*, *5*(1), 113.

Lu, H., Wang, X., Zhang, Y., Huang, P., Xing, C., Zhang, M., & Zhu, X. (2023). Increased interbrain synchronization and neural efficiency of the frontal cortex to enhance human coordinative behavior: A combined hyper-tes and fnirs study. *NeuroImage*, *282*, 120385.

Lu, K., Qiao, X., & Hao, N. (2019). Praising or keeping silent on partner's ideas: Leading brainstorming in particular ways. *Neuropsychologia*, *124*, 19–30.

Lyons, D. E., Santos, L. R., & Keil, F. C. (2006). Reflections of other minds: How primate social cognition can inform the function of mirror neurons. *Current Opinion in Neurobiology*, *16*(2), 230–234.

Martin, R. S., & Huettel, S. A. (2022). Cognitive functions as revealed by imaging of the human brain. In *Neuroscience in the 21st century: From basic to clinical* (pp. 3087–3113). Springer.

Mazzonetto, I., Castellaro, M., Cooper, R. J., & Brigadoi, S. (2022). Smartphone-based photogrammetry provides improved localiza-

tion and registration of scalp-mounted neuroimaging sensors. *Scientific Reports*, *12*(1), 10862.

Meng, X., Sun, C., Du, B., Liu, L., Zhang, Y., Dong, Q., Georgiou, G. K., & Nan, Y. (2022). The development of brain rhythms at rest and its impact on vocabulary acquisition. *Developmental Science*, *25*(2), e13157.

Metz, A. J., Wolf, M., Achermann, P., & Scholkmann, F. (2015). A new approach for automatic removal of movement artifacts in near-infrared spectroscopy time series by means of acceleration data. *Algorithms*, *8*(4), 1052–1075.

Mohammad, S. M. (2016). Sentiment analysis: Detecting valence, emotions, and other affectual states from text. In *Emotion measurement* (pp. 201–237). Elsevier.

Molavi, B., & Dumont, G. A. (2012). Wavelet-based motion artifact removal for functional near-infrared spectroscopy. *Physiological measurement*, *33*(2), 259.

Montague, P. R., Berns, G. S., Cohen, J. D., McClure, S. M., Pagnoni, G., Dhamala, M., Wiest, M. C., Karpov, I., King, R. D., Apple, N., et al. (2002). Hyperscanning: Simultaneous fmri during linked social interactions. *Neuroimage*, *16*(4), 1159–1164.

Morgan, J. K., Santosa, H., Conner, K. K., Fridley, R. M., Forbes, E. E., Iyengar, S., Joseph, H. M., & Huppert, T. J. (2023). Mother–child neural synchronization is time linked to mother–child positive affective state matching. *Social Cognitive and Affective Neuroscience*, *18*(1), nsad001.

Moskalenko, V., Zolotykh, N., & Osipov, G. (2020). Deep learning for ecg segmentation. *Advances in Neural Computation, Machine Learn-*

ing, and Cognitive Research III: Selected Papers from the XXI International Conference on Neuroinformatics, October 7-11, 2019, Dolgoprudny, Moscow Region, Russia, 246–254.

Newman, M. (2018). *Networks*. Oxford university press.

Nguyen, T., Banki, A., Markova, G., & Hoehl, S. (2020). Studying parent-child interaction with hyperscanning. *Progress in brain research*, *254*, 1–24.

Nguyen, T., Hoehl, S., & Vrtička, P. (2021). A guide to parent-child fnirs hyperscanning data processing and analysis. *Sensors*, *21*(12), 4075.

Nguyen, T., Kungl, M. T., Hoehl, S., White, L. O., & Vrtička, P. (2024). Visualizing the invisible tie: Linking parent–child neural synchrony to parents' and children's attachment representations. *Developmental Science*, *27*(6), e13504.

Nguyen, T., Schleihauf, H., Kayhan, E., Matthes, D., Vrtička, P., & Hoehl, S. (2020). The effects of interaction quality on neural synchrony during mother-child problem solving. *cortex*, *124*, 235–249.

Nguyen, T., Schleihauf, H., Kayhan, E., Matthes, D., Vrtička, P., & Hoehl, S. (2021). Neural synchrony in mother–child conversation: Exploring the role of conversation patterns. *Social Cognitive and Affective Neuroscience*, *16*(1-2), 93–102.

Nguyen, T., Schleihauf, H., Kungl, M., Kayhan, E., Hoehl, S., & Vrtička, P. (2021). Interpersonal neural synchrony during father–child problem solving: An fnirs hyperscanning study. *Child Development*, *92*(4), e565–e580.

Nguyen, T., Zimmer, L., & Hoehl, S. (2023). Your turn, my turn. neural synchrony in mother–infant proto-conversation. *Philosophical Transactions of the Royal Society B*, *378*(1875), 20210488.

Noponen, T., Kotilahti, K., Nissilä, I., Kajava, T., & Meriläinen, P. (2010). Effects of improper source coupling in frequency-domain near-infrared spectroscopy. *Physics in Medicine & Biology*, *55*(10), 2941.

Novembre, G., & Iannetti, G. D. (2021). Hyperscanning alone cannot prove causality. multibrain stimulation can. *Trends in Cognitive Sciences*, *25*(2), 96–99.

Nozawa, T., Sakaki, K., Ikeda, S., Jeong, H., Yamazaki, S., Kawata, K. H. d. S., Kawata, N. Y. d. S., Sasaki, Y., Kulason, K., Hirano, K., et al. (2019). Prior physical synchrony enhances rapport and inter-brain synchronization during subsequent educational communication. *Scientific reports*, *9*(1), 12747.

Nozawa, T., Sasaki, Y., Sakaki, K., Yokoyama, R., & Kawashima, R. (2016). Interpersonal frontopolar neural synchronization in group communication: An exploration toward fnirs hyperscanning of natural interactions. *Neuroimage*, *133*, 484–497.

Nummenmaa, L., Glerean, E., Viinikainen, M., Jääskeläinen, I. P., Hari, R., & Sams, M. (2012). Emotions promote social interaction by synchronizing brain activity across individuals. *Proceedings of the National Academy of Sciences*, *109*(24), 9599–9604.

Ogwok, D., & Ehlers, E. M. (2022). Jaccard index in ensemble image segmentation: An approach. *Proceedings of the 2022 5th International Conference on Computational Intelligence and Intelligent Systems*, 9–14.

Pan, Y., Cheng, X., Zhang, Z., Li, X., & Hu, Y. (2017). Cooperation in lovers: An f nirs-based hyperscanning study. *Human Brain Mapping*, *38*(2), 831–841.

Pan, Y., Guyon, C., Borragán, G., Hu, Y., & Peigneux, P. (2021). Interpersonal brain synchronization with instructor compensates for learner's sleep deprivation in interactive learning. *Biochemical pharmacology*, *191*, 114111.

Parkinson, C., Kleinbaum, A. M., & Wheatley, T. (2018). Similar neural responses predict friendship. *Nature communications*, *9*(1), 332.

Paszke, A., Gross, S., Massa, F., Lerer, A., Bradbury, J., Chanan, G., Killeen, T., Lin, Z., Gimelshein, N., Antiga, L., et al. (2019). Pytorch: An imperative style, high-performance deep learning library. *Advances in neural information processing systems*, *32*.

Perpetuini, D., Cardone, D., Filippini, C., Chiarelli, A. M., & Merla, A. (2021). A motion artifact correction procedure for fnirs signals based on wavelet transform and infrared thermography video tracking. *Sensors*, *21*(15), 5117.

Pilon, F., Boisvert, M., Mottron, L., & Potvin, S. (2025). A fmri meta-analysis of emotion processing in the psychosis spectrum reveals no significant alterations in at-risk individuals. *Psychiatry Research*, *351*, 116565.

Pinti, P., Devoto, A., Greenhalgh, I., Tachtsidis, I., Burgess, P. W., & de C Hamilton, A. F. (2021). The role of anterior prefrontal cortex (area 10) in face-to-face deception measured with fnirs. *Social Cognitive and Affective Neuroscience*, *16*(1-2), 129–142.

Pinti, P., Tachtsidis, I., Hamilton, A., Hirsch, J., Aichelburg, C., Gilbert, S., & Burgess, P. W. (2020). The present and future use of func-

tional near-infrared spectroscopy (fnirs) for cognitive neuroscience. *Annals of the new York Academy of Sciences*, *1464*(1), 5–29.

Plutchik, R. (1980). A general psychoevolutionary theory of emotion. In *Theories of emotion* (pp. 3–33). Elsevier.

Poeppel, D., Emmorey, K., Hickok, G., & Pylkkänen, L. (2012). Towards a new neurobiology of language. *Journal of Neuroscience*, *32*(41), 14125–14131.

Polkinghorne, D. E. (2005). Language and meaning: Data collection in qualitative research. *Journal of counseling psychology*, *52*(2), 137.

Price, C. J. (2012). A review and synthesis of the first 20 years of pet and fmri studies of heard speech, spoken language and reading. *Neuroimage*, *62*(2), 816–847.

Qian, X., Wang, M., Wang, X., Wang, Y., & Dai, W. (2022). Intelligent method for real-time portable eeg artifact annotation in semiconstrained environment based on computer vision. *Computational Intelligence and Neuroscience*, *2022*(1), 9590411.

Quispe, L. V., Tohalino, J. A., & Amancio, D. R. (2021). Using virtual edges to improve the discriminability of co-occurrence text networks. *Physica A: Statistical Mechanics and its Applications*, *562*, 125344.

Raposo, A., Moss, H. E., Stamatakis, E. A., & Tyler, L. K. (2006). Repetition suppression and semantic enhancement: An investigation of the neural correlates of priming. *Neuropsychologia*, *44*(12), 2284–2295.

Reindl, V., Gerloff, C., Scharke, W., & Konrad, K. (2018). Brain-to-brain synchrony in parent-child dyads and the relationship with

emotion regulation revealed by fnirs-based hyperscanning. *NeuroImage*, *178*, 493–502.

Rissman, J., Eliassen, J. C., & Blumstein, S. E. (2003). An event-related fmri investigation of implicit semantic priming. *Journal of cognitive neuroscience*, *15*(8), 1160–1175.

Rizzolatti, G., & Craighero, L. (2004). The mirror-neuron system. *Annu. Rev. Neurosci.*, *27*, 169–192.

Rizzolatti, G., & Fabbri-Destro, M. (2008). The mirror system and its role in social cognition. *Current Opinion in Neurobiology*, *18*(2), 179–184.

Ronneberger, O., Fischer, P., & Brox, T. (2015). U-net: Convolutional networks for biomedical image segmentation. *Medical image computing and computer-assisted intervention–MICCAI 2015: 18th international conference, Munich, Germany, October 5-9, 2015, proceedings, part III 18*, 234–241.

Roy, M., Shohamy, D., & Wager, T. D. (2012). Ventromedial prefrontal-subcortical systems and the generation of affective meaning. *Trends in cognitive sciences*, *16*(3), 147–156.

Russell, J. A. (1980). A circumplex model of affect. *Journal of personality and social psychology*, *39*(6), 1161.

Sachs, O., Weis, S., Zellagui, N., Sass, K., Huber, W., Zvyagintsev, M., Mathiak, K., & Kircher, T. (2011). How different types of conceptual relations modulate brain activation during semantic priming. *Journal of Cognitive Neuroscience*, *23*(5), 1263–1273.

Saint-Georges, C., Chetouani, M., Cassel, R., Apicella, F., Mahdhaoui, A., Muratori, F., Laznik, M.-C., & Cohen, D. (2013). Motherese

in interaction: At the cross-road of emotion and cognition?(a systematic review). *PloS one*, *8*(10), e78103.

Samson, D., Apperly, I. A., Chiavarino, C., & Humphreys, G. W. (2004). Left temporoparietal junction is necessary for representing someone else's belief. *Nature Neuroscience*, *7*(5), 499–500.

Sanchez-Lopez, A., Vanderhasselt, M.-A., Allaert, J., Baeken, C., & De Raedt, R. (2018). Neurocognitive mechanisms behind emotional attention: Inverse effects of anodal tdcs over the left and right dlpfc on gaze disengagement from emotional faces. *Cognitive, Affective, & Behavioral Neuroscience*, *18*(3), 485–494.

Sandler, M., Howard, A., Zhu, M., Zhmoginov, A., & Chen, L.-C. (2018). Mobilenetv2: Inverted residuals and linear bottlenecks. *Proceedings of the IEEE conference on computer vision and pattern recognition*, 4510–4520.

Sänger, J., Müller, V., & Lindenberger, U. (2012). Intra-and interbrain synchronization and network properties when playing guitar in duets. *Frontiers in human neuroscience*, *6*, 312.

Sänger, J., Müller, V., & Lindenberger, U. (2013). Directionality in hyperbrain networks discriminates between leaders and followers in guitar duets. *Frontiers in human neuroscience*, *7*, 234.

Santamaria, L., Noreika, V., Georgieva, S., Clackson, K., Wass, S., & Leong, V. (2020). Emotional valence modulates the topology of the parent-infant inter-brain network. *NeuroImage*, *207*, 116341.

Santosa, H., Aarabi, A., Perlman, S. B., & Huppert, T. J. (2017). Characterization and correction of the false-discovery rates in resting state connectivity using functional near-infrared spectroscopy. *Journal of biomedical optics*, *22*(5), 055002–055002.

Santosa, H., Zhai, X., Fishburn, F., Sparto, P. J., & Huppert, T. J. (2020). Quantitative comparison of correction techniques for removing systemic physiological signal in functional near-infrared spectroscopy studies. *Neurophotonics*, *7*(3), 035009–035009.

Scholkmann, F., Spichtig, S., Muehlemann, T., & Wolf, M. (2010). How to detect and reduce movement artifacts in near-infrared imaging using moving standard deviation and spline interpolation. *Physiological measurement*, *31*(5), 649.

Schwartz, L., Levy, J., Endevelt-Shapira, Y., Djalovski, A., Hayut, O., Dumas, G., & Feldman, R. (2022). Technologically-assisted communication attenuates inter-brain synchrony. *Neuroimage*, *264*, 119677.

Schwartz, L., Levy, J., Hayut, O., Netzer, O., Endevelt-Shapira, Y., & Feldman, R. (2024). Generation whatsapp: Inter-brain synchrony during face-to-face and texting communication. *Scientific reports*, *14*(1), 2672.

Semeraro, A., Vilella, S., Improta, R., De Duro, E. S., Mohammad, S. M., Ruffo, G., & Stella, M. (2025). Emoatlas: An emotional network analyzer of texts that merges psychological lexicons, artificial intelligence, and network science. *Behavior Research Methods*, *57*(2), 77.

Semeraro, A., Vilella, S., Ruffo, G., & Stella, M. (2022). Emotional profiling and cognitive networks unravel how mainstream and alternative press framed astrazeneca, pfizer and covid-19 vaccination campaigns. *Scientific reports*, *12*(1), 14445.

Shao, C., Zhang, X., Wu, Y., Zhang, W., & Sun, B. (2023). Increased interpersonal brain synchronization in romantic couples is asso-

ciated with higher honesty: An fnirs hyperscanning study. *Brain Sciences*, *13*(5), 833.

Sharp, D. J., Awad, M., Warren, J. E., Wise, R. J., Vigliocco, G., & Scott, S. K. (2010). The neural response to changing semantic and perceptual complexity during language processing. *Human brain mapping*, *31*(3), 365–377.

Siew, C. S., Wulff, D. U., Beckage, N. M., & Kenett, Y. N. (2019). Cognitive network science: A review of research on cognition through the lens of network representations, processes, and dynamics. *Complexity*, *2019*.

Song, X., Dong, M., Feng, K., Li, J., Hu, X., & Liu, T. (2024). Influence of interpersonal distance on collaborative performance in the joint simon task—an fnirs-based hyperscanning study. *NeuroImage*, *285*, 120473.

Sorella, S., Grecucci, A., Piretti, L., & Job, R. (2021). Do anger perception and the experience of anger share common neural mechanisms? coordinate-based meta-analytic evidence of similar and different mechanisms from functional neuroimaging studies. *NeuroImage*, *230*, 117777.

Stella, M. (2022). Cognitive network science for understanding online social cognitions: A brief review. *Topics in Cognitive Science*, *14*(1), 143–162.

Stella, M., Citraro, S., Rossetti, G., Marinazzo, D., Kenett, Y. N., & Vitevitch, M. S. (2024). Cognitive modelling of concepts in the mental lexicon with multilayer networks: Insights, advancements, and future challenges. *Psychonomic Bulletin & Review*, 1–24.

Stella, M., De Nigris, S., Aloric, A., & Siew, C. S. (2019). Forma mentis networks quantify crucial differences in stem perception between students and experts. *PloS one*, *14*(10), e0222870.

Stern, D. N. (2009). *The first relationship*. Harvard University Press.

Strangman, G. E., Li, Z., & Zhang, Q. (2013). Depth sensitivity and source-detector separations for near infrared spectroscopy based on the colin27 brain template. *PloS one*, *8*(8), e66319.

Tang, Y., Mo, L., Peng, Z., Li, Y., & Zhang, D. (2025). Causal enhancement of cognitive reappraisal through synchronized dorsolateral and ventrolateral prefrontal cortex activity. *Emotion*, *25*, 1418–1428.

Tausczik, Y. R., & Pennebaker, J. W. (2010). The psychological meaning of words: Liwc and computerized text analysis methods. *Journal of language and social psychology*, *29*(1), 24–54.

Thompson-Schill, S. L., D'Esposito, M., Aguirre, G. K., & Farah, M. J. (1997). Role of left inferior prefrontal cortex in retrieval of semantic knowledge: A reevaluation. *Proceedings of the National Academy of Sciences*, *94*(26), 14792–14797.

Tomasello, M. (2010). *Origins of human communication*. MIT press.

Toppi, J., Borghini, G., Petti, M., He, E. J., De Giusti, V., He, B., Astolfi, L., & Babiloni, F. (2016). Investigating cooperative behavior in ecological settings: An eeg hyperscanning study. *PloS one*, *11*(4), e0154236.

Trehub, S. E., Ghazban, N., & Corbeil, M. (2015). Musical affect regulation in infancy. *Annals of the New York Academy of Sciences*, *1337*(1), 186–192.

Tremblay, P., & Dick, A. S. (2016). Broca and wernicke are dead, or moving past the classic model of language neurobiology. *Brain and language*, *162*, 60–71.

Trevarthen, C. (1998). The concept and foundations of infant intersubjectivity. In S. Bråten (Ed.), *Intersubjective communication and emotion in early ontogeny* (pp. 15–46). Cambridge University Press.

Turk, E., Endevelt-Shapira, Y., Feldman, R., van den Heuvel, M. I., & Levy, J. (2022). Brains in sync: Practical guideline for parent–infant eeg during natural interaction. *Frontiers in Psychology*, *13*, 833112.

Twenge, J. M., Baumeister, R. F., DeWall, C. N., Ciarocco, N. J., & Bartels, J. M. (2007). Social exclusion decreases prosocial behavior. *Journal of personality and social psychology*, *92*(1), 56.

Tyler, L. K., Marslen-Wilson, W. D., Randall, B., Wright, P., Devereux, B. J., Zhuang, J., Papoutsi, M., & Stamatakis, E. A. (2011). Left inferior frontal cortex and syntax: Function, structure and behaviour in patients with left hemisphere damage. *Brain*, *134*(2), 415–431.

Van Overwalle, F. (2009). Social cognition and the brain: A meta-analysis. *Human Brain Mapping*, *30*(3), 829–858.

Van Overwalle, F., & Baetens, K. (2009). Understanding others' actions and goals by mirror and mentalizing systems: A meta-analysis. *NeuroImage*, *48*(3), 564–584.

Virtanen, J., Noponen, T., Kotilahti, K., Virtanen, J., & Ilmoniemi, R. J. (2011). Accelerometer-based method for correcting signal baseline changes caused by motion artifacts in medical near-infrared spectroscopy. *Journal of biomedical optics*, *16*(8), 087005–087005.

Vitevitch, M. S., Pisoni, D. B., Soehlke, L., & Foster, T. A. (2024). Using complex networks in the hearing sciences. *Ear and Hearing*, *45*(1), 1–9.

von Lühmann, A., Boukouvalas, Z., Müller, K.-R., & Adalı, T. (2019). A new blind source separation framework for signal analysis and artifact rejection in functional near-infrared spectroscopy. *Neuroimage*, *200*, 72–88.

Vygotsky, L. S. (1978). *Mind in society: The development of higher psychological processes* (Vol. 86). Harvard university press.

Wang, J., Yang, Y., Zhao, X., Zuo, Z., & Tan, L.-H. (2020). Evolutional and developmental anatomical architecture of the left inferior frontal gyrus. *NeuroImage*, *222*, 117268.

Wang, J., Meng, F., Xu, C., Zhang, Y., Liang, K., Han, C., Gao, Y., Yu, X., Li, Z., Zeng, X., et al. (2025). Simultaneous intracranial recordings of interacting brains reveal neurocognitive dynamics of human cooperation. *Nature Neuroscience*, *28*(1), 161–173.

Wang, X., Lu, K., He, Y., Gao, Z., & Hao, N. (2022). Close spatial distance and direct gaze bring better communication outcomes and more intertwined neural networks. *NeuroImage*, *261*, 119515.

Waugh, C. E., Hamilton, J. P., & Gotlib, I. H. (2010). The neural temporal dynamics of the intensity of emotional experience. *Neuroimage*, *49*(2), 1699–1707.

Waugh, C. E., Lemus, M. G., & Gotlib, I. H. (2014). The role of the medial frontal cortex in the maintenance of emotional states. *Social Cognitive and Affective Neuroscience*, *9*(12), 2001–2009.

Wernicke, C. (1969). The symptom complex of aphasia. In R. S. Cohen & M. W. Wartofsky (Eds.), *Proceedings of the boston colloquium for the philosophy of science 1966/1968* (pp. 34–97, Vol. 4). Springer.

Wikström, V., Saarikivi, K., Falcon, M., Makkonen, T., Martikainen, S., Putkinen, V., Cowley, B. U., & Tervaniemi, M. (2022). Inter-brain synchronization occurs without physical co-presence during cooperative online gaming. *Neuropsychologia*, *174*, 108316.

Wilson, M., & Wilson, T. P. (2005). An oscillator model of the timing of turn-taking. *Psychonomic Bulletin & Review*, *12*, 957–968.

Wu, C.-Y., Xu, Q., & Neumann, U. (2021). Synergy between 3dmm and 3d landmarks for accurate 3d facial geometry. *2021 International Conference on 3D Vision (3DV)*, 453–463.

Wu, J., Liu, Y., Du, X., Zhang, X., & Xue, C. (2025). Influence of design interaction modes on conceptual design behavior and inter-brain synchrony in designer teams: A fnirs hyperscanning study. *Advanced Engineering Informatics*, *65*, 103223.

Xiao, Q., Shen, L., He, H., Wang, X., Fu, Y., Ding, J., Jiang, F., Zhang, J., Zhang, Z., Grecucci, A., et al. (2024). Alteration of prefrontal cortex and its associations with emotional and cognitive dysfunctions in adolescent borderline personality disorder. *European child & adolescent psychiatry*, *33*(11), 3937–3949.

Yang, J., Zhang, H., Ni, J., De Dreu, C. K., & Ma, Y. (2020). Within-group synchronization in the prefrontal cortex associates with intergroup conflict. *Nature Neuroscience*, *23*(6), 754–760.

Yang, Y., Li, L., de Deyne, S., Li, B., Wang, J., & Cai, Q. (2024). Unraveling lexical semantics in the brain: Comparing internal, exter-

nal, and hybrid language models. *Human Brain Mapping*, *45*(1), e26546.

Yang, Y.-H., Marslen-Wilson, W. D., & Bozic, M. (2017). Syntactic complexity and frequency in the neurocognitive language system. *Journal of Cognitive Neuroscience*, *29*(9), 1605–1620.

Yeshurun, Y., Swanson, S., Simony, E., Chen, J., Lazaridi, C., Honey, C. J., & Hasson, U. (2017). Same story, different story: The neural representation of interpretive frameworks. *Psychological science*, *28*(3), 307–319.

Yücel, M. A., Luke, R., Mesquita, R. C., von Lühmann, A., Mehler, D. M., Lührs, M., Gemignani, J., Abdalmalak, A., Albrecht, F., de Almeida Ivo, I., et al. (2025). Fnirs reproducibility varies with data quality, analysis pipelines, and researcher experience. *Communications biology*, *8*(1), 1149.

Yücel, M. A., Selb, J., Cooper, R. J., & Boas, D. A. (2014). Targeted principle component analysis: A new motion artifact correction approach for near-infrared spectroscopy. *Journal of innovative optical health sciences*, *7*(02), 1350066.

Zhao, Q., Zhao, W., Lu, C., Du, H., & Chi, P. (2024). Interpersonal neural synchronization during social interactions in close relationships: A systematic review and meta-analysis of fnirs hyperscanning studies. *Neuroscience & Biobehavioral Reviews*, *158*, 105565.

Zhu, L., Lotte, F., Cui, G., Li, J., Zhou, C., & Cichocki, A. (2018). Neural mechanisms of social emotion perception: An eeg hyper-scanning study. *2018 International Conference on Cyberworlds (CW)*, 199–206.

Zimeo Morais, G. A., Balardin, J. B., & Sato, J. R. (2018). Fnirs optodes' location decider (fold): A toolbox for probe arrangement guided by brain regions-of-interest. *Scientific Reports*, *8*(1), 3341.